

Chromosome aberrations in human lymphocytes irradiated with heavy ions

Vom Fachbereich Physik
der Technischen Universität Darmstadt

zur Erlangung des Grades
eines Doktors der Naturwissenschaften
(Dr. rer. nat.)

genehmigte Dissertation von
M.A.-Sc. Ryonfa Lee
aus Yamagata, Japan

Darmstadt 2006

D17

Referent: Prof. Dr. G. Kraft
Korreferent: Prof. Dr. D. H. H. Hoffmann
Tag der Einreichung: 18.04.2006
Tag der Prüfung: 07.06.2006

Zusammenfassung

Im Hinblick auf den wachsenden Einsatz von Schwerionenstrahlen in der Tumorthherapie und für die Planung bemannter Weltraumflüge ist eine realistische Abschätzung des Gesundheitsrisikos von Teilchenstrahlen unerlässlich. Die Standardmethode zur Quantifizierung einer Strahlendosis und zur Abschätzung des Gesundheitsrisikos von Strahlung ist die Analyse von Chromosomenschäden in peripheren Blutlymphozyten. Hierzu werden die Zellen zu einem festgelegten Untersuchungszeitpunkt, nämlich 48 Stunden nach der *in vitro* Stimulierung, in der ersten Mitose nach Bestrahlung untersucht. Die Anwendung dieser Methode resultiert für hoch-LET Strahlung in einer niedrigen RBW. Mittlerweile gibt es vermehrt Hinweise, dass die Anzahl der Aberrationen, die in Metaphasezellen sichtbar ist, durch hoch-LET induzierte Zellzyklusverzögerungen und Apoptose beeinflusst werden können. Um diese Fragen zu untersuchen, wurden Lymphozyten eines gesunden Spenders mit Röntgenstrahlen, C-, Fe- und Fe-ähnlichen Ionen mit LET Werten im Bereich von 2 bis 3160 keV/ μm bestrahlt. Zur Untersuchung von Chromosomenschäden wurden Zellen in dreistündigen Intervallen zwischen 48 und 84 Stunden nach Bestrahlung gesammelt und Aberrationen in Metaphasen des ersten Zellzyklus untersucht. Parallel dazu wurden Aberrationen in G_2 -Phasezellen bestimmt und die Zellzyklusprogression sowie die strahleninduzierte Apoptose gemessen. Die Untersuchung ergab, dass die durch hoch-LET Strahlung induzierte Apoptose nicht die Anzahl der Aberrationen in Metaphasezellen beeinflusst. In Gegensatz dazu wurde ein Zusammenhang zwischen hoch-LET induzierten Zellzyklusverzögerungen und der Anzahl der Aberrationen der Zellen gefunden. Der verzögerte Eintritt von schwergeschädigten Zellen in die Mitose wird durch einen Arrest in der G_2 -Phase verursacht, und die Dauer der Verzögerung hängt von der Dosis und dem LET ab. Eine detaillierte statistische Analyse der Verteilung der Aberrationen in der Zellpopulation zeigte eine Korrelation zwischen der Zellzyklusverzögerung schwergeschädigter Zellen und der Anzahl der Teilchendurchgänge pro Zellkern. Zusammenfassend zeigen die Daten, dass der Standardtest, der auf der Untersuchung von Metaphasezellen 48 Stunden nach der Bestrahlung beruht, die RBW von hoch-LET Teilchen unterschätzt. Die Anwendung alternativer zytogenetischer Methoden (Analyse von Zellen in der G_2 -Phase, Integrationsanalyse) bestätigt diese Schlussfolgerung.

Abstract

Because of the increasing use of heavy ions in cancer therapy and for the planning of manned space travels, a realistic estimate of the health risks associated with particle exposure is indispensable. The standard method to quantify the exposed dose and to assess the health risks of radiation is the analysis of chromosome aberrations in peripheral blood lymphocytes at the first post-irradiation mitosis at one fixed time, 48 h, after *in vitro* stimulation. Using this procedure very low RBE values for high LET particles are reported. However, evidence is accumulating that high LET induced cell cycle delays and apoptosis may influence the aberration yield observable in metaphase cells. To address these questions, lymphocytes obtained from a healthy donor were irradiated with X-rays, C-, Fe- and Fe-like particles with LETs ranging from 2-3160 keV/ μm and chromosome aberrations were measured in first cycle metaphase cells at multiple 3 h collection intervals from 48 to 84 h post-irradiation. In parallel, aberrations were determined in G_2 -phase cells and cell cycle progression as well as radiation-induced apoptosis were examined. Analysis of the data sets shows that high LET-induced apoptosis does not affect the observable aberration yield. However, a relationship between high LET induced cell cycle delays and the number of aberrations carried by a cell was found: the delayed entry of heavily damaged cells into mitosis results from a prolonged arrest in G_2 and the delay is dose- and LET-dependent. Detailed statistical analysis of the frequency distributions of aberrations among cells revealed a correlation between the selective delay of heavily damaged cells and the number of particle hits per cell nucleus. Altogether, the data demonstrate that the application of the standard metaphase assay 48 h post-irradiation results in an underestimation of the RBE of high LET particles. Application of alternative cytogenetic approaches (G_2 -PCC analysis, the integration analysis) confirmed this conclusion.

Contents

1	Introduction	1
1.1	High LET radiation exposure to humans	1
1.2	Physics of charged particles	3
1.2.1	Macroscopic characteristics of charged particles	3
1.2.2	Microscopic characteristics of charged particles	5
1.3	Biological effects of ionizing radiation	7
1.3.1	Relative biological effectiveness (RBE) and its characteristics	7
1.3.2	DNA damage and repair	8
1.3.3	Cell cycle and checkpoints and apoptosis	11
1.3.4	Chromosome aberrations and their fate	13
1.4	Chromosome aberration analysis for biological dosimetry	15
1.4.1	Analysis of structural aberrations in metaphase cells	15
1.4.2	Confounding factors for biological dosimetry	16
1.4.3	Analysis of chromosome aberrations in interphase cells	17
1.5	Objective of the study	18
2	Materials and methods	21
2.1	Cell culture and irradiation	21
2.1.1	Isolation of lymphocytes	21
2.1.2	Irradiation procedure	21
2.1.3	Cell culture	23
2.2	Cytogenetic analysis	24
2.2.1	Cell fixation and chromosome preparation	24
2.2.2	Fluorescence-plus-Giemsa staining	25
2.2.3	Metaphase analysis	26
2.2.4	PCC analysis	27
2.3	Cell proliferation analysis	27
2.3.1	Mitotic and PCC indices and cell generations	27
2.3.2	BrdU-labeling	28
2.4	Apoptosis measurement	29
2.4.1	Analysis of cell morphology	29
2.4.2	TUNEL-method	30

2.5	Data analysis	31
2.5.1	Integration analysis of chromosome aberrations	31
2.5.2	Comparison of theoretical distributions with experimental distributions of aberrations among cells	32
2.5.3	Error calculation and curve fitting	37
3	Results	39
3.1	Cell proliferation analysis	39
3.1.1	BrdU-labeling	39
3.1.1.1	Radiation-induced cell cycle delay	39
3.1.1.2	LET dependence of the labeling index	40
3.1.2	The mitotic index	41
3.1.3	The fraction of cells at first G_2 -phase and first mitosis	43
3.2	Investigation of the cytogenetic damage	44
3.2.1	Number of aberrant first cycle metaphases and corresponding aberration yield	44
3.2.1.1	Number of aberrant first cycle metaphases	44
3.2.1.2	Aberration yields in first cycle metaphases	46
3.2.2	Aberration spectrum	47
3.2.3	Number of aberrant first cycle G_2 -PCCs and corresponding aberration yield	48
3.2.3.1	Number of aberrant first cycle G_2 -cells	48
3.2.3.2	Aberration yields in first cycle G_2 -cells	48
3.2.3.3	Comparison of cytogenetic damage detected in metaphases and G_2 -PCC cells	50
3.2.4	Inter-experimental variations in the cytogenetic response to X-ray exposure	51
3.2.5	RBE values for the induction of aberrations in metaphases and G_2 -PCC cells	51
3.3	Integration analysis	53
3.3.1	Fraction of lymphocytes completing first mitosis	53
3.3.2	Total amount of chromosome damage in the initial cell population	54
3.4	Distribution of chromosome aberrations	56
3.4.1	Distribution of aberrations among first cycle metaphases after exposure to low LET radiation	56
3.4.2	Distribution of aberrations among first cycle metaphases after exposure to high LET particles	58
3.4.3	Distribution of aberrations among first cycle G_2 -PCCs	58
3.4.4	Verification of the theoretical fit to the experimental data	60
3.4.5	Parameter λ derived from aberration analysis at early and late sampling time	61

3.4.6	LET dependence of the value of parameter μ	63
3.4.7	Fit of the convoluted Poisson-Neyman statistics to the experimental data	64
3.5	Radiation-induced apoptosis	66
3.5.1	Analysis of the effects of sampling time, dose, LET and inter-experimental variations in proliferating lymphocytes	67
3.5.2	Time-course of apoptosis in non-proliferating lymphocytes	69
4	Discussion	71
4.1	Biological effects of high LET radiation: importance for cancer therapy and manned space explorations	71
4.2	Cytogenetic analysis for radiation risk assessment	72
4.2.1	Metaphase analysis at single versus multiple sampling times	72
4.2.2	RBE estimates based on metaphase data	73
4.3	Application of new methods for a more reliable biodosimetry	74
4.3.1	Integration analysis	74
4.3.2	Chromosome aberration measurement in G_2 -PCCs	76
4.4	Factors that may confound the yield of radiation-induced chromosome damage	77
4.4.1	Radiation-induced cell cycle effects	77
4.4.2	Spectrum of aberrations	78
4.4.3	Radiation-induced apoptosis	80
4.4.4	Inter-experimental variations	82
4.5	Insights into radiation quality gained by the distribution of aberrations among cells	83
4.5.1	Overdispersion of the frequency distribution in lymphocytes irradiated with high-LET particles	83
4.5.2	Analysis of data by Neyman and Poisson-Neyman statistics fit to experimental distributions	85
5	Summary	87
A	Tables	89
B	Abbreviated terms	107
C	List of materials, products and laboratory equipments	109
C.1	Materials	109
C.1.1	Chemicals	109
C.1.2	Test kits	110
C.1.3	Solutions and buffers	110
C.2	Disposable products	111

Contents

C.3 Laboratory equipments	111
Bibliography	124

List of Figures

1.1	Energy spectrum of H, He, C and Fe ions in the GCR	2
1.2	Comparison of the depth dose profile of photons with carbon ions .	4
1.3	Energy loss of particles as a function of energy	5
1.4	C-ion track structure in nanometer resolution	6
1.5	Local dose distributions for C-, Cr- and Fe-ions	7
1.6	Microscopic dose distribution of X-rays or different ions	8
1.7	Dose dependence of RBE for the induction of chromosome aberrations	9
1.8	LET dependence of RBE of C-ions	10
1.9	Schematic diagram of radiation induced DNA damages	11
1.10	Standard eucaryotic cell cycle stages and checkpoints	12
1.11	Giemsa-stained and FISH-painted human chromosomes	14
1.12	Human cells at anaphase with bridged chromosomes	15
2.1	Flow diagram illustrating the experiments	24
2.2	Mitotic cells in first, second or later cycles after BrdU-incorporation	25
2.3	Schematic diagram of aberration types at metaphase	26
2.4	Prematurely condensed chromosomes in different cell cycle stages .	28
2.5	BrdU positive- and negative-lymphocytes stained with modified FPG-technique	29
2.6	Normal and typical apoptotic lymphocyte stained with fluorescent dye	30
2.7	Theoretical distributions of aberrations per cell	34
3.1	BrdU-labeling index as a function of time	40
3.2	Fraction of BrdU-labeled lymphocytes 72 h after exposure to X-rays or heavy ions.	41
3.3	Mitotic indices after exposure to X-rays or Fe-ions	42
3.4	The fraction of first cycle G_2 and metaphase cells after exposure to X-rays or Fe-ions	43
3.5	The frequencies of aberrant cells and the aberration yields in first metaphases exposed to X-rays or particles	45
3.6	The frequencies of aberrant cells and the aberration yields in first metaphases exposed to Cr-ions	46
3.7	The chromosome aberration spectrum as a function of LET	47

3.8	The frequencies of aberrant cells and the yields of excess fragments in first G_2 -PCC cells exposed to X-rays or particles	49
3.9	The frequencies of aberrant cells and aberration yields in first G_2 PCC cells exposed to Cr-ions	50
3.10	RBE as a function of LET	52
3.11	Corrected mitotic indices and reconstructed growth curves for lymphocytes exposed to Fe-ions or X-rays	53
3.12	Fraction of cells completing first mitosis after X-ray or particle exposure.	54
3.13	Total number of aberrant cells and aberrations after X-ray or particle exposure	55
3.14	Distributions of chromosome aberrations induced by X-rays or C-ions	57
3.15	Distributions of chromosome aberrations induced by Fe-ions	59
3.16	Determination of the λ according to the fit by Neyman statistics for aberration distributions in metaphases	62
3.17	Determination of the λ according to the fit by Neyman statistics for aberration distributions in G_2 -PCCs	63
3.18	$\Delta\lambda/\Delta t$ as a function of particle fluences	64
3.19	LET dependence of the parameter μ	65
3.20	Time-response of apoptosis in lymphocytes after X-ray or particle exposure	66
3.21	Dose-response of apoptotic in lymphocytes after exposure to X-rays or particles	67
3.22	Time-averaged apoptotic index among independent experiments	68
3.23	Time-response of apoptosis in non-proliferating lymphocytes exposed to X-rays or C-ions	69
4.1	RBE values derived from total aberrations and dicentrics	79
4.2	Microscopic dose and event distribution of X-rays or C-ions with different energies	84

List of Tables

2.1	Energies and LETs of the applied ion beams	22
2.2	Information of the applied doses, the fluences, the number of particle hits per nucleus and the track radii	23
A.1	Effects of X-ray irradiation on the frequency of chromosome aberrations in first cycle metaphases	90
A.2	Effects of 90 MeV/u C-ion irradiation on the frequency of chromosome aberrations in first cycle metaphases	91
A.2	Continued	92
A.3	Effects of 990 MeV/u Fe-ion irradiation on the frequency of chromosome aberrations in first cycle metaphases	93
A.4	Effects of 177 MeV/u Fe-ion irradiation on the frequency of chromosome aberrations in first cycle metaphases	94
A.4	Continued	95
A.5	Effects of 4.1 MeV/u Cr-ion irradiation on the frequency of chromosome aberrations in first cycle metaphases	96
A.6	Effects of X-ray irradiation on the frequency of excess fragments in first cycle G_2 -PCCs	97
A.7	Effects of 90 MeV/u C-ion irradiation on the frequency of excess fragments in first cycle G_2 -PCCs	98
A.8	Effects of 990 MeV/u Fe-ion irradiation on the frequency of excess fragments in first cycle G_2 -PCCs	99
A.9	Effects of 177 MeV/u Fe-ion irradiation on the frequency of excess fragments in first cycle G_2 -PCCs	100
A.10	Effects of 4.1 MeV/u Cr-ion irradiation on the frequency of excess fragments in first cycle G_2 -PCCs	101
A.11	Analysis of the frequency distributions of aberrations in first cycle metaphases produced by X-rays and 90 MeV/u C-ions	102
A.12	Analysis of the frequency distributions of aberrations in first cycle metaphases produced by 990 MeV/u Fe-ions, 177 MeV/u Fe-ions and 4.1 MeV/u Cr-ions	103
A.13	Analysis of the frequency distributions of aberrations in first cycle G_2 -PCCs produced by X-rays and 90 MeV/u C-ions	104

A.14 Analysis of the frequency distributions of aberrations in first cycle G_2 -PCCs produced by 990 MeV/u Fe-ions, 177 MeV/u Fe-ions and 4.1 MeV/u Cr-ions	105
---	-----

Chapter 1

Introduction

1.1 High LET radiation exposure to humans

On Earth, humans are exposed to ionizing radiations such as natural background radiations or man-made radiation sources used for example for medical applications. High linear energy transfer (LET) radiation exposure in environment originates mainly from radon (α -particles). Radon accumulates in enclosed areas such as underground mines or residences (National Research Council, 1999). Another high LET source are neutrons which are produced by the interactions of space radiation with the atmosphere. Humans are exposed to neutrons during air-flights (Lewis et al., 2001). Furthermore, neutrons are generated by atomic bombing (Roesch, 1987; Cullings and Fujita, 2003) or accidents at nuclear facilities (Tanaka, 2001).

In addition, an increasing number of cancer patients is treated with charged particles due to the advantages of the dose-depth profile (fig. 1.2) and their greater biological effectiveness compared to photons (fig. 1.7 and 1.8). The first clinical trial started in 1954 at Berkeley (USA) using protons. Later, Helium and heavier particles were also applied. When the facility was closed in 1992 a total of 2500 patients had been treated (Sisterson, 2005). At present, 23 proton therapy centers are in operation and more than 43000 patients have been exposed (Sisterson, 2005). Radiotherapy with heavier particles, i.e. carbon ions (C-ions), is performed at three facilities at Chiba (Japan) since 1994, at Darmstadt (Germany) since 1997 and at Hyogo (Japan) since 2002 and more than 2000 cancer patients received this new technique (Sisterson, 2005). Based on the successes of hadron therapy (e.g. Tsujii et al., 2004; Schulz-Ertner et al., 2004), several new facilities all over the world are planned or are already approved (Amaldi and Kraft, 2005; PTCOG, 2006).

High LET exposure has also to be considered for planning manned space missions. The major radiation source in space is galactic cosmic radiation (GCR) and solar particle events (SPE). GCR is composed of about 85 % protons, 12 % helium ions, 1 % heavier ions and 2 % electrons and positrons (Simpson, 1983). The energy spectrum of GCR has a maximum around 10^2 MeV/u followed by a steep decay with increasing energies (fig 1.1). SPE consist of high energy 90-95 % protons, 5-10 % helium ions and 0.1 % heavier ions emanated from the Sun. They are sporadic

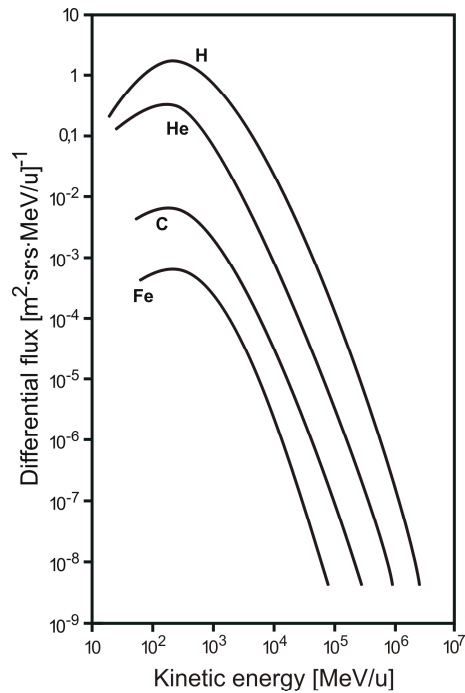


Figure 1.1: Energy spectrum of H, He, C and Fe ions in the galactic cosmic rays (GCR) measured at Earth, adapted from Simpson (1983).

and unpredictable and can double the annual estimated dose of GCR (NASA, 1997, and references therein).

Although much is known about the composition of radiation environment of outer space, there is a lack of data on the biological effects of dose, dose-rate and high LET radiations (Schimmerling et al., 2003). In particular Fe-ions are of concern because of their relative dose contribution (Space Studies Board, 1996). As a result large uncertainties exist with regard to the health risk posed to astronauts. For example, the current uncertainties in cancer risk for long-term space missions are estimated as 400-600 % (Cucinotta et al., 2001).

To contribute to this issue, the genetic consequences of Fe-ions and Fe-ion like particles with differing LET were examined in detail in the present study (table 2.1). Furthermore, the effects of C-ions which have to be known for both, space research (fig. 1.1) and heavy ion therapy were investigated. In the following the physics of charged particles (section 1.2), their biological effects (section 1.3) and methods that allow to estimate the risk associated with particle exposure (section 1.4) are described.

1.2 Physics of charged particles

In radiation physics, biology and therapy the absorbed dose in units of Gray (1 Gy=1 J/kg) is defined as the energy deposited per unit mass (ICRU, 1970). When a thin target is irradiated by a parallel beam of particles, the absorbed dose is given as

$$D[Gy] = 1.602 \times 10^{-9} \times \frac{dE}{dx} \left[\frac{keV}{\mu m} \right] \times F[cm^{-2}] \times \frac{1}{\rho} \left[\frac{cm^3}{g} \right] \quad (1.1)$$

where F is the particle fluence (i.e. the number of particles traversing per unit area) and ρ is the target mass density. $\frac{dE}{dx}$ is the energy loss, equivalent to LET when all energy transfer processes are included (ICRU, 1970).

1.2.1 Macroscopic characteristics of charged particles

Both, photons and charged particles (protons or heavier ions) produce damages to biological systems via emission of secondary electrons when penetrating matter. However, the spatial energy deposition of charged particles is different from that of photons on a macroscopic and also a microscopic scale. Recent overviews are given by Kraft (2000); Scholz (2003).

Differences on macroscopic scale are shown in fig. 1.2. For lower energy photons the stochastic interactions with matter by photoelectric, Compton or pair-production processes yield an exponential decay of absorbed dose with penetration depth (e.g. 120 keV X-rays in fig. 1.2). With increasing photon energy, the maximum dose is shifted to deeper depth, since forwardly scattered Compton electrons are transported further into the material. In contrast, heavy charged particles like C-ions have an inverted depth-dose relationship: the energy deposition of particles increases with penetration depth and reaches a maximum at a certain range. This depth-dose profile results from the dependence of the energy loss on the particle energy.

Within the range of therapeutically relevant energies (10^2 to 10^3 MeV/u) the process of energy loss is dominated by electronic collisions as described by the Bethe-Bloch formula (Bethe, 1930; Bloch, 1933):

$$\frac{dE}{dx} = \frac{4\pi e^4 Z_{eff}^2 Z N}{m_e v^2} \ln \frac{2m_e v^2}{I} + \text{relativistic terms} \quad (1.2)$$

with the energy loss per length $\frac{dE}{dx}$, the electron charge e and mass m_e , the projectile velocity v , the target atomic number Z , the electron density of the target N , and the average excitation energy I of the target. The effective ion charge Z_{eff} is empirically approximated as following:

$$Z_{eff} = Z[1 - \exp(-125\beta Z^{-\frac{2}{3}})] \quad (1.3)$$

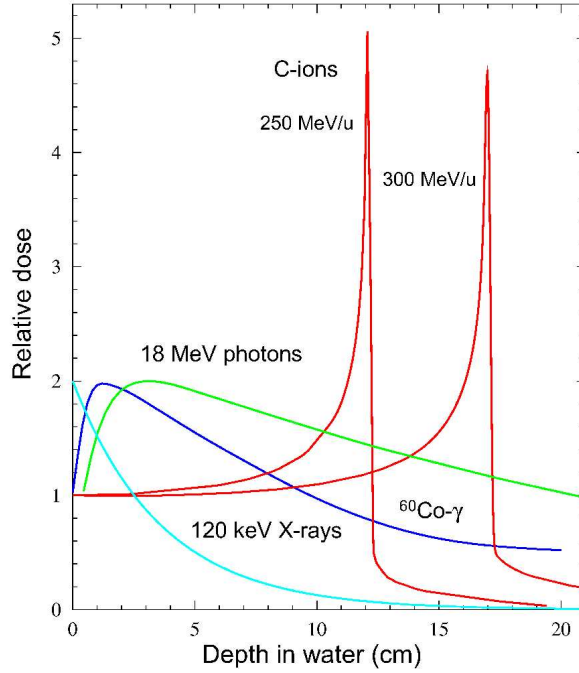


Figure 1.2: Comparison of the depth dose profile of X-rays, bremsstrahlung and ^{60}Co γ -rays with carbon ions of 250 and 300 MeV/u. For photons the maximum dose is shifted to deeper depth with increasing energy and the dose decreases exponentially. For carbon ions the maximum dose is deposited at the end of the track (Bragg peak) depending on the initial energy. The dose sharply drops off after the Bragg peak (Courtesy U. Weber).

with $\beta = \frac{v}{c}$ (Barkas, 1963). In the eq. 1.2 the $\frac{1}{v^2}$ term is dominating at high energies. As shown in fig. 1.3, the energy loss is comparably lower for higher energies, i.e. higher velocities. Thus, with increasing penetration depth, the velocity of the ions is reduced and the energy loss rises up to a maximum just before the end of the particle range which is called Bragg peak (fig. 1.2). The position of the Bragg peak depends on the initial particle energy. When the velocity is small enough that electrons from the target are captured by primary ions and Z_{eff} decreases, the energy loss is reduced (eq. 1.2). The small fraction of dose deposition after the Bragg peak is due to the nuclear interaction of the projectiles with the target atoms, causing fragmentation of primary ions into lighter particles. These lighter particles further travel in a forward direction and deposit energy at deeper depth, (e.g. Schall et al., 1996; Sihver et al., 1998).

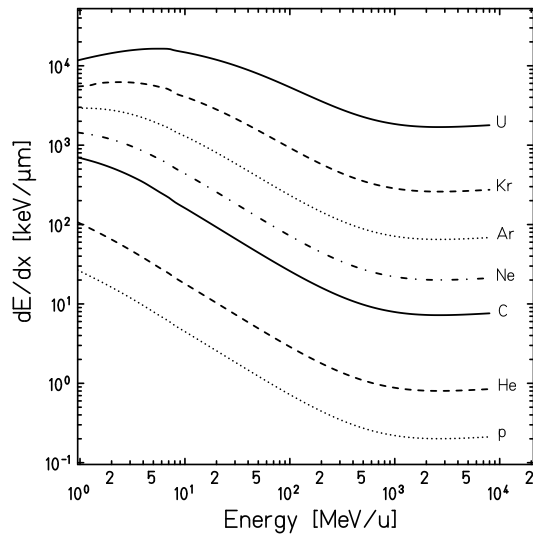


Figure 1.3: Energy loss of different particles as a function of energy. The energy loss is lower at higher energy. Data were taken from Heinrich et al. (1991).

1.2.2 Microscopic characteristics of charged particles

Also, on a microscopic scale, the local energy deposition of charged particles is different from photons. Secondary electrons produced by the energy deposition of photons are randomly distributed within the target. In contrast, charged particles produce secondary electrons (i.e. δ -electrons) localized along the track of a particle. In fig. 1.4, simulations of δ -electron emission by C-ions at different energies in water are shown (Krämer and Kraft, 1994). Water has been used in the simulation since the density of biological tissue is assumed to be equivalent to that of water. Furthermore, fig. 1.4 is displayed at the scale of deoxyribonucleic acid (DNA) molecules, which are the main target of the radiation effect and are located in the cell nucleus (Munro, 1970). With decreasing particle energy, more electron tracks are produced along the trajectory of a primary ion that cause higher numbers of locally multiply damaged sites (clustered damages) within the DNA (overview in Nikjoo et al., 1999). The effect of radiation on biological systems is described in more detail in section 1.3.2.

The radial energy dose distribution within a particle track can be described in terms of the average dose deposition $D(r)$ as a function of distance r from the track center, i.e. $D(r) \propto \frac{1}{r^2}$. The maximum radial range of δ -electrons R_{max} increases with the energy of the primary particle and can be described by a power law (Kiefer and Straaten, 1986):

$$R_{max} = 0.05 \cdot E^{1.7} \quad (1.4)$$

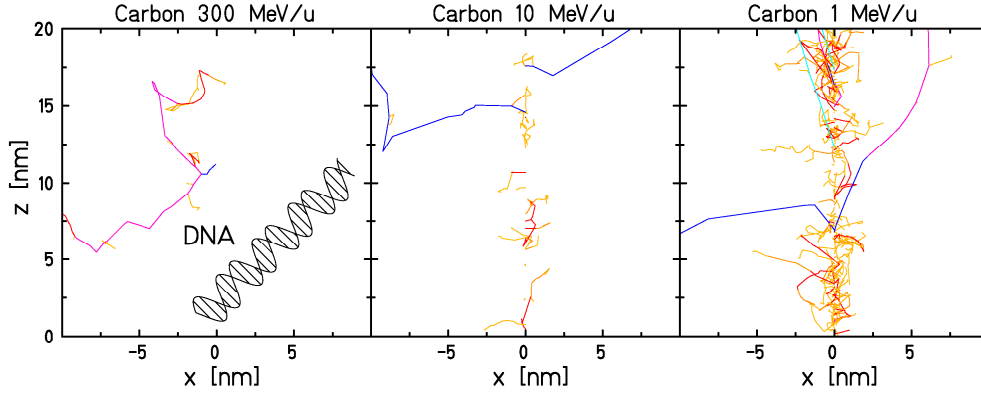


Figure 1.4: Track structure of C-ions at different energies in nanometer resolution compared to a schematic representation of a DNA molecule. A primary ion is injected at the zero position ($x = 0$) in vertical direction. The emission and transport of δ -electrons by a carbon ion are simulated using the Monte-Carlo model explained in detail in Krämer and Kraft (1994) (Courtesy M. Krämer).

where R_{max} is measured in μm and E is the specific energy of the ion in MeV/u . Exemplarily in fig. 1.5 the radial dose distributions of 90 MeV/u C-ions, 990 MeV/u and 177 MeV/u Fe-ions and 4.1 MeV/u Cr-ions are shown, which were examined in the present study. When the biological effects of particle radiation are studied, the microscopic dose deposition at the scale of the cell nucleus are important. For human lymphocytes, that are routinely used for radiation risk assessment, the nuclear cross sectional area is about $25 \mu\text{m}^2$ (Anderson et al., 2000), i.e. their radius is $\sim 3 \mu\text{m}$. Consequently, a particle fluence of $4 \times 10^6 \text{ ions/cm}^2$ leads to a mean number of one direct particle hit per nucleus of human lymphocytes. According to Poisson statistics, 37 % of the nuclei receive no direct hit, while 37 % are hit once, 18 % are hit twice and 8 % are hit three times or more. As can be inferred from fig. 1.5, in the case of Cr-ions the track radius is comparable to that of the cell nucleus, while for the other ions studied the track radii are much larger than that of the biological target. Thus, when human lymphocytes are exposed to 90 MeV/u C-ions, 990 or 177 MeV/u Fe-ions, individual tracks overlap and lead to decreasing heterogeneity of the microscopic dose deposition (e.g. fig. 1.6a-c). Similarly, an increase in particle fluences contributes to an increase in the homogeneity of dose deposition (e.g. fig. 1.6a). For photons, on the other hand, the absorbed dose is homogeneous for the dimensions of a cell nucleus since independent electron tracks are produced within the target (fig. 1.6e).

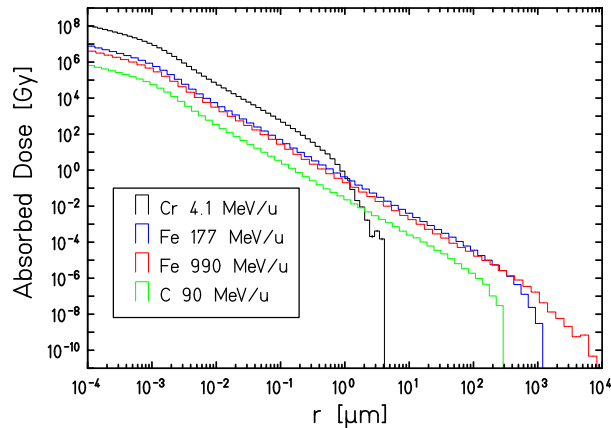


Figure 1.5: Local dose distributions for 4.1 MeV/u chrome (Cr), 90 MeV/u carbon (C) and 177 and 990 MeV/u iron (Fe) ions which were investigated in the present study. Locally absorbed dose is plotted along the trajectory of ions, where r is the distance from the track center. The simulation using the Monte-carlo method is explained in Krämer and Kraft (1994) (Courtesy M. Krämer).

1.3 Biological effects of ionizing radiation

The effectiveness of charged particles is described in terms of the Relative Biological Effectiveness (RBE). In the following section the definition of RBE is given and several biological effects of charged particles are described.

1.3.1 Relative biological effectiveness (RBE) and its characteristics

Numerous studies have shown that the induction of biological effects induced by high and low LET radiation are different due to the difference in spatial energy deposition of radiation. To compare the effectiveness of different radiation qualities, i.e. LET, the RBE has been introduced (ICRU, 1986). RBE of ion is defined as the ratio of photon dose (D_{photon}) and ion dose (D_{ion}) producing the same biological effect:

$$RBE = \frac{D_{photon}}{D_{ion}} \quad (1.5)$$

The general trend is that the RBE increases with LET up to a maximum followed by a decrease. The maximum value depends on particle types as reviewed by Kraft (1997). Furthermore, RBE values depend on the the absorbed dose, the cell type and the biological endpoints. For example, fig. 1.7 shows the dose-response curves for the induction of chromosome aberrations in mammalian cells following

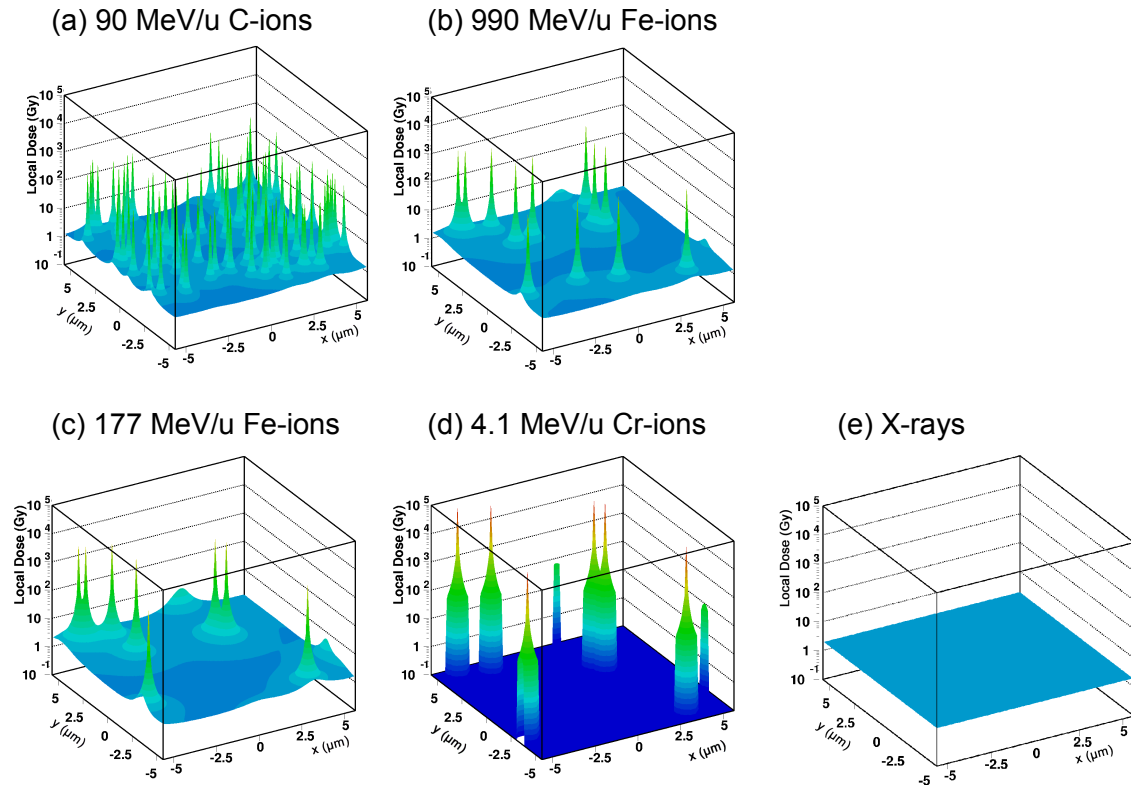


Figure 1.6: Microscopic dose distribution of X-rays or different ions investigated in the present study. For the simulation, broadening of the initial energy deposition through radical (e.g. $H\cdot$, $OH\cdot$) diffusion is taken into account (Brons et al., 2003) and leads to the reduction of the maximum dose deposition in the track center. (a) 2 Gy of 90 MeV/u C-ions (43×10^6 ions/cm²), (b) 2.3 Gy of 990 MeV/u Fe-ions (9×10^6 ions/cm²), (c) 2 Gy of 177 MeV/u Fe-ions (3.7×10^6 ions/cm²), (d) 20.3 Gy of 4.1 MeV/u Cr-ions (4×10^6 ions/cm²) (e) 2 Gy of X-rays (Courtesy M. Scholz)

particle exposure. As indicated by arrows, for lower doses and consequently low aberration yields the RBE is higher than that derived for higher doses and higher aberration yields. In fig. 1.8, the effect of the genetic background of the cells studied on the RBE is shown: Following C-ion exposure a RBE maximum around 150 keV/ μ m was measured for repair-proficient Chinese hamster cells (CHO), while no RBE maximum was detected when repair-deficient xrs5 Chinese hamster cells were examined (Weyrather et al., 1999).

1.3.2 DNA damage and repair

As mentioned above, the biological effects of radiation result basically from damage to DNA as shown in an early study by Munro (1970). DNA, which contain the

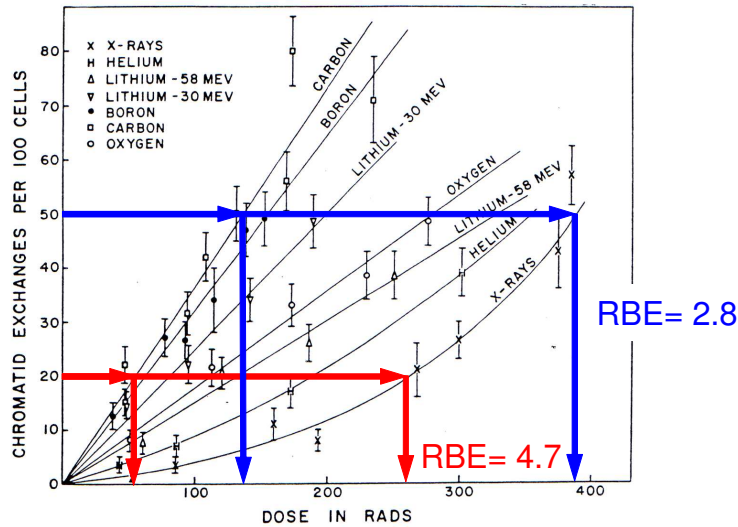


Figure 1.7: Dose dependence of RBE for the induction of chromosome aberrations. The RBE of C-ions for the induction of 0.2 and 0.5 chromatid exchanges per cell. Data are taken from Skarsgard et al. (1967).

genetic information, is a helical polymer composed of two strands. Each strand consists of four types of subunits (nucleotides) which are composed of sugar, phosphate and four different bases: A (adenine), T (thymine), G (guanine) and C (cytosine). The two DNA strands are held together by complementary base pairs between A and T and between G and C and form a double helix. DNA molecules are associated with proteins and folded into a compact structure. The DNA in eucaryotes such as mammals is located in the nucleus and separated from the surrounding cytoplasm by the nuclear envelope. A typical human cell contains about 3×10^9 nucleotide pairs of DNA (Alberts et al., 1994).

Ionizing radiation induces several types of DNA damages such as single- and double-strand breaks (SSBs and DSBs, respectively), base damages and DNA-protein cross links (fig. 1.9). Among these, DSBs are regarded as the most important lesion determining the fate of the injured cell, since non-repaired or misrepaired DSBs can give rise to chromosome aberrations, mutations or cell transformation.

Both, experimental data and modelling studies suggest that the quality of lesions changes as LET increases. This effect is related to the spatial distribution of ionizations, i.e. in the case of low LET radiation ionizations are randomly distributed, while after high LET exposure ionizations occur in a correlated manner (see fig. 1.6). Owing to the high local energy deposition in a particle track clustered damages are produced (e.g. Nikjoo et al., 1999), comprising one or more DSBs as well as associated SSBs, base damages and cross links within about ten base pairs (overview in Jenner et al., 2001). Because of the complexity, such clusters are

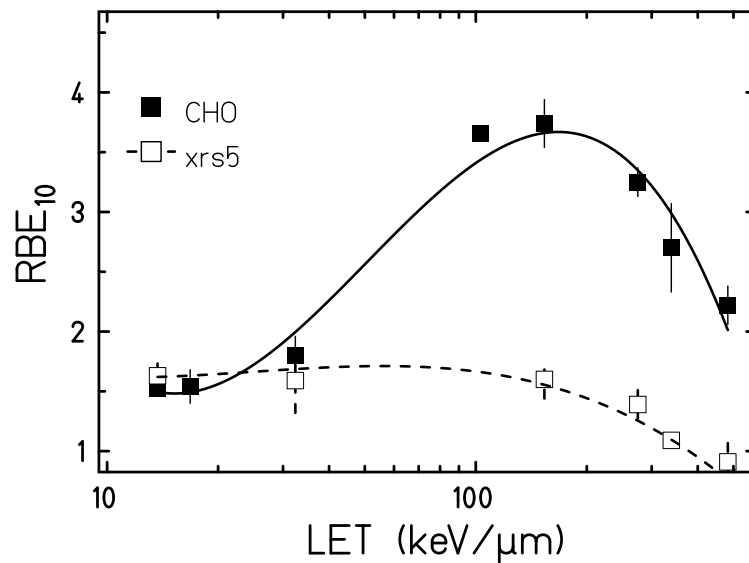


Figure 1.8: LET dependence of RBE of C-ions measured in repair-proficient (CHO) and repair-deficient (xrs5) cell lines. RBE was determined at a survival level of 10 %. Data are taken from Weyrather et al. (1999).

less repairable than sparsely distributed single damages (Ward, 1994; Goodhead, 1994). By an immunofluorescence-staining of proteins involved in the DNA damage response, localized DNA damages along particle tracks have been visualized in individual cells. In contrast, after X-ray exposure DNA damages were distributed over the whole nucleus (Jakob et al., 2000).

Accordingly, DNA-rejoining studies showed that after high LET exposure a significant fraction of DSBs remained unrejoined confirming that the DSBs produced by high LET radiation are more complex than those induced by X-rays or γ -rays (Rydberg et al., 1994; Heilmann et al., 1996). Moreover, when an assay was applied that allows to distinguish between the joining of correct and incorrect DNA ends, it was shown that the yields of misrejoined DSBs are significantly higher after particle exposure than after X-ray irradiation (Rydberg et al., 2005). Similarly, on chromosomal level marked differences in the aberration spectrum were found. For example, the fraction of chromosome and chromatid breaks increased with LET, while the proportion of dicentrics decreased (Durante et al., 1992; Nasonova et al., 1998; Ritter et al., 2002b). In addition, recent studies applying fluorescence *in situ* hybridization (FISH) for chromosome staining (see section 1.3.4) revealed that a greater proportion of complex exchanges is produced by high LET radiation compared to low LET exposure (Anderson et al., 2000; Durante et al., 2002). This

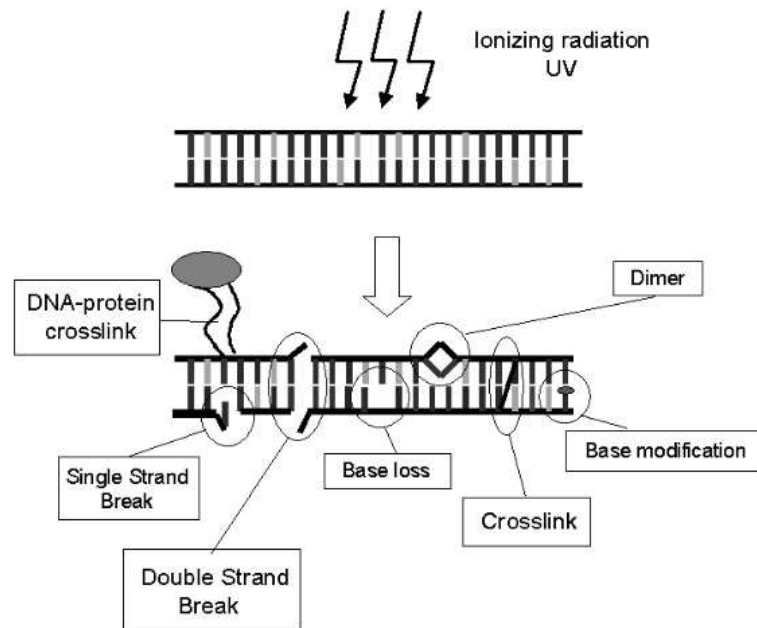


Figure 1.9: Schematic diagram of radiation induced DNA damages. To simplify the diagram, DNA double helix is drawn as a flat and ladder-like structure (Courtesy M. Scholz).

aberration-type arises from three or more breaks in two or more chromosomes. The fate of aberrations visible at mitosis are described in detail in section 1.3.4.

1.3.3 Cell cycle and checkpoints and apoptosis

The cell cycle is the sequence of events between mitotic cell divisions of eucaryotic cells. As shown in fig. 1.10, the cycle is divided into four phases, G_1 (G standing for gap), S (DNA synthesis), G_2 and M (mitosis). The interval between the completion of mitosis and the beginning of DNA synthesis is called G_1 -phase. During G_1 -phase, cells grow and monitor their environment to take a decisive step for DNA replication. During S-phase DNA is replicated and at the end of S-phase each chromosome consists of two identical chromatids joined together at a region called centromere. The interval between the end of DNA synthesis and the onset of mitosis is called G_2 -phase. The G_2 -phase provides a safety gap, to ensure that DNA replication is complete and to monitor the cell growth and the environment before cell division. During mitosis, chromosomes become shorter and condensed and the spindle microtubules attach to the centromere to ensure that the sister-chromatids are equally divided between the daughter cells. Finally, two daughter cells are formed, which will enter a new cell cycle. Certain cell types such as human

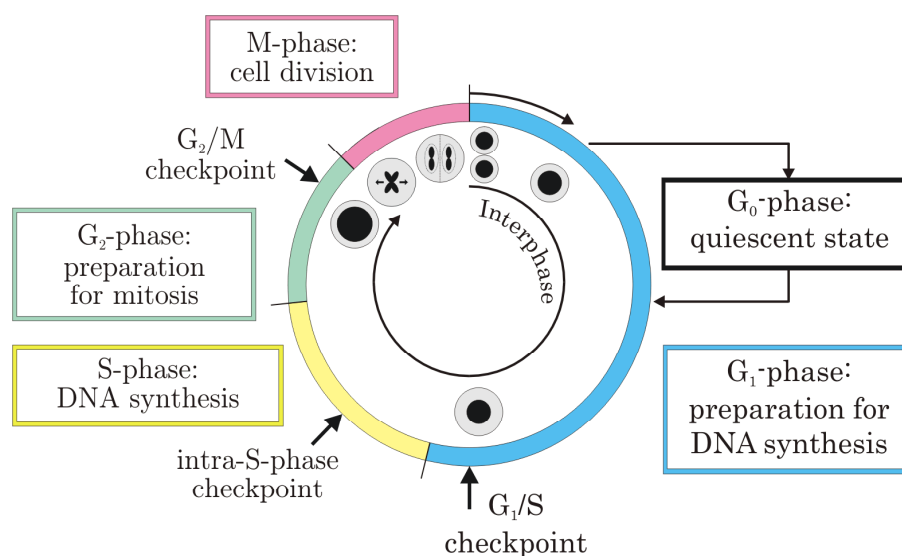


Figure 1.10: Standard eucaryotic cell cycle stages and checkpoints adapted from Alberts et al. (1994) and Sancar et al. (2004). The cell cycle is divided into four successive phases, G_1 , S (DNA synthesis), G_2 and M (mitosis). Certain cell types leave the cell cycle and enter a resting state called G_0 . The cell cycle is controlled by three main checkpoints: G_1/S , intra-S-phase and G_2/M checkpoint.

peripheral blood lymphocytes, which have been used in the present study, are not cycling. They are in a resting stage called G_0 -phase.

When cells progress from one cell cycle stage to another, the integrity of the DNA is examined at specific points, called checkpoints (reviewed by Sancar et al., 2004). There are three main checkpoints, i.e. G_1/S checkpoint, intra-S-phase checkpoint and G_2/M checkpoint as shown in fig. 1.10. The checkpoints employ sensor proteins to detect DNA damages as well as complex signal transduction pathways to inhibit the cell cycle progression. The arrest is thought to provide additional time for the repair of lesion and the extent of this effect depends on the genetic background of the cells as reviewed by Fournier and Taucher-Scholz (2004). In particular, after heavy ion exposure pronounced cell cycle delays were observed (Collyn-d’Hooghe et al., 1981; Scholz et al., 1994; Ritter et al., 1996) and extended genetic studies with Chinese hamster cells and human fibroblasts confirmed that the cell cycle delays are related to aberration burden of cells (e.g. Ritter et al., 2000, 2002b; Gudowska-Nowak et al., 2005). However, for human lymphocytes, usually used to estimate the radiation risk of humans (see section 1.4.1), little is known on the relationship between cell cycle progression delay and aberration yield (George et al., 2001; Ritter et al., 2002a; Nasonova and Ritter, 2004).

When cellular damage cannot be properly repaired, checkpoint signaling may result in the activation of pathways leading to programmed cell death called apop-

tosis (Pietenpol and Stewart, 2002). Cells undergoing apoptosis show characteristic morphological features such as chromatin aggregation, nuclear and cytoplasmic condensation and partition (e.g. see fig. 2.6, Kerr et al., 1972). Nuclear changes have been linked to endonuclease activation (Wyllie, 1980). The general hypothesis is that the apoptotic process removes damaged cells from the cell population and thus, minimizes the transmission of damage to daughter cells and reduces the risk of cell transformation and tumorigenesis. In other cell systems such as normal fibroblasts checkpoint signaling results in an accelerated aging of cells to prevent the transmission of genetic changes to further cell generations (Fournier et al., 2001).

For human lymphocytes, frequently used for radiation risk assessment, DNA damage-induced apoptosis is the typical response after exposure to ionizing radiation. Yet, little is known up to now on the LET-dependence of this effect. Moreover, a recent study indicates that the proliferative status of lymphocytes influences their sensitivity to radiation-induced apoptosis, i.e. stimulation was found to rescue cells from apoptosis (Carloni et al., 2001). This aspect is important, because apoptosis has been generally examined in G_0 -phase lymphocytes (Meijer et al., 1998, and references therein), but cycling cells are used in most radiobiological studies (section 1.4). To improve the knowledge on the relationship between apoptosis and the expression of cytogenetic changes, in the present study both endpoints were investigated in lymphocytes under the same experimental conditions.

1.3.4 Chromosome aberrations and their fate

Normal human cell contains 46 chromosomes consisting of 22 pairs of autosomes and one pair of sex chromosomes: XX in the female and XY in the male (fig. 1.11). After exposure to physical agents including ionizing radiation as well as chemicals DNA damage is induced. These damages can be either repaired, misrepaired to form an exchange-type aberration or remain unrepaired. Generally, aberrations are investigated in mitotic cells by an optical microscope.

Chromosome aberrations can be classified in several ways. When aberrations are induced in G_0/G_1 -phase cells that consist of a single chromatid, they are also replicated during S-phase giving rise to "chromosome-type" aberrations involving both chromatids at identical positions. In contrast, when damages are induced in S- or G_2 -phase cells containing replicated DNA, each chromatid acts independently. In this case, aberrations seen at metaphase affect only one of the two chromatids of a chromosome and are referred to as "chromatid-type" aberrations.

Another classification scheme is based on the number of breaks involved and the interaction of broken chromatids. If unrepaired (or misrepaired), a single break results in an acentric fragment (fig. 2.3, csb). If two breaks occur on separate arms of a single chromosome, misrepair can give rise to a centric ring accompanied by a fragment (fig. 2.3, r). In contrast, two breaks within one arm usually generate a shortened chromosome and an acentric ring (fig. 2.3, dmin). Two breaks in different

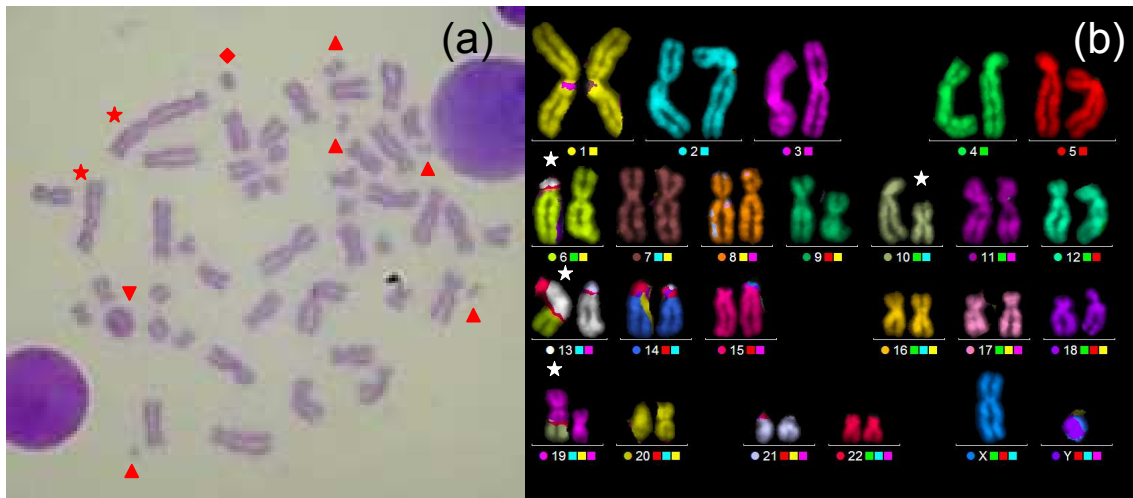


Figure 1.11: Giemsa-stained and FISH-painted human chromosomes as viewed at metaphase, consist of a pair of identical chromatids. (a) Original chromosome spread stained with Giemsa. The metaphase cell contains two dicentric (stars), a centric ring (reversed triangle), an acentric ring (diamond) and five acentric fragments (triangles). (b) Chromosomes painted with FISH probes which allow to identify each chromosome pair. Chromosomes are arranged according to the length and the position of the centromere. The cell contains a chromosome exchanges between chromosome 6 and 13 and an exchange between chromosome 10 and 19 as indicated by white stars (Courtesy S. Sommer).

chromosomes can result in the formation of a dicentric chromosome plus an acentric fragment (fig. 2.3, dic) or a reciprocal exchange (fig. 2.3, lower right) is produced.

Due to mechanical reasons chromosome aberrations are modified or lost during subsequent cell divisions. For example, acentric fragments which lack the attachment region for the spindle microtubules are unable to move with the sister chromatids to the daughter cells and thus are rapidly eliminated from the cell population. Similarly, the number of dicentric and ring chromosomes declines rapidly during subsequent divisions, since most dicentrics and ring chromosomes form anaphase bridges during mitosis (fig. 1.12). As acentric fragments, bridged chromosomes are often not included in the daughter nuclei and are lost. Generally, the loss of chromosomes results in cell death. Completely rejoined symmetrical aberrations such as reciprocal translocations do not result in mechanical problems at division and thus, will be transmitted to further cell generations. Therefore, this group has been referred to as "stable aberrations", while the former group has been termed "unstable aberrations". Stable aberrations have been found in many tumors and are implicated in cell transformation and carcinogenesis.

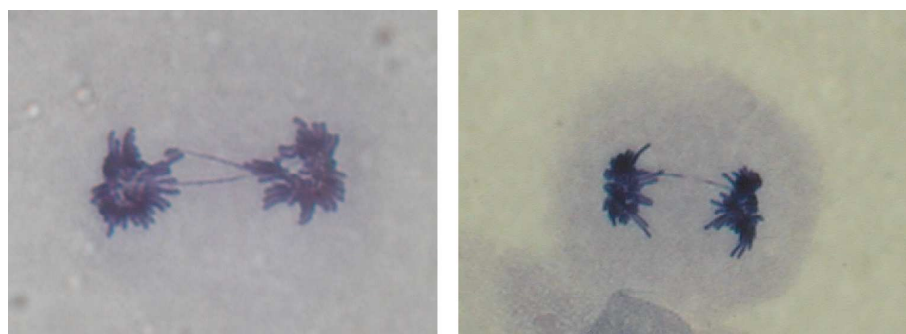


Figure 1.12: Human cells at anaphase. Left: two chromosome bridges, right: one broken bridge (Courtesy E. Nasonova).

The aberration types that can be detected depend on the applied chromosome staining technique. Originally, solid staining was applied, that allows the detection of unstable aberrations and some stable aberrations, i.e. translocations with an extraordinary long chromosome arm (fig. 2.3). However, by advanced staining techniques such as fluorescence *in situ* hybridization (FISH) stable (fig. 1.11b) and unstable aberrations can be visualized (Pinkel et al., 1986; Durante et al., 1998) .

1.4 Chromosome aberration analysis for biological dosimetry

Biological dosimetry of radiation-exposed people is usually applied when physical dosimetry is unavailable or has to be confirmed (e.g. Sasaki et al., 2001; Hayata et al., 2001). Today, several methods are available for biodosimetry. These include the analysis of dicentrics and/or translocations in metaphase cells or in prematurely condensed interphase cells and the micronucleus assay (IAEA, 2001).

Generally, to estimate the dose, a venipuncture blood sample is taken as soon as possible after the exposure and the whole blood or separated lymphocytes are cultured *in vitro*. Lymphocytes are chosen, because they can be easily obtained and remain in the body for a long time in a non-dividing state. Lymphocytes consist of two main types, which have different immunological functions, namely T cells and B cells. Among these T-cells represent the majority (~70-80 %) and are therefore examined for cytogenetic damage.

1.4.1 Analysis of structural aberrations in metaphase cells

The analysis of structural aberrations in lymphocytes at mitosis is regarded as the most sensitive method which can detect aberrations following exposure to ≥ 0.05 Gy

sparsely or densely ionizing radiation (Cornforth and Goodwin, 1991; Bauchinger, 1995; Edwards, 1997, and references therein). For the first time, biological dosimetry was performed in the mid 1960s by Bender and Gooch (1966) based on the yield of dicentric chromosomes. Since that time the technique was refined and a standard protocol was developed that has been applied for accidental exposures as well as for radiobiological *in vitro* studies (last update in IAEA, 2001).

According to the recommended protocol lymphocytes are cultivated *in vitro* for 48 h since at that time a high number of cells reaches first mitosis. Peripheral blood lymphocytes are resting in G_0 -phase (see section 1.3.3). Therefore, they have to be stimulated by a mitogen to enter the cell cycle. In most studies phytohemagglutinin (PHA) is used that primarily activates T-lymphocytes. Prior to fixation, a spindle inhibitor (colchicine or colcemid) is added to the samples to accumulate metaphase cells. Then, chromosome spreads are prepared and aberrations are scored in first generation metaphases, because the aberration yield declines during subsequent cell divisions.

To estimate the dose to which an individual has been exposed, the measured aberration yields are compared to a calibration curve, which has been generated by the exposure of blood cells *in vitro*. To reduce statistical uncertainty, calibration curves should be based on about 10 doses in the range 0.25-5 Gy (IAEA, 2001).

Till now, one important aberration-type for radiation risk assessment is the dicentric chromosome (e.g. Di Giorgio et al., 2004). The analysis of dicentrics is regarded as the most reliable cytogenetic endpoint for biological dosimetry, because dicentrics are easily scorable and the control level is low (IAEA, 2001). However, dicentrics are eliminated over time from the peripheral blood pool and this effect is directly correlated with the life time of lymphocytes. In contrast to dicentrics, translocations, that are detectable by FISH, are considered to be stable. They are therefore more suitable for the detection of old or long-term exposures than the dicentric assay. Since information on the persistence of translocations is still limited, the application of translocation frequencies to biological dosimetry is currently validated.

1.4.2 Confounding factors for biological dosimetry

During recent years evidence is accumulating that several factors may influence the observed aberration yield. One important factor is the inter-laboratory difference in aberration scoring. For example, a recent intercomparison study of 13 laboratories revealed up to three-fold differences in the dicentric yields (Roy et al., 2004). To reduce the uncertainty of dose estimation arising from differences in aberration analysis between laboratories, IAEA (2001) recommends that any laboratory establishes its own calibration curve. Further confounding factors are the variation in radiation sensitivity among different donors (inter-individual differences) or within the same donor (intra-individual differences). Great inter-individual variability has,

for example, been reported for patients overexposed to ionizing radiation resulting in a lack of correlation between accident dose and the frequency of aberrations (Wojcik et al., 2003). Also, a significant variation of radiosensitivity within the same donor was observed when samples were taken on different occasions (e.g. Vral et al., 2004; Kakati et al., 1986).

Furthermore, evidence is accumulating that the standard metaphase assay is not reliable in the case of high LET exposure. Heavy charged particles produce pronounced cell cycle delays (Collyn-d'Hooghe et al., 1981; Scholz et al., 1994; Ritter et al., 1996) and experiments with V79 Chinese hamster cells and human fibroblasts performed during the last 15 years at GSI have shown that these delays are related to aberration burden of cells, i.e. cells reaching mitosis at later times carry more aberrations than those arriving at mitosis at earlier times (Ritter et al., 2000, 2002b; Gudowska-Nowak et al., 2005). In contrast, after photon irradiation which has a minor influence on the cell cycle transition time, a constant aberration yield or a slight increase in the number of aberrations with time was observed (Ritter et al., 1996; Nasonova et al., 1998). For human lymphocytes, usually used to estimate the radiation risk of humans, little is known on the relationship between particle induced cell cycle progression delay and aberration yield. Generally, the standard method for aberration analysis (IAEA, 2001) is applied, which does not account for cell cycle delays, since lymphocytes are only collected at one sampling time post-irradiation as described in section 1.4.1. Therefore, it can be expected that the efficiency of high LET particles for the induction of cytogenetic damage is systematically underestimated, because heavily damaged and delayed cells are excluded from the analysis.

1.4.3 Analysis of chromosome aberrations in interphase cells

To overcome the problems resulting from the selective delay of heavily damaged cells, the analysis of aberrations in interphase cells by means of the premature chromosome condensation (PCC) technique has been proposed (Pantelias and Maillie, 1984; Durante et al., 1997, 1998; Kanda et al., 1999). Originally, PCC was induced in G_0 -phase lymphocytes by the fusion with mitotic cells (Pantelias and Maillie, 1984). However, the PCC-fusion method has several drawbacks: the procedure is technically difficult and the PCC index is usually much lower than the mitotic index (Durante et al., 1998). More recently, a simpler PCC-method has been developed using inhibitors of type A and type 2A serine/threonine protein phosphatases such as okadaic acid or calyculin A (Gotoh et al., 1995; Coco-Martin and Begg, 1997). This method results in a much higher frequency of scorable cells than the fusion-technique and is therefore suitable for high overexposures which are accompanied by a rapid fall in peripheral white blood cell counts like the criticality accident at Tokai-mura (Hayata et al., 2001).

However, okadaic acid or calyculin A induce PCC only in proliferating cells. Therefore, lymphocytes have to be stimulated first. For the analysis of cytogenetic damage PCC-cells are usually harvested 48-50 h after exposure and aberrations are analyzed in G_2 or G_2/M cells to account for the delay of heavily damaged cells (Durante et al., 2002; Ritter et al., 2002a; George et al., 2003; Nasonova and Ritter, 2004). As expected, these studies showed that the PCC-analysis results in higher RBE values than the standard metaphase assay.

In order to examine, to what extent the PCC-assay accounts for the delay of heavily damaged cells, aberrations were measured in first cycle G_2 -PCCs collected at different sampling times after exposure and the aberration yields were compared to that measured in metaphase samples.

1.5 Objective of the study

Detailed information on the biological effects of heavy ions are needed for both, the application of particle beams in tumor therapy and for the planning of manned missions to the moon or Mars. Since a few years carbon ion radiotherapy is applied in Japan and Germany. However, due to the short follow-up, little is known on late effects from radiation such as the induction of secondary tumors or fibrosis. Similarly, there is only limited experience on the health risks of a prolonged exposure to space radiation and the current uncertainties in risk estimates are >400 % as described in section 1.1.

Chromosome aberrations are an important biomarker of cancer risk and are used since the mid 1960s for biological dosimetry. In general, aberration yields are measured in human lymphocytes, because they can be easily obtained by venipuncture. For cytogenetic analysis, cells are harvested at a single early time-point, i.e. 48 h after initiation of the culture, based on the assumption that the sample reflects the damage induced within the whole cell population. However, extended time-course studies performed previously in our group with Chinese hamster cells and human fibroblasts showed, that this assay is not reliable in the case of high LET exposure.

Heavy charged particles produce dramatic cell cycle delays and these delays are correlated with the number of aberrations carried by a cell. Consequently, currently available RBE values underestimate the cytogenetic effects of high LET radiation. To overcome the problems resulting from the delay of heavily damaged cells the use of alternative cytogenetic approaches have been recently proposed: one is the integration analysis based on a multiple fixation regime together with a mathematical analysis; the other assay is based on the aberration analysis in G_2 -cells collected 48 h post-irradiation by means of chemically induced premature chromosome condensation (G_2 -PCC assay). However, with respect to the latter technique, it has not been experimentally demonstrated that indeed all aberrant cells arrive at the first G_2 -phase by 48 h. Thus, the validity of the G_2 -PCC assay is still ques-

tionable. Furthermore, there is evidence that besides cell cycle delays several other factors may affect the aberration yield observable in human lymphocytes at mitosis. These include radiation-induced apoptosis and inter- and intra-donor variations in radiosensitivity.

To address these problems, a complex set of endpoints was investigated in human lymphocytes after exposure to X-rays, carbon, iron and iron-like ions over a broad range of LET values. To account for cell cycle delays, lymphocytes were collected at several sampling times up to 84 h post-irradiation and the effect of sampling time on the RBE in metaphase and G_2 -phase cells was studied in detail. Additionally, the frequency distributions of chromosome aberrations among cells were analyzed to gain insights into track structure effects. Furthermore, special emphasis was placed to minimize experiment-to-experiment variability. To account for inter-individual difference in the radiation response, for all experiments lymphocytes of the same donor were used.

Chapter 2

Materials and methods

2.1 Cell culture and irradiation

2.1.1 Isolation of lymphocytes

For all experiments peripheral blood lymphocytes were obtained from a female donor (non-smoking). The age at the donations was 42 to 44 years. Lymphocytes were isolated from whole blood and cultured as described in detail by Durante et al. (1998) with minor modification. Briefly, eight ml of whole blood were collected in a isolation tube for blood cells (Vacutainer CPT). The sample was centrifuged at 1600 g (2900 rpm) for 20 min, and the layer of mononuclear cells and platelets was collected by a pipette and transferred to 10 ml centrifuge tube. RPMI 1640 medium was added up to 8 ml and the sample was centrifuged at 390 g (1500 rpm) for 10 min. After the removal of the supernatant, the cell pellet was resuspended at a density of 6×10^6 cells/ml medium RPMI 1640 supplemented with 20 % fetal calf serum, 2 mM L-glutamine, 100 U/ml penicillin, 100 μ g/ml streptomycin and 5 IE/ml sodium heparin (complete medium). Cells were kept in a culture flask in an incubator at 37 °C in a 5 % CO₂ humidified atmosphere until radiation exposure.

2.1.2 Irradiation procedure

Lymphocytes were exposed to heavy charged particles or X-rays at room temperature (RT). The beam characteristics, such as the primary energy, the average energy in the sample, the LET value and the residual range were calculated by the computer code ATIMA (ATIMA, 2006) developed at GSI and are shown in table 2.1. ATIMA calculates various physical quantities of protons and heavy ions in matter for specific kinetic energies between 1 keV/u and 500 GeV/u. The calculation for a primary particle energy above 30 MeV/u is based on the theory of Lindhard and Sorensen (1996) and includes the following corrections: the shell corrections, a Barkas term and the Fermi-density effect (Scheidenberger and Geissel, 1998, and references therein). Below 10 MeV/u an older version of Ziegler's SRIM program is used (Ziegler et al., 1985). In the intermediate energy range the value is interpolated between the two calculations.

Particle type	E_{prim} (MeV/u)	E_{av} (MeV/u)	LET_{av} (keV/ μ m)	Residual range (mm)
C-ions ¹	100	89.1 \pm 2.4	28.9 \pm 0.6	19.0
Fe-ions ¹	1000	989 \pm 2.5	155 \pm 0.1	258.5
Fe-ions ¹	200	177 \pm 6.0	335 \pm 7.5	16.2
Cr-ions ²	11.4	4.1 \pm 0.45	3161 \pm 121	0.07

Table 2.1: Energies and LETs of the applied ion beams. Irradiation was performed at either SIS¹ or UNILAC² at GSI. E_{prim} is the primary energy of the particles delivered by the accelerator. E_{av} is the average energy value in the sample and LET_{av} is the corresponding LET value. Residual range is the range of particles in water.

Exposure to 90 MeV/u C-ions, 177 MeV/u Fe-ions or 990 MeV/u Fe-ions was performed at the heavy ion synchrotron SIS at GSI (Darmstadt) with the intensity controlled raster scanning technique as described in detail elsewhere (Haberer et al., 1993). Twenty min before the exposure, cells were resuspended at a maximum density of 6×10^6 cells/ml and transferred to the irradiation holder. The holder consists of polyethylene (height: 8 cm, width: 3.5 cm) with a 2 mm thick well for the sample and 1 mm plastic (CR39) between the cells and the beam.

Low energy Cr-ion irradiation was performed at the UNILAC facility (GSI). A detailed description of the irradiation procedure and dosimetry is given elsewhere Kraft et al. (1980). For the exposure 10μ l cell suspension at a density of 9×10^7 /ml was sandwiched between a polycarbonate foil (thickness: 14 μ m, diameter: 29 mm) and a 35 mm petri dish resulting in a liquid layer thickness of about 15 μ m. After irradiation cells were washed off from the foil and the Petri dish with complete medium. The whole process did not exceed 40 min to prevent cell death because of the reduction of oxygen concentration and evaporation of the culture medium.

For comparison X-irradiation was performed with a Seifert X-ray machine (Ahrensberg, Germany) operated at 250 kV and 16 mA with a 1 mm Al and a 1 mm Cu filter at a dose rate of ~ 1 Gy/min. In a detailed X-ray study (e.g. see fig. 3.5, a) lymphocytes were irradiated in a cell culture flasks with dose of 0.3 to 4 Gy. To obtain information on experimental variations in the radiation response, in parallel to a particle experiment cells were irradiated with 2 Gy X-rays using the same experimental set up (i.e. irradiation holder) as for the particle exposure. This datum point was referred to as internal reference.

For the particle experiments, the applied doses, the fluences, the track radii and the mean number of hits per nucleus are summarized in table 2.2. The relationship between dose and fluence was derived from eq. 1.1. The track radius was calculated by eq. 1.4. The mean geometrical cross-section of a lymphocyte cell nucleus is about $25 \mu\text{m}^2$ (Anderson et al., 2000). Therefore, particle fluence of 4×10^6 / cm^2 results in a mean number of one particle traversal per cell nucleus. Accordingly, 37 % of

Particle type	E_{prim} (MeV/u)	R_{max} (μm)	Dose (Gy)	Fluence (particles/ cm^2)	mean hits/nucleus
C-ions	100	104 ± 5	0.3	6.5×10^6	1.6
			0.6	13×10^6	3.2
			1.0	22×10^6	5.4
			2.0	43×10^6	10.8
			3.0	65×10^6	16.1
			4.0	86×10^6	21.5
Fe-ions	1000	6172 ± 27	1.0	4×10^6	1.0
			2.3	9×10^6	2.3
			3.0	12×10^6	3.0
Fe-ions	200	332 ± 19	0.54	1×10^6	0.25
			1.1	2×10^6	0.5
			2.2	4×10^6	1.0
			3.2	6×10^6	1.5
			4.3	8×10^6	2.0
Cr-ions	11.4	0.56 ± 0.11	5.1	1×10^6	0.25
			20.3	4×10^6	1.0
			40.5	8×10^6	2.0
			60.8	12×10^6	3.0

Table 2.2: Information of the applied doses, the fluences, the number of particle hits per nucleus and the track radii. R_{max} is the maximum radial range of energy deposition in the sample calculated by eq. 1.4. The dose was converted to fluence by eq. 1.1. For further details see table 2.1.

the population receives no hits, 37 % of the nuclei get one hit, 18 % of the nuclei receive two hits and 8 % of the nuclei get three or more hits.

2.1.3 Cell culture

After radiation exposure cells were resuspended at a concentration of $0.5 \times 10^6/\text{ml}$ in complete medium supplemented with 1 % phytohemagglutinin (PHA) to stimulate lymphocytes to traverse the cell cycle. Additionally, $6 \mu\text{g}/\text{ml}$ 5-bromo-2-deoxyuridine (BrdU) and $4.8 \mu\text{g}/\text{ml}$ deoxycytidine were added to differentiate cell generations. For each dose- and time-point studied (see fig. 2.1) 3 ml of cell suspension was seeded into a 10 ml tube. All procedures from the addition of BrdU up to the fixation of cells were performed under subdued light to avoid photolysis of BrdU. During cell culture, the cap of the tube was loosened to allow oxygen and CO_2 exchange. For the same purpose tubes were inclined in a incubator to increase the surface area of the cell culture medium.

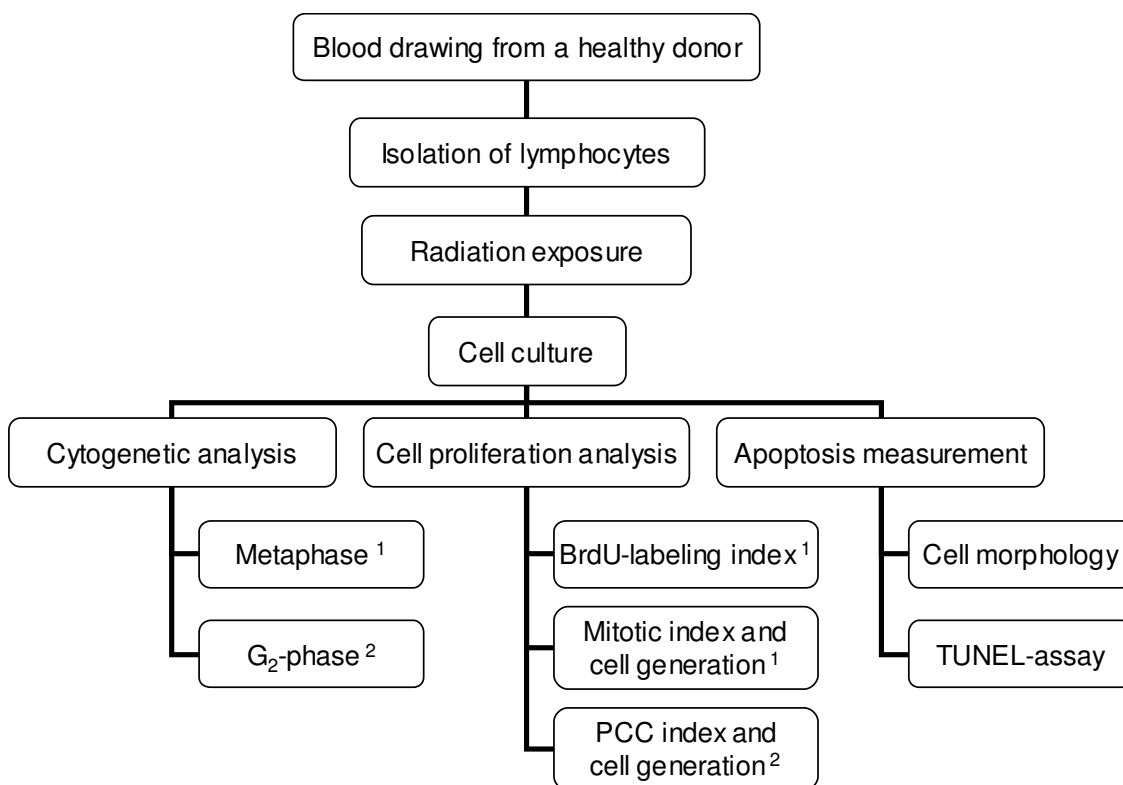


Figure 2.1: Flow diagram illustrating the experiments. After blood drawing lymphocytes were isolated, irradiated and finally seeded into 10 ml tubes for the analysis of cytogenetic damage and apoptosis. Information on cell proliferation was derived from the samples prepared for cytogenetic analysis indicated by the indices (1: metaphase sample, 2: G_2 -PCC sample).

2.2 Cytogenetic analysis

Chromosome aberrations were analyzed in both metaphase and prematurely condensed G_2 -phase cells. For metaphase analysis lymphocytes were collected between 30 and 90 h after radiation exposure. To accumulate mitotic cells 200 ng/ml colcemid was added to the samples 3 h before harvest. For G_2 -cell analysis premature chromosome condensation (PCC) was chemically induced by applying 50 nM calyculin A dissolved in ethanol for 45 min before fixation (Durante et al., 1998). PCC cells were harvested between 48 and 84 h after irradiation.

2.2.1 Cell fixation and chromosome preparation

Chromosome spreads were prepared according to standard techniques (IAEA, 2001). If not indicated, procedures were performed at RT. Samples were centrifuged

at 170 g (1000 rpm) for 6 min and the pellet was resuspended in 10 ml 75 mM KCl solution. After 10 min the samples were again centrifuged (170 g, 1000 rpm, 8 min) and the cell pellets were resuspended in freshly prepared fixative (methanol:acetic acid = 3:1). After a further centrifugation (250 g, 1200 rpm, 10 min), samples were resuspended in a small volume of fixative (e.g. 1×10^6 cells/0.1 to 0.3 ml fixative). Then, chromosome spreads were prepared, i.e. slide glasses were humidified with ultrapure water and one or two drops (18 μl /drop) of cell suspension were applied on each slide by the use of an Eppendorf pipette. Slides were air-dried and stored at RT overnight.

2.2.2 Fluorescence-plus-Giemsa staining

Fluorescence-plus-Giemsa (FPG) technique enables to differentiate between cells in the first, second and later cell cycle after BrdU-treatment. Briefly, samples were stained with the FPG-method developed by Perry and Wolff (1974) with minor modifications (Ritter et al., 1996). Slides were incubated in 10 $\mu\text{g}/\text{ml}$ Hoechst 33258 for 1 h at RT, washed in ultrapure water and air-dried. Then, about 0.3 ml of buffer (194.5 mM Na_2HPO_4 , 2.75 mM citric acid) was dropped on each slide and covered with a cover glass. Samples were irradiated for 1 h with a low-pressure UV lamp ($\lambda=360\text{-}365$ nm). Slides were washed with ultrapure water, air-dried and afterwards incubated in $2 \times \text{SSC}$ for 30 min at 55 $^\circ\text{C}$. Then, slides were washed with ultrapure water, air-dried and stored overnight. Finally, samples were stained with 3 % Giemsa in phosphate buffer (33.3 mM Na_2HPO_4 and 33.3 mM KH_2PO_4) for 10 min, dried overnight and embedded in Eukitt. Examples of metaphases stained with FPG-technique are shown in fig. 2.2. Chromosomes of first-post irradiation mitoses are uniformly darkly stained, second generation mitoses show harlequin chromosomes consisting of one dark and one light chromatid, while in subsequent

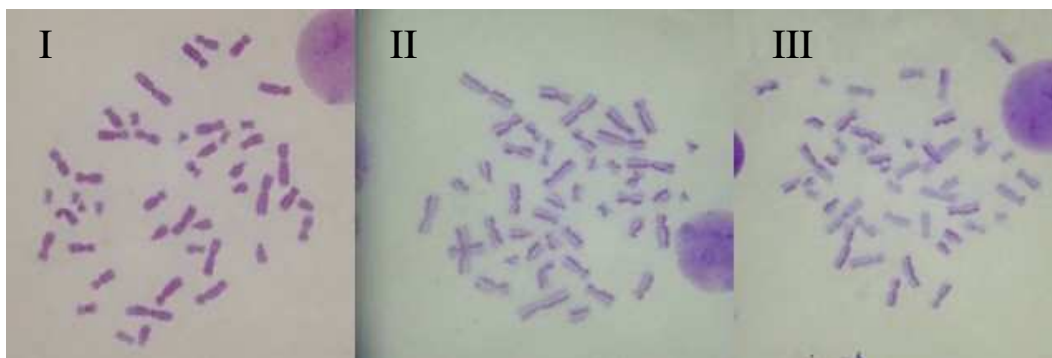


Figure 2.2: Mitotic cells in first (I), second (II) or later cycles (III) after BrdU-incorporation. Lymphocytes were stained with FPG-technique.

generations >50 % of the chromatids are stained lightly. Similarly, in G_1 and G_2 PCCs the cell cycle generation can be determined after FPG-staining.

2.2.3 Metaphase analysis

The frequencies of aberrant metaphases and aberrations were determined in lymphocytes collected between 48 and 84 h post-irradiation. At each dose- and time-point 50 to 300 first cycle metaphases were scored. Chromosome aberrations were analyzed based on the classification of Savage (1976). Examples of aberrations are shown in fig. 2.3. After Giemsa staining the following aberration types can be detected: chromatid break (ctb), chromosome acentric fragment (csb), acentric ring (dmin), dicentric (dic), centric ring (r) and chromatid exchange (cte). Chromatid exchanges include symmetrical- and asymmetrical chromatid exchanges (shown in fig 2.3), sister-unions and triradials. Furthermore, a subgroup of translocations (t) can be detected resulting in a chromosome with anomalous arm length, i.e. the abnormal arm is longer than the longest arm of chromosome 1 (see fig. 1.11b). In the

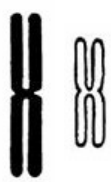







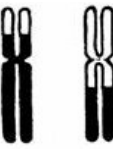
Normal	Chromatid break (ctb)	Chromosome fragment (csb)	Acentric ring (dmin)	Centric ring with fragment (r)	Translocation (t)
					
Chromatid exchange (cte)		Dicentric with fragment (dic)		Reciprocal exchange (not observable)	
					

Figure 2.3: Schematic diagram of aberration types at metaphase (Evans, 1974, modified). Abbreviated terms were used in accordance with ISCN (1978).

case of dicentric chromosomes, centric rings, triradials or sister-chromatid unions, one acentric fragment was subtracted from the number of fragments present in the cell. Polycentrics were included as dicentrics, e.g. tricentrics or quadracentrics were counted as two or three dicentrics respectively.

2.2.4 PCC analysis

PCC was chemically induced in interphase cells by applying calyculin A. Generally, in human lymphocytes calyculin A condenses chromosomes in S-, early and late G_2 -phase. G_0 and first-cycle G_1 cells are not effected probably due to the lack of maturation promoting factor (MPF) (Durante et al., 1998). However, chromatin condensation occurs in G_1 -cells of the second or later cell generations. Early G_2 -PCCs were distinguished from late G_2 -PCCs based on the degree of chromosome condensation. As shown in fig. 2.4, chromosome condensation is incomplete in early G_2 -PCC, while late G_2 -cells display fully condensed, bivalent chromatids. Late G_2 -cells were discriminated from metaphases based on the centromere structure: metaphase cells have a visible centromere region, while late G_2 -PCCs lack a visible centromere.

Aberrations were analyzed in first cycle late G_2 -phase cells (fig. 2.4c). Because of the chromosome morphology, aberrations such as dicentrics can not be detected in G_2 -PCCs. Therefore, the analysis of cytogenetic damage was restricted to the number of chromosome pieces in excess of 46. At each dose- and time-point aberrations were measured in 100 to 200 first-cycle late G_2 -PCC cells collected between 48 h and 84 h post-irradiation (see table A.6 to A.10).

2.3 Cell proliferation analysis

To gain information on the cell progression following radiation exposure several methods were used. Firstly, the number of mitotic cells and their cell generation were scored in metaphase samples. Secondly, the cell cycle stages and the cell generation were determined in calyculin A treated samples. Thirdly, the number of cells that entered at least S-phase were scored using the BrdU-labeling technique.

2.3.1 Mitotic and PCC indices and cell generations

The mitotic index ($MI = \text{number of mitotic cells} \div \text{total number of cells}$) was measured in samples prepared for metaphase analysis by scoring at least 2000 cells per dose- and time-point (from 30 h to 90 h post-irradiation). Similarly, the frequency of each first, second, and third cycle metaphase was determined by scoring 100-700 mitoses per sample.

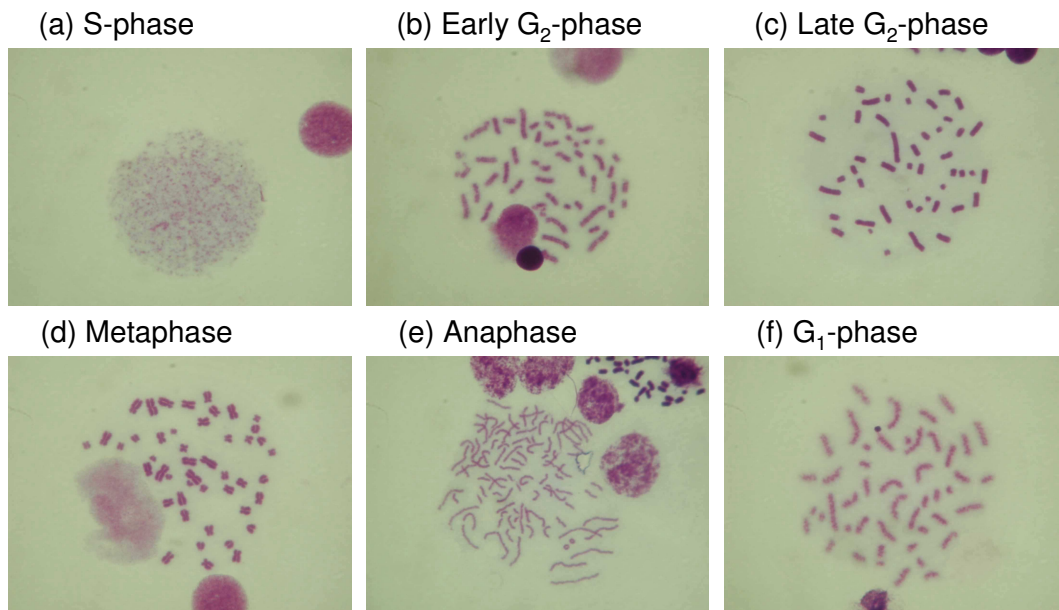


Figure 2.4: Prematurely condensed chromosomes in different cell cycle stages. Premature chromosome condensation (PCC) was induced in lymphocytes by calyculin A. DNA does not condense in G_0 and first cycle G_1 -cells but condenses in S-phase (a). The condensation is incomplete during early G_2 -phase (b). Chromosomes are fully condensed during late G_2 -phase (c) but the centromere is not detectable. Centromeres can be clearly seen in metaphase (d). In anaphase chromatids are separated (e) resulting in second cycle G_1 cells (f) with single chromatids.

In PCC samples the PCC index ($PI = \text{number of PCC cells} \div \text{total number of cells}$) was measured among 2000 cells. Samples were collected between 48 h and 84 h after irradiation. Furthermore, as shown in fig. 2.4, the cell cycle phase (G_1 , S, G_2 and M) and the cell generation was determined in calyculin treated samples by analyzing 300 to 900 PCC cells. As mentioned above, only second and third cycle G_1 -PCC are detectable, but not first cycle G_1 -phase. All S-phase cells were pooled because their morphology does not allow a clear distinction of cell generations.

2.3.2 BrdU-labeling

During S-phase BrdU is incorporated into DNA instead of thymidine and can be visualized in samples prepared for metaphase analysis (section 2.2.3). For the detection of BrdU-positive cells slides were stained with a modified FPG-technique described in detail in Nasonova et al. (2004). Briefly, after Giemsa-staining slides were immersed for 2-10 min in ultrapure water to differentiate labeled cells from non-labeled cells. Differentiation was controlled under a light microscope. BrdU-

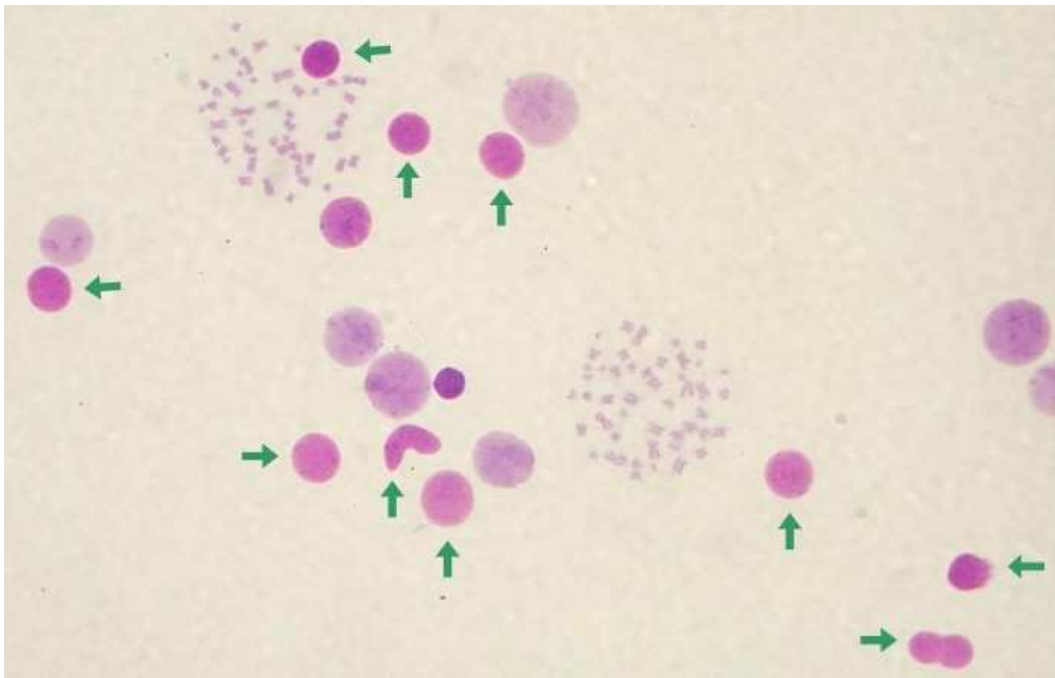


Figure 2.5: BrdU positive-lymphocytes (blue) and negative-lymphocytes (rose, indicated by green arrows) stained with modified FPG-technique.

labeled nuclei and chromosome spreads appear blue, while unlabelled nuclei are rose as shown in fig. 2.5. At each dose- and time-point about 2000 cells were scored to determine the BrdU-labeling index (number of BrdU-labeled cells \div total number of cells).

2.4 Apoptosis measurement

Cells undergoing apoptosis show characteristic morphological and biochemical features. To determine the number of apoptotic cells two methods were applied. The first assay was based on apoptosis-related morphological changes of the cell nucleus and the cell membrane after dual fluorescent staining. To verify these data, apoptosis was also determined by the TUNEL-assay (Terminal deoxynucleotidyl transferase-mediated X-deoxyuridine triphosphate nick end-labeling), which detects apoptosis-related DNA breakage.

2.4.1 Analysis of cell morphology

In parallel to the cytogenetic studies, apoptosis was measured in proliferating lymphocytes. Apoptotic cells were determined under a fluorescence microscope by the

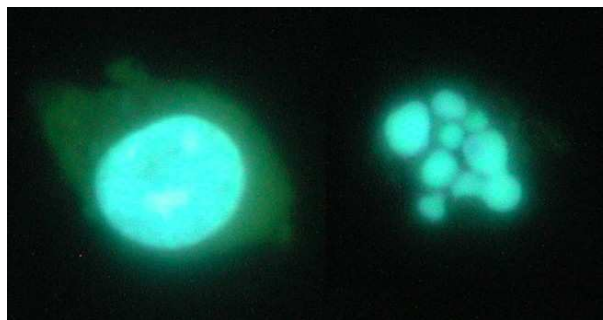


Figure 2.6: Human lymphocytes stained with Hoechst and acridine orange. A normal cell (left) and a typical apoptotic cell with a fragmented nucleus (right).

typical changes of the cell morphology such as nuclear condensation and fragmentation (apoptotic bodies) as described by Meijer et al. (1998). An example is shown in fig. 2.6. Samples were fixed with 1 % formaldehyde between 24 and 72 h post-irradiation and stained with 2 $\mu\text{g}/\text{ml}$ Hoechst 33342 to visualize the cell nucleus and 10 $\mu\text{g}/\text{ml}$ acridine orange to stain both nucleus and cytoplasm (Holgersson et al., 2003).

Since radiation induced cell death is routinely measured in non-proliferating lymphocytes, the number of apoptotic cells was additionally measured in unstimulated cells. At least 500 cells were scored for each dose- and time-point to calculate apoptotic indices.

2.4.2 TUNEL-method

One of the characteristics of apoptosis is the occurrence of DNA fragmentation caused by the activation of endonucleases. This process can be detected by enzymatic labeling of the free 3'-OH termini of the fragmented DNA with modified nucleotides (e.g. fluorescein-12-deoxyuridine triphosphate: FITC-dUTP) using terminal deoxynucleotidyl transferase (TdT). The end-labeling method is termed TUNEL (TdT-mediated X-dUTP Nick End-Labeling) assay.

The TUNEL-method was performed according to the instructions of the manufacturer (Apo-DIRECTTM in situ DNA fragmentation assay kit). Briefly, at the indicated time-points (see fig. 3.20) samples were centrifuged at 300 g (1300 rpm) for 5 min. The pellet was resuspended in 0.5 ml PBS and cells were fixed for 15 min on ice by adding 5 ml of PBS containing 1 % formaldehyde. After two washes with PBS, the pellet was resuspended in 0.5 ml of PBS. Then, 5 ml of ice-cold 70 % ethanol was added and the cells were kept on ice for at least 30 min. Samples were rinsed twice in wash buffer provided by the supplier and incubated for 1 h at 37 °C in 50 μl of the staining solution containing TdT enzyme and FITC-dUTP. Then, cells were washed twice with rinse buffer, resuspended in 0.5 ml of propid-

ium iodide (PI) containing RNase A solution and incubated in the dark for 30 min. Apoptotic cells showed FITC (green) fluorescence (emission: 500-560 nm), while PI (red) fluorescence was used to counter-stain all cell nuclei (emission: 608-652 nm). The apoptotic index was determined by the analysis of at least 1000 cells under a fluorescence microscope.

2.5 Data analysis

2.5.1 Integration analysis of chromosome aberrations

The experimental data obtained in the present study revealed that there is a drastic increase in the aberration yield with time after high LET exposure. Therefore, aberration yields can be misleading when the damages are scored at only one sampling time. In order to overcome this problem the use of multiple fixation times together with a mathematical analysis was proposed by Kaufman et al. (1974). In this study, a slightly modified approach developed by Scholz et al. (1998) was applied.

The basic idea of the method is to collect all aberrant cells passing through first mitosis in order to determine the total amount of damage induced in the initial cell population. To perform the integration analysis, samples were taken until all cells have passed the first mitosis. Since previous reports have shown a constant increase in chromosome aberration yields with time after high LET exposure (Ritter et al., 1996; Nasonova et al., 1998; Ritter et al., 2000, 2002a,b; Gudowska-Nowak et al., 2005), aberrations were analyzed at 48, 60, 72 and 84 h post-irradiation and the time-course of aberrations was interpolated between the data points. In contrast, pronounced fluctuations of the mitotic indices with times were reported by Größer (2002) who measured mitotic indices between 48 and 96 h post-irradiation. These data suggest that the interpolation of mitotic index is not appropriate. Therefore, in this study, cells were generally collected every 3 h between 30 and 90 h post-irradiation for mitotic index and cell generation analysis.

In the integration analysis, a linear interpolation is performed which results in data points over the whole sampling interval with 1 h steps. Since mitotic cells were collected by 3 h colcemid treatment (see section 2.2), the measured mitotic indices were divided by 3, thus giving the passage of cells through mitosis per hour. Furthermore, it has to be taken into account that mitotic indices for late dividing cells are underestimated due to the increase in cell number by the division of undamaged or slightly damaged cells. This can be corrected when the increase in cell number is known Scholz et al. (1998): the increase in cell number from time step $i - 1$ to time step i can be described as:

$$N_i = N_{i-1}(1 + MI_i) \quad (2.1)$$

where N_i is the number of cells and MI_i is the measured mitotic index at time i . Therefore, the total number of cells at time step k are calculated iteratively from the formula:

$$N_k = \prod_{i=1}^k N_0(1 + MI_i) \quad (2.2)$$

where N_0 represents the initial cell number. The measured mitotic indices are further corrected for the increase in cell number in order to obtain the mitotic indices with respect to the initial cell population:

$$MI_k^* = MI_k \frac{N_k}{N_0} = MI_k \prod_{i=1}^k (1 + MI_i) \quad (2.3)$$

The formula 2.3 is applied to obtain the corrected fraction of aberrant cells Φ_i^* at a given time i :

$$\Phi_i^* = f_i MI_i^* \quad (2.4)$$

where f_i is the frequency of aberrant mitosis. In the same way, the corrected flux of aberrations A_i^* through mitosis at a time i can be determined as following:

$$A_i^* = a_i MI_i^* \quad (2.5)$$

where a_i represents the number of aberrations found in a metaphase. Thus, the total fraction of aberrant cells Φ_{tot} (eq. 2.6) and the total number of aberrations A_{tot} (eq. 2.7) with respect to the initial cell population can be obtained by summing up all aberrant metaphases during the time slot until first mitosis is completed:

$$\Phi_{tot} = \sum_i \Phi_i^* \quad (2.6)$$

$$A_{tot} = \sum_i A_i^* \quad (2.7)$$

2.5.2 Comparison of theoretical distributions with experimental distributions of aberrations among cells

For X-rays the energy deposition in micrometer scale, i.e. in the dimension of a cell nucleus, is homogeneous (see fig. 1.6e). In contrast, high LET particles distribute their energy inhomogeneously (e.g. fig. 1.6a-d) with two characteristics. One is that the number of hits per nucleus is randomly distributed among the cells. The other is that the ionizations are localized along the trajectory of the primary ion. Because of the differences in energy deposition, also the distribution of chromosome aberrations among cells is expected to be different.

In the present study, the distributions of aberrations in lymphocytes exposed to different radiation qualities were investigated by means of three different stochastic distributions: a Poisson distribution, a compound Poisson-Poisson (Neyman type A) distribution (Neyman, 1939) and a convoluted Poisson-Neyman distribution. A pure Poisson distribution is expected after low LET radiation exposure, where chromosome aberrations are randomly produced due to an uniform dose distribution in a cell nucleus (fig. 1.6e). In this case, the random variable, the number of aberrations per cell, is described by the Poisson distribution:

$$P_P(k) = \frac{a^k e^{-a}}{k!} \quad (2.8)$$

where k is the number of aberrations per individual cell and a is the average number of aberrations per cell in the population. An example of frequency distributions with the different mean numbers of aberrations/cell predicted by a Poisson statistics is shown in fig. 2.7 (left panel).

On the other hand, after heavy ion exposure the distribution of aberrations reflects the microscopic inhomogeneity of energy depositions (e.g. fig. 1.6d). To describe this effect, the following two random variables are assumed to be independent and explained by a Poisson statistics: the number of particle traversals per cell nucleus and the number of aberrations induced by a particle hit. The number of particle hits per cell is given by:

$$P_\lambda(n) = \frac{\lambda^n e^{-\lambda}}{n!} \quad (2.9)$$

here, λ stands for the mean number of particle traversals through a cell nucleus. Then, the number of aberrations per cell induced by n hits is described by:

$$P_{n\mu}(m) = \frac{(n\mu)^m e^{-n\mu}}{m!} \quad (2.10)$$

where μ represents the mean number of aberrations per particle traversal through a nucleus. Thus, the distribution of aberrations can be represented by a compound Poisson (Neyman type A) statistics (Virsik and Harder, 1981):

$$P_N(k) = \sum_{n=0}^{\infty} P_{n\mu}(k) P_\lambda(n) = \sum_{n=0}^{\infty} \frac{(n\mu)^k e^{-n\mu}}{k!} \frac{\lambda^n e^{-\lambda}}{n!} = \frac{\mu^k}{k!} e^{-\lambda} \sum_{n=0}^{\infty} \frac{n^k}{n!} (e^{-\mu} \lambda)^n \quad (2.11)$$

Fig. 2.7 (middle panel) shows an example of frequency distributions predicted by Neyman statistics. The main characteristics of a Neyman distribution compared to a Poisson distribution is the higher number of non-aberrant cells and the higher frequency of cells carrying multiple aberrations. The increased fraction of non-aberrant cells can be interpreted as that part of the cell population that is not

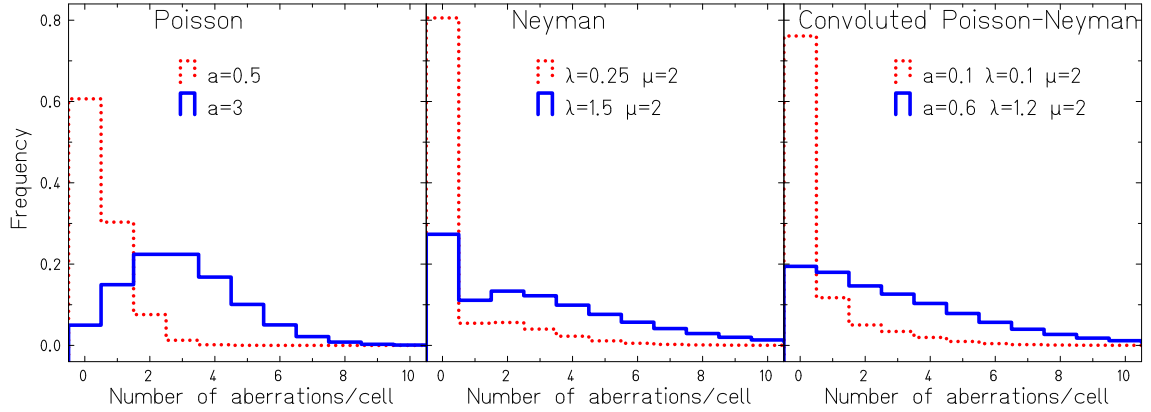


Figure 2.7: Theoretical distributions of chromosome aberrations per cell predicted by Poisson (left panel), Neyman (middle panel) and convoluted Poisson-Neyman statistics (right panel). Each distribution is fit with the given parameters indicated in the figure resulting that the average number of aberrations per cell is either 0.5 aberrations/cell (dotted red lines) or 3 aberrations/cell (blue lines).

traversed by a particle, while the elevated number of cells with multiple aberrations per cell may represent cells hit by multiple particles.

The third theoretical distribution that has been applied to the data was obtained by convoluting a Neyman distribution with an independent Poisson distribution in order to account for the radial extension of the particle tracks. For example, for an 990 MeV/u Fe-ion (see fig. 1.5 and 1.6b) the track radius ($R_{max} \approx 6200 \mu\text{m}$) is much larger than the radius of the nucleus of a lymphocyte ($\sim 3 \mu\text{m}$) and thus, several cells will be hit in the passage of a single ion. Under the applied exposure conditions particle tracks overlap contributing to a homogeneous dose distribution. As a consequence, the frequency distribution of aberrations is not appropriate described by Neyman statistics. In this case, the distribution of aberrations is characterized by two independent random variables, i.e. the number of aberrations induced by the center part of the tracks and the aberrations produced by the outer, overlapping parts of the tracks which contribute to a "photon-like" dose deposition. Consequently the distribution can be expressed as a mixture of a Neyman distribution with a Poisson distribution called the convoluted Poisson-Neyman distribution:

$$P_{N+P}(k) = \sum_{s=0}^{\infty} P_P(s)P_N(k-s) \quad (2.12)$$

As shown in fig. 2.7 (right panel) the convoluted Poisson-Neyman distributions are located between the Poisson and Neyman distributions since the distribution is convoluted by the two statistics. The comparison between the blue and the dotted

red lines in Neyman and compound Poisson-Neyman distributions shows that the shape of the frequency distribution changes significantly when the mean number of aberrations/cell increases.

For each radiation-type, the frequency distribution of the number of aberrations per metaphase (tables A.11 and A.12) or G_2 -cell (tables A.13 and A.14) measured at several dose- and time-points was fit to either Poisson, Neyman or convoluted Poisson-Neyman distribution. Fits to the experimental data were performed using the **gd** program and a fit software package available for UNIX workstation at GSI (GD, 2006). Then, the optimal parameters were chosen according to the lowest value of χ^2 which is the result of the goodness-of-fit test.

By introducing the probability generating function, the mean values and dispersions for three distributions can be calculated (e.g. see Beyer, 1968). The generating function of the random variable X is defined as

$$G(Z) = \langle Z^k \rangle = \sum_{k=0}^{\infty} P_X(k) Z^k \quad (2.13)$$

where Z is a complex variable, $P_X(k)$ is the distribution of a random variable X with $P_X(k) \geq 0$ and $\sum_{k=0}^{\infty} P_X(k) = 1$. Derivatives of $G(Z)$ evaluated at $Z = 1$ are related to the moments:

$$\frac{dG(Z)}{dZ} = G'(Z) = \sum_{k=0}^{\infty} k Z^{k-1} P_k|_{Z=1} = \langle X \rangle \quad (2.14)$$

$$\frac{d^2G(Z)}{d^2Z} = G''(Z) = \sum_{k=0}^{\infty} k(k-1) Z^{k-2} P_k|_{Z=1} = \langle X^2 \rangle - \langle X \rangle \quad (2.15)$$

The probability generating function for the Poisson distribution is obtained by eq. 2.8 and 2.13:

$$G_P(Z) = \sum_{k=0}^{\infty} P_P(k) Z^k = \sum_{k=0}^{\infty} \frac{e^{-a} a^k}{k!} Z^k = e^{-a} e^{aZ} = e^{a(Z-1)} \quad (2.16)$$

Together with eq. 2.14 and 2.16 the direct calculation of the moment gives the mean value:

$$\langle X \rangle = G'_P(Z)|_{Z=1} = a \quad (2.17)$$

where $\langle X \rangle$ corresponds to the mean number of aberrations per cell. The moment of the second order is (eq. 2.15 and 2.16):

$$\langle X^2 \rangle = G''_P(Z)|_{Z=1} + \langle X \rangle = a^2 + a \quad (2.18)$$

Here the variance σ^2 is defined as following:

$$\sigma^2 = \langle (X - \langle X \rangle)^2 \rangle = \langle X^2 \rangle - \langle X \rangle^2 \quad (2.19)$$

Then the variance and relative variance are obtained:

$$\begin{aligned}\sigma^2 &= \langle X^2 \rangle - \langle X \rangle^2 = a^2 + a - a^2 = a \\ \frac{\sigma^2}{\langle X \rangle} &= 1\end{aligned}\quad (2.20)$$

The probability generating function for the Neyman distribution is obtained by eq. 2.11 and 2.13:

$$G_N(Z) = \sum_{k=0}^{\infty} P_N(k) Z^k = \sum_{k=0}^{\infty} \sum_{n=0}^{\infty} \frac{(n\mu)^k e^{-n\mu}}{k!} \frac{\lambda^n e^{-\lambda}}{n!} Z^k = e^{\lambda[e^{\mu(Z-1)} - 1]} \quad (2.21)$$

Calculations of moments yields the following relations:

$$\langle X \rangle = G'_N(Z)|_{Z=1} = \lambda\mu \quad (2.22)$$

$$\begin{aligned}\langle X^2 \rangle &= G''_N(Z)|_{Z=1} + \langle X \rangle = \lambda^2\mu^2 + \lambda\mu^2 + \lambda\mu \\ \sigma^2 &= \langle X^2 \rangle - \langle X \rangle^2 = \lambda^2\mu^2 + \lambda\mu^2 + \lambda\mu - \lambda^2\mu^2 = \lambda\mu(1 + \mu) \\ \frac{\sigma^2}{\langle X \rangle} &= 1 + \mu\end{aligned}\quad (2.23)$$

The parameter μ can be determined from the relative dispersion $\sigma^2/\langle X \rangle$ of the measured distribution of aberrations which is generally broader than the corresponding Poisson distribution with the same mean.

The probability generating function for the convoluted Poisson-Neyman distribution is given by eq. 2.12 and 2.13:

$$G_{N+P}(Z) = G_P(Z)G_N(Z) = \exp[\lambda(e^{\mu(Z-1)} - 1) + a(Z - 1)] \quad (2.24)$$

Evaluation of moments leads to the following relations:

$$\langle X \rangle = G'_{N+P}(Z)|_{Z=1} = \lambda\mu + a \quad (2.25)$$

$$\begin{aligned}\langle X^2 \rangle &= G''_{N+P}(Z)|_{Z=1} + \langle X \rangle = (\lambda\mu + a)^2 + \lambda\mu^2 + \lambda\mu + a \\ \sigma^2 &= \langle X^2 \rangle - \langle X \rangle^2 = \lambda\mu^2 + \lambda\mu + a \\ \frac{\sigma^2}{\langle X \rangle} &= \frac{\lambda\mu^2 + \lambda\mu + a}{\lambda\mu + a} = 1 + \frac{\lambda\mu^2}{\lambda\mu + a}\end{aligned}\quad (2.26)$$

2.5.3 Error calculation and curve fitting

Errors bars on the proportions $\frac{X}{N}$ were estimated as standard deviations of a binomial distribution:

$$\Delta x = \Delta \left(\frac{X}{N} \right) = \frac{\sqrt{N \cdot x \cdot (1 - x)}}{N} \quad (2.27)$$

where x is the frequency under consideration (i.e. mitotic index, PCC index, BrdU-labeling index, apoptotic indices and the fraction of aberrant cells) and N is the total number of cells scored.

The statistical uncertainties of the chromosome aberration yields and the distribution of chromosome aberrations were calculated assuming Poisson statistics:

$$\Delta x = \sqrt{\frac{x}{N}} \quad (2.28)$$

where x is the frequency under consideration.

The dose effect curves of aberration yields in metaphase or G_2 -PCC cells were approximated by a linear-quadratic response curve:

$$y = C + \alpha D + \beta D^2 \quad (2.29)$$

where y is the aberration yield, C is an offset parameter, α is the linear coefficient and β is the dose (D) squared coefficient. Fits were determined using the **gd** program.

The error of the RBE value (eq. 1.5), ΔRBE is obtained by error propagation from the error of photon and ion doses as given by:

$$\frac{\Delta RBE}{RBE} = \sqrt{\left(\frac{\Delta D_{photon}}{D_{photon}} \right)^2 + \left(\frac{\Delta D_{ion}}{D_{ion}} \right)^2} \quad (2.30)$$

where the photon dose (D_{photon}) and the ion dose (D_{ion}) producing the same biological effect are derived from the dose response curves fit by the **gd** program. Errors of the photon dose (ΔD_{photon}) and the ion dose (ΔD_{ion}) are obtained from the confidence limits of the fit curve at one standard deviation as given by the same program.

Chapter 3

Results

3.1 Cell proliferation analysis

3.1.1 BrdU-labeling

To investigate whether lymphocytes remain in the G_0/G_1 -phase after exposure or initiate cell cycle progression and enter at least S-phase, BrdU-incorporation into DNA was measured. After irradiation with X-rays, 29 keV/ μm C-ions, 155 keV/ μm and 335 keV/ μm Fe-ions and 3160 keV/ μm Cr-ions, BrdU was added to the cultures as described in section 2.3.2. At different time-points cells were fixed, slides were prepared and BrdU-positive cells were differentiated from BrdU-negative cells by the modified FPG-technique (fig. 2.5).

3.1.1.1 Radiation-induced cell cycle delay

Measurement of the labeling indices at several sampling times after exposure to X-ray or particles revealed a dose-dependent delay in the progression of the cells to S-phase. As an example, in fig. 3.1 (left panel) the BrdU labeling curves for cells exposed to 335 keV/ μm Fe-ions at two doses or X-rays are shown. Both exposures were performed in parallel. In control cultures BrdU-positive cells started to appear around 30 h after PHA stimulation. When lymphocytes were exposed to radiation, a delayed entry into S-phase was observed. For cells exposed to 4.3 Gy 335 keV/ μm Fe-ions a delay of about 10 h was measured. Furthermore, in control cultures the number of labeled lymphocytes increased steadily with time and saturated around 70 h. A similar effect was observed in irradiated cultures, but for increasing doses lower maximum BrdU-labeling indices were reached and when a comparable dose was applied, the saturation level was higher after X-ray irradiation compared to Fe-ion exposure (fig. 3.1, left panel). The saturation effect was confirmed by other experiments measured up to 90 h (data not shown). If the low labeling indices observed in irradiated cultures result from the inability of cells to initiate cell cycle progression, a pronounced cell cycle progression delay or death of BrdU-positive cells remains to be elucidated.

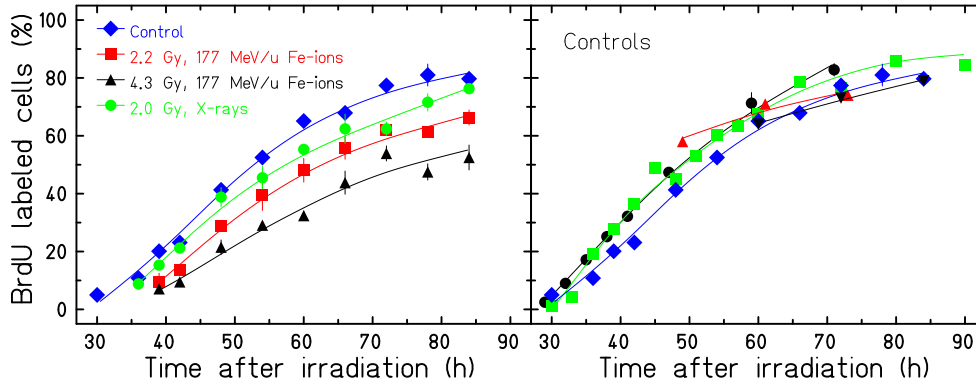


Figure 3.1: BrdU-labeling index as a function of time after stimulation. Left panel: Effect of 177 MeV/u Fe-ion (LET=335 keV/ μ m) and X-ray exposure. Both irradiations were done in parallel. Right panel: BrdU-labeling index measured in control samples. Data result from 5 experiments as indicated by different symbols. Control data in the left panel are also included in the right panel (blue diamond). Error bars are standard deviation of 3 measurements on the same slide and were in average 7 %.

Furthermore, as shown in fig. 3.1 (right panel) a comparison of the labeling index curves (five experiments) demonstrated small inter-experimental variations in the cell cycle progression, although for all experiments blood samples were taken from the same donor. For example, the time to reach an index of 70 % ranged from 60 to 68 h after initiation of the culture. The variation between experiments is also visible in the time-course of the mitotic index (section 3.1.2) and in the fraction of first G_2 -cells as mentioned in section 3.1.3.

3.1.1.2 LET dependence of the labeling index

To investigate the effect of different radiation qualities on cell proliferation, labeling indices measured at 72 h were normalized to the control level and compared. The indices for cultures exposed to comparable doses of X-rays and particles with $LET \leq 335$ keV/ μ m were similar as shown in fig.3.2 (left panel), i.e. the RBE is about one for this LET range. In contrast, isodoses of low energy Cr-ions (LET=3160 keV/ μ m) were less effective resulting in a RBE \sim 0.4 (data not shown). However, when similar particle fluences are compared, it is evident that a traversal of a high LET particle through a cell nucleus affects the cell cycle progression more than a hit by a low LET particle (see fig.3.2, right panel). For example, after exposure to 4×10^6 particles/ cm^2 corresponding to a mean number of one particle hit per a cell nucleus, the labeling indices were 0.96, 0.8 and 0.67 in samples irradiated with 990 MeV/u Fe-ions (LET=155 keV/ μ m), 177 MeV/u Fe-ions (LET=335 keV/ μ m) and 4.1 MeV/u Cr-ions (LET=3160 keV/ μ m), respectively.

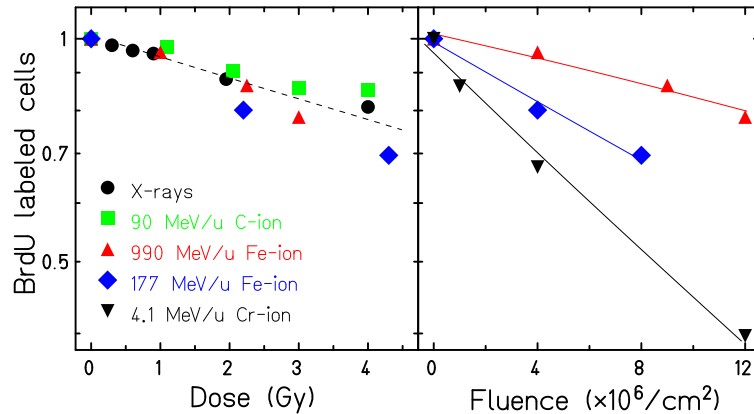


Figure 3.2: Fraction of BrdU-labeled lymphocytes 72 h after exposure to X-rays, 90 MeV/u C-ions (29 keV/ μm), 990 MeV/u Fe-ions (155 keV/ μm), 177 MeV/u Fe-ions (LET=335 keV/ μm) or 4.1 MeV/u Cr-ions (3160 keV/ μm). Data were normalized to the control level. The indices were plotted as a function of dose (left) or particle fluence (right). A particle fluence of $4 \times 10^6 / \text{cm}^2$ corresponds to one direct hit per cell nucleus.

3.1.2 The mitotic index

Additional information on the cell cycle progression was obtained by the determination of the mitotic index on slides prepared for cytogenetic analysis. Lymphocytes were fixed between 30 to 90 h after exposure to X-rays or ions. Each sampling time was preceded by a 3 h colcemid treatment to accumulate mitotic cells. Then, the number of metaphases was scored from the whole cell population. Additionally, the cell generation of mitotic cells was determined. Tables A.1 to A.5 show the results for selected sampling times.

Investigation of the mitotic index revealed a delayed entry of lymphocytes into metaphase and a depression of the mitotic activity after irradiation. Exemplary, the time-course of the mitotic index measured in cultures exposed to 335 keV/ μm Fe-ion or X-rays is plotted in fig. 3.3 (left panel). In control samples, mitotic cells appeared around 36 h after stimulation. At 45 h the mitotic index was about 2 % and thereafter the values fluctuated in the range of 3.5 to 6 %. Similarly, after exposure to ionizing radiation, the mitotic indices fluctuated. This kinetics is typical for human lymphocytes (e.g. Größer, 2002). However, irradiated cells entered mitosis at later times and the mitotic indices were generally lower than in control cultures.

Since the FPG-staining technique was used, a detailed analysis of the time-course of first generation metaphases, that are most relevant for radiation risk assessment (see section 1.4.1), can be performed. When the frequencies of first cycle metaphases are plotted as shown in fig. 3.3 (right panel), again a radiation-induced mitotic delay is observable. Additionally, it is evident that with increasing dose and

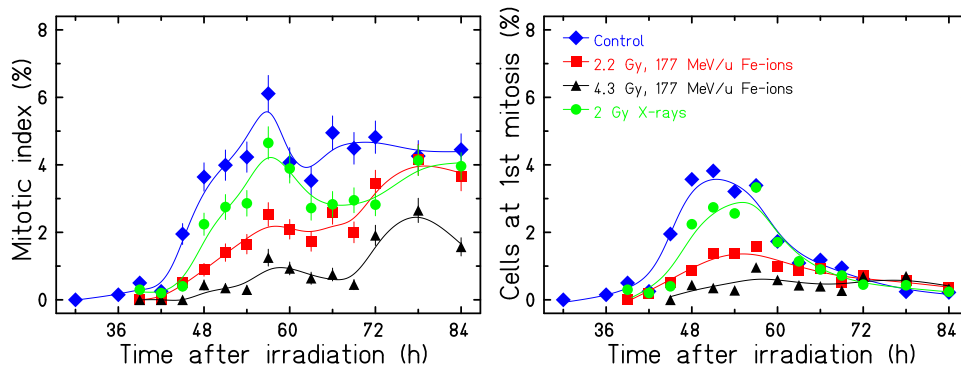


Figure 3.3: The mitotic index (left panel) and the frequency of cells at first mitosis (right panel) as a function of time after exposure to 177 MeV/u Fe-ions (335 keV/ μm) or 2 Gy X-rays. Both irradiations were performed in parallel. The indices were derived from samples treated with colcemid to accumulate mitotic cells. Lines are drawn to guide the eye. Error bars in the left panel were obtained by eq. 2.27.

LET cells were less capable to proceed to the first mitosis, i.e. the peak index of first cycle mitosis and the area under the curve decreased. For example, in control sample the index peaked at 3.8 %, after exposure to 2 Gy X-rays the peak index was 3.3 % and in samples exposed to higher LET, 2.2 Gy 335 keV/ μm Fe-ions the peak decreased 1.6 %. Following 4.3 Gy Fe-ion exposure, the indices did not exceed 1 % and a maximum was not detectable.

Accordingly, cell generation analysis revealed a dose-dependent progression delay to the second or later cycle metaphase. At 72 h after stimulation, in the control 13 % of metaphases belonged to the first cycle, while in samples exposed to 2 Gy X-rays 16 % were first cycle metaphases. For lymphocyte cultures exposed to 2.2 and 4.3 Gy 335 keV/ μm Fe-ions this value changed to 21 and 36 %, respectively (see tables. A.4 and A.3).

Furthermore, in three experiments cultures were analyzed at multiple subsequent time intervals (tables A.1, A.2, A.4 and fig. 3.3, left panel). When the mitotic indices of control samples were compared, a similar time-course was observed. However, the mitotic activity, reflected in the height of the mitotic index, varied between experiments. For example, at a given sampling time the mitotic indices differed up to a factor of two. The same trend was observed, when only the proportions of cells at the first mitosis were compared. This inter-experimental difference has been analyzed in more detail by the integration analysis (see section 3.3.1).

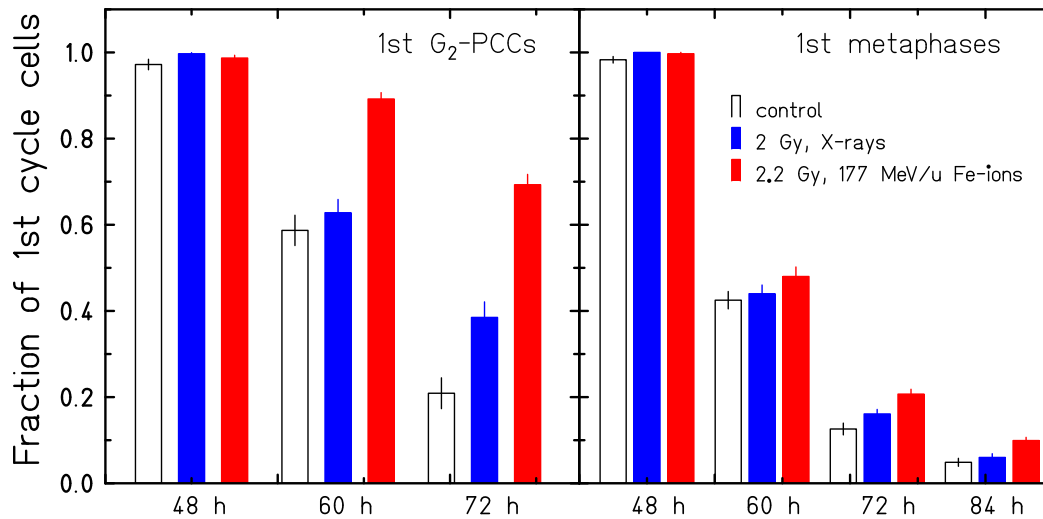


Figure 3.4: The fraction of first cycle G_2 (left panel) and metaphase cells (right panel) among all G_2 -PCC or mitotic cells collected at 48, 60, 72 and 84 h after exposure to X-rays or 177 MeV/u Fe-ions (335 keV/ μ m). Both irradiations were done in parallel. The fraction of first mitosis was scored in samples treated with colcemid. Error bars were obtained by eq. 2.27.

3.1.3 The fraction of cells at first G_2 -phase and first mitosis

Since recent studies suggest (section 1.4.2) that the delayed entry of lymphocytes into mitosis results from a prolonged arrest in G_2 , at each dose- and time-point the fraction of first cycle G_2 -cells among all G_2 -PCCs and the fraction of first cycle metaphases among all mitoses were compared. The analysis revealed that at 48 h for both control and irradiated cultures most of G_2 and metaphase cells (>97 %) belonged to the first cycle (fig. 3.4 and tables A.1 to A.10). With increasing time lymphocytes moved from G_2 -phase to mitosis and progressed to the second or later cycles, i.e. the fraction of first cycle G_2 and metaphase cells decreased. However, at a given time point a higher fraction of first cycle G_2 -PCCs was found in irradiated samples than in control cultures and this effect was more pronounced after high LET exposure compared to X-irradiation indicative for an arrest of cells in the first G_2 -phase. In contrast, radiation has only a minor effect on the cell cycle progression through the first mitosis.

Exemplarily, the response of lymphocytes exposed to ~ 2 Gy X-rays and 335 keV/ μ m Fe-ions is shown in fig. 3.4. While 72 h after initiation of the control culture ~ 20 % of all G_2 -phase cells belonged to the first cycle, this fraction increased to 40 and 70 % after X-ray and Fe-ion exposure. On the other hand, the fraction of first cycle metaphases decreased rapidly with time and this effect was

similar in the control and in irradiated samples. Obviously, cells that were able to overcome the G_2 -block move rapidly through mitosis and enter the second cell cycle.

3.2 Investigation of the cytogenetic damage

3.2.1 Number of aberrant first cycle metaphases and corresponding aberration yield

In the study the frequency of aberrant first generation metaphases and the number of chromosome aberration per cell were measured in 50 to 300 cells collected at several time-points after exposure to X-rays and particles of different LETs (fig. 3.5, fig. 3.6 and tables A.1 to A.5). Mitotic cells were accumulated by a 3 h colcemid treatment.

3.2.1.1 Number of aberrant first cycle metaphases

For all radiation types the number of aberrant first cycle cells increased with dose in the dose range of 0 to 2 Gy, then the frequencies saturated at higher doses (fig. 3.5, left panels). At any dose- and time-point 29 keV/ μm C-ion and 155 keV/ μm Fe-ion were more effective in inducing aberrant cells than X-rays. For instance, the fraction of aberrant metaphases was about 62 % in samples exposed to 1 Gy C-ions, while the same dose of X-rays induced about 30 %. Following irradiation with 1 Gy 155 keV/ μm Fe-ions, the frequencies of aberrant cells ranged from 50 to 77 % at different collection times. When samples were collected at 48 and 60 h after irradiation with 335 keV/ μm Fe-ions, less aberrant metaphases were found than in cultures exposed to isodoses of X-rays. However, due to a pronounced increase in the number of aberrant cells with time after Fe-ion exposure, the effectiveness of 335 keV/ μm Fe-ions and X-rays was comparable at later sampling times. Finally, 3160 keV/ μm Cr-ions were less effective than X-rays (fig. 3.6).

Analysis of the time-course of chromosomal damage induced by X-rays and C-ions revealed that the number of aberrant first cycle cells did not change with sampling time as shown in fig. 3.5a and b. However, a time-dependent increase in the number of aberrant cells was detected after high-LET irradiation: when samples were irradiated with 1 Gy 155 keV/ μm Fe-ions, 50 % of first cycle metaphases were aberrant at 48 h post-irradiation, while this value increased to 77 % at 84 h after exposure (fig. 3.5c). The time-effect was more pronounced in cultures irradiated with 335 keV/ μm Fe-ions. Under this irradiation condition two to three times more aberrant mitotic cells were detected in samples collected at 84 h than in lymphocytes harvested at 48 h post-irradiation (see fig. 3.5d). Accordingly, for

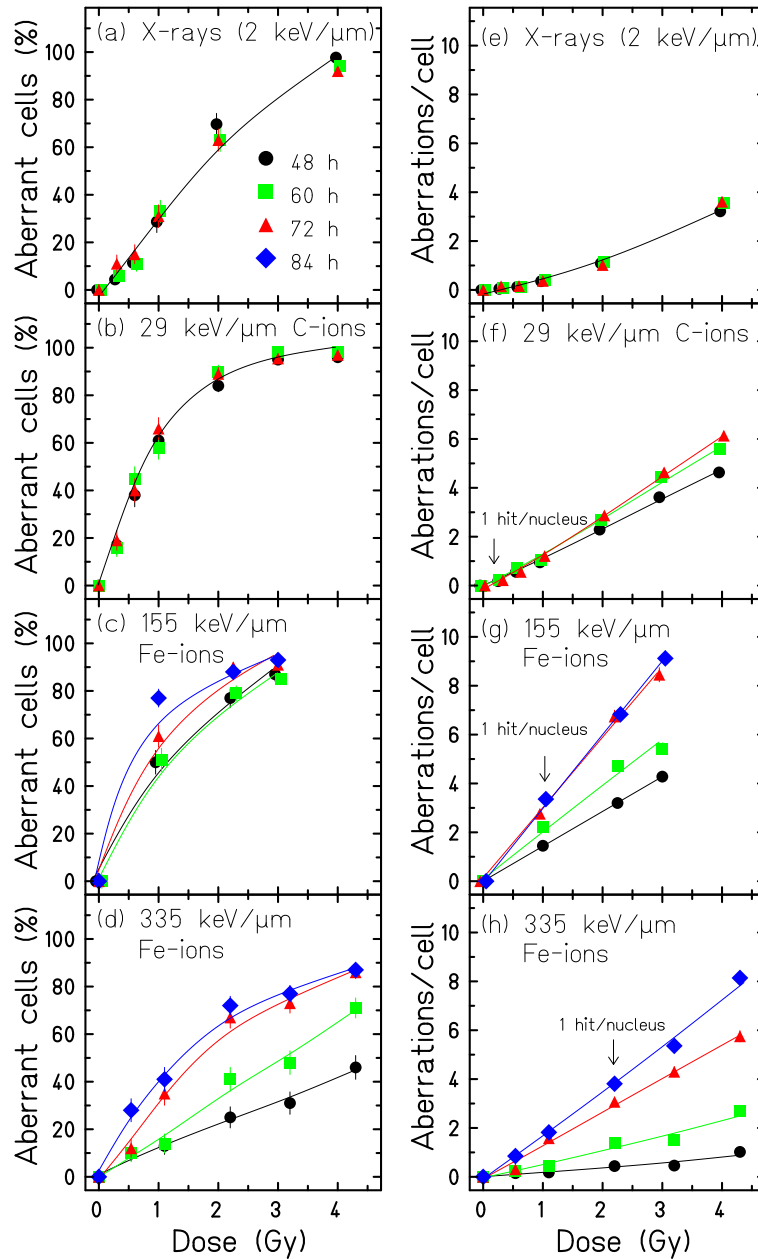


Figure 3.5: The frequencies of aberrant first cycle metaphases (a-d) and the corresponding aberration yields (e-h) as a function of dose. Cells were analyzed at 3 to 4 sampling times after exposure to X-rays (a and e), 90 MeV/u C-ions with LET=29 keV/μm (b and f), 155 keV/μm Fe-ions with LET=155 keV/μm (c and g) or 177 MeV/u Fe-ions with LET=335 keV/μm (d and h). Background values were subtracted. Error bars were calculated by eq. 2.27 (a-d) or eq. 2.28 (e-h). The doses corresponding to 1 particle hit per nucleus ($4 \times 10^6/cm^2$) are indicated by an arrow.

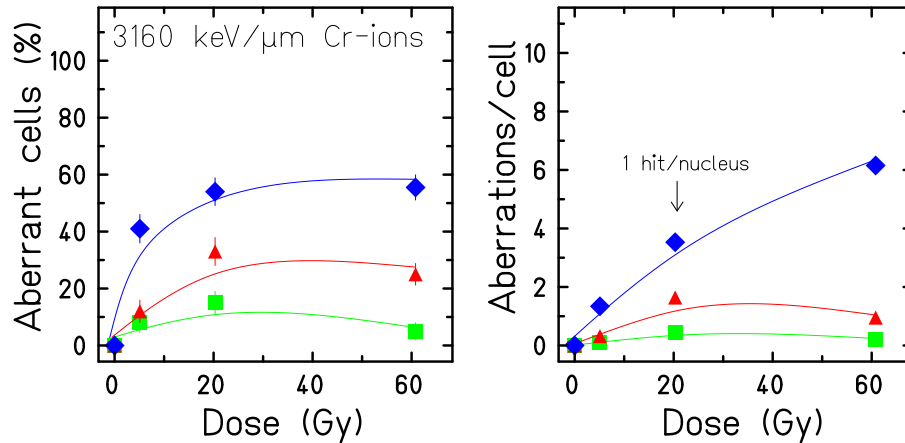


Figure 3.6: The frequencies of aberrant first cycle metaphases (left panel) and the corresponding aberration yields (right panel) as a function of dose after exposure to 4.1 MeV/u Cr-ions with LET=3160 keV/ μm . For further details, see figure caption 3.5.

3160 keV/ μm Cr-ions, the fractions increased more than fivefold with sampling time (fig. 3.6 left panel).

3.2.1.2 Aberration yields in first cycle metaphases

Analysis of the aberration yields revealed a linear-quadratic dose-response after X-irradiation, while a linear increase was observed after exposure to 29 keV/ μm C-ions, 155 keV/ μm and 335 keV/ μm Fe-ions (fig. 3.5e to h). After irradiation with 3160 keV/ μm Cr-ions, the number of chromosome aberrations saturated as shown in fig. 3.6 (right panel). When the effectiveness of isodoses is compared the following picture emerged: C-ions induced about two times more aberrations than X-rays (fig. 3.5f). Cells reaching the first mitosis 48 h after exposure to 155 keV/ μm Fe-ions carried already more aberrations than those detected in samples exposed to X-rays (see fig. 3.5g). On the other hand, when cultures were exposed to 335 keV/ μm Fe-ions, the aberration yield was at 48 h four times lower than after X-irradiation, while at 84 h two times more aberrations were measured than after X-ray exposure. In samples exposed to 3160 keV/ μm Cr-ions, less aberrations were found at any dose-point than after X-ray exposure.

When the time-course of aberrations was analyzed in lymphocytes, after X-irradiated similar yields were found at early and late sampling times as shown in fig. 3.5e. Following C-ion irradiation, the aberration frequencies increased slightly with time and were at 72 h about 25 % higher than at 48 h. The time-dependent rise was significant in cultures irradiated with high LET particles: after irradiation with 155 keV/ μm and 335 keV/ μm Fe-ions, two and eight times higher yields were measured at late sampling times (fig. 3.5g, h). Following 3160 keV/ μm Cr-ion

irradiation, only a few aberrations were detected in cells collected at 60 h, while >20 times more aberrations were found in cells harvested at 84 h (fig. 3.6, right panel). Thus, the number of aberrant mitotic cells and the aberration yields increased drastically with sampling time in lymphocytes after high LET exposure, while there was only a minimal effect after with low LET radiation. Consequently, if RBE values are determined for high LET induced cytogenetic damage, the values will rise with sampling time as described in detail in section 3.2.5.

3.2.2 Aberration spectrum

In metaphase samples seven categories of aberration can be distinguished following giemsa-staining as shown in fig. 2.3. When lymphocytes were exposed to any radiation (tables A.1 to A.5), the majority of aberrations consisted of dicentrics and breaks (i.e. chromatid and chromosome breaks). In order to gain information to what extent the aberration spectrum is influenced by LET, the percentage of dicentrics and breaks among all aberrations was determined for each data set. The analysis showed that for a given radiation type these proportions varied only slightly with dose- or sampling-time. Therefore, the time- and dose-averaged frequencies were determined (mean \pm SD from 3 to 13 measurements) and used for the comparison. As shown in fig. 3.7 the proportion of breaks or dicentrics among all aberrations did not change up to LET=155 keV/ μ m. At higher LET values the fraction of breaks increased, while the fraction of dicentrics decreased. This change

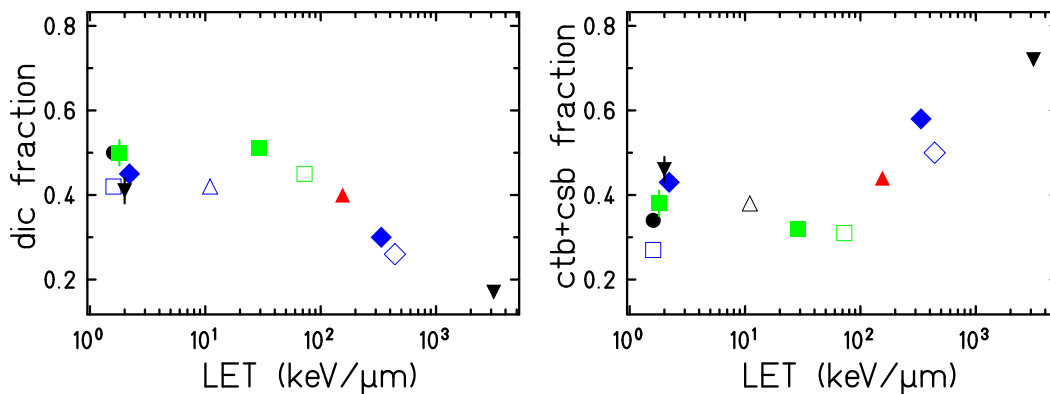


Figure 3.7: The fraction of dicentrics (dic, left panel) and the fraction of both chromatid breaks (ctb) and chromosome breaks (csb, right panel) among all aberrations induced in human lymphocytes by X-rays or heavy ions with different LET. Key as in fig. 3.2. Open symbols show recently published data obtained for the same donor (Größer, 2002; Ritter et al., 2002a; Nasonova and Ritter, 2004). Each datum point represent the time- and dose-averaged mean from 3 to 13 measurements (mean \pm SD).

in the aberration spectrum has important implications for the determination of reliable RBE values of heavy ions as described in detail in section 4.4.2.

3.2.3 Number of aberrant first cycle G_2 -PCCs and corresponding aberration yield

To overcome the problems resulting from pronounced mitotic delay of heavily damaged cells after high LET exposure as shown in section 3.2.1, the technique of calyculin A induced premature chromosome condensation (PCC) was applied, which allows to measure chromosome aberrations in late G_2 -phase cells (fig. 2.4c). Since in late G_2 -cells the centromere region of chromosomes is invisible, only aberrations resulting in the formation of excess fragments such as chromosome breaks, acentric and centric rings can be detected, while dicentrics cannot be recorded. G_2 -cells were collected between 48 and 84 h post-irradiation and at each dose and sampling time 50 to 250 first cycle cells were analyzed. Tables A.6 to A.10 summarize the results.

In control samples, first cycle G_2 -cells carried more excess fragments than first cycle metaphases. In addition, more excess fragments were detected in control cultures at later sampling times than controls at early times suggesting that calyculin A is cytotoxic for lymphocytes.

3.2.3.1 Number of aberrant first cycle G_2 -cells

Fig. 3.8 and 3.9 (left panels) display the frequency of damaged first generation G_2 -cells collected at 48 to 84 h after exposure to X-rays and charged particles. The dose-effect curves for the induction of aberrant G_2 -cells show the same trend as those for aberrant metaphases, i.e. for X-rays, C-ions and Fe-ions (155 keV/ μm and 335 keV/ μm) the number of aberrant cells increased significantly in the dose range of 0 to 1 Gy. At higher doses the frequencies saturated (fig. 3.8a to d). As shown in fig. 3.9 (left panel) for 3160 keV/ μm Cr-ions the yields saturated at 5 Gy.

Comparison of the time-course data revealed that the number of aberrant G_2 -cells varied only slightly with time after irradiation with X-rays, 29 keV/ μm C-ions and 155 keV/ μm Fe-ions. However, following C-ion irradiation, less aberrant cells were found in the cultures collected at 72 h than at earlier times (fig. 3.8b). This effect may result from the elevated number of aberrant cells in control cultures at 72 h. Finally, after exposure to 335 keV/ μm Fe-ions and Cr-ions, up to two times more aberrant cells were measured at late times compared to the early times.

3.2.3.2 Aberration yields in first cycle G_2 -cells

The analysis of excess PCC fragments in first G_2 -cells revealed that the yields increased linearly with dose after exposure to all radiation qualities except for

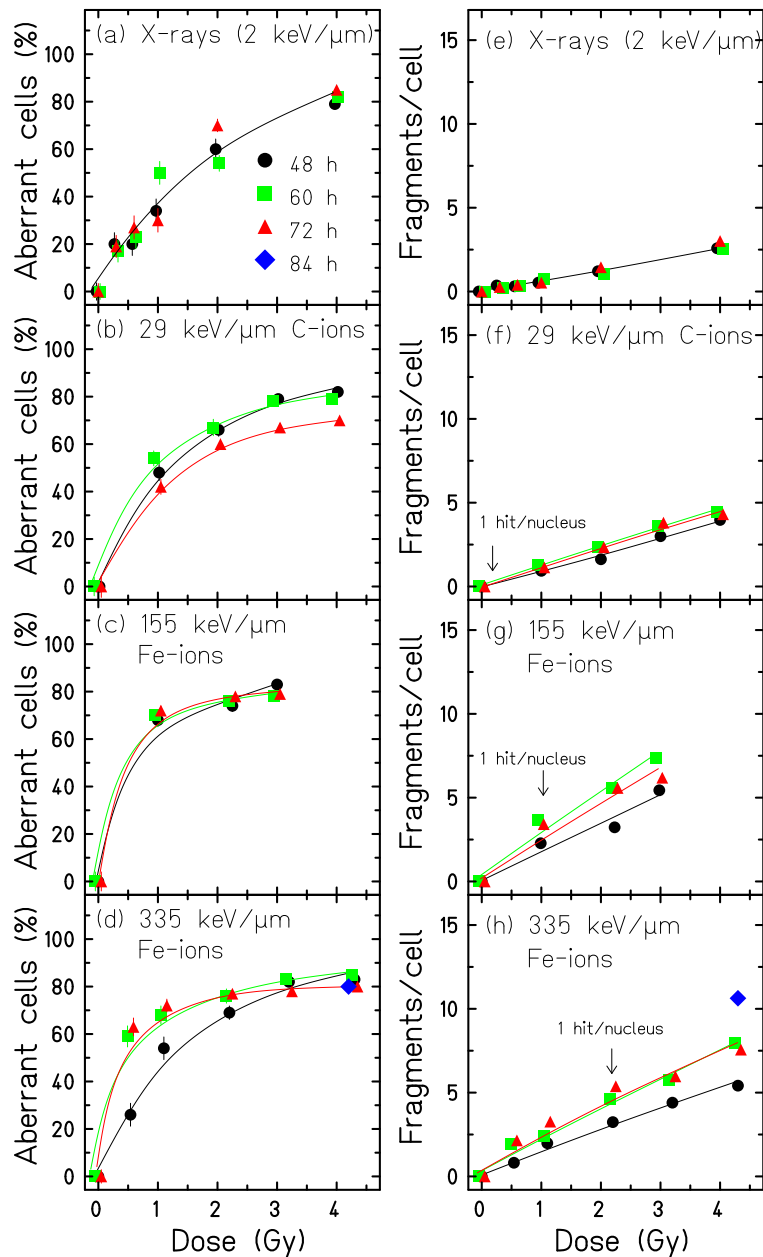


Figure 3.8: The frequencies of aberrant first G_2 -cells (a to d) obtained by premature chromosome condensation technique and the corresponding yields of excess fragments (e to h) as a function of dose. The aberration analysis has been restricted to excess fragments because of chromosome morphology (see section 2.2.4). Cells were analyzed at 3 to 4 sampling times after exposure to X-rays (a and e), 90 MeV/u C-ions with LET=29 keV/μm (b and f), 155 keV/μm Fe-ions with LET=155 keV/μm (c and g) or 177 MeV/u Fe-ions with LET=335 keV/μm (d and h). Background values were subtracted. Error bars were calculated by eq. 2.27 (a-d) or eq. 2.28 (e-h). The doses corresponding to 1 particle hit per nucleus ($4 \times 10^6/cm^2$) are indicated by an arrow.

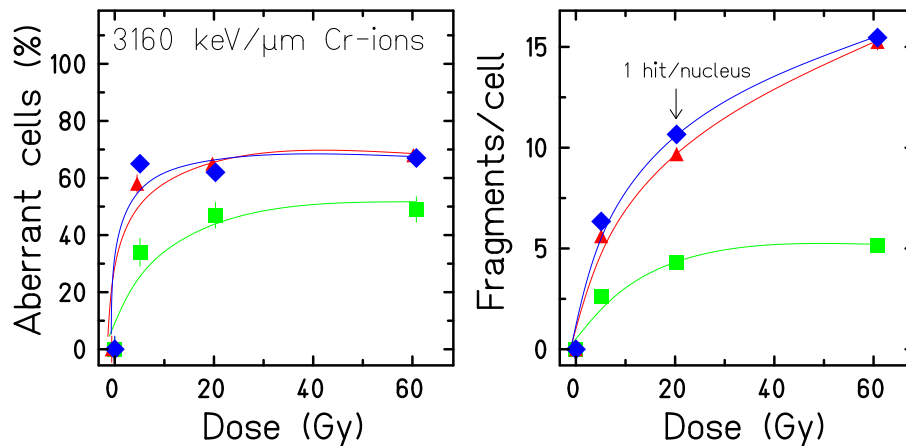


Figure 3.9: The frequencies of aberrant first G_2 -cells (left panel) and the corresponding yields of excess fragments (right panel) as a function of dose after exposure to 4.1 MeV/u Cr-ions with LET=3160 keV/ μ m. For further details, see figure caption 3.8.

the high LET Cr-ions (fig. 3.8, right panels), where the yields saturated (fig. 3.9, right panel). When the time-course of excess fragments was compared, a stable yield was detected after irradiation with X-rays and C-ions. On the other hand, after exposure to high LET particles (LET \geq 155 keV/ μ m) the aberration frequency increased with sampling time. For example, following 155 keV/ μ m Fe-ion exposure the aberration yields in lymphocytes collected at 48 h to 72 h post-irradiation increased 1.5-fold (see fig. 3.8g). This trend was more pronounced in lymphocytes exposed to higher LET particles. For cells irradiated with 335 keV/ μ m Fe-ions and 3160 keV/ μ m Cr-ions, the increase was twofold and threefold, respectively (fig. 3.8h and fig. 3.9, right panel) indicating that for these radiation conditions the RBE values will increase with sampling time as described in section 3.2.5.

3.2.3.3 Comparison of cytogenetic damage detected in metaphases and G_2 -PCC cells

The number of excess fragments measured in metaphase cells were compared with the yields found in G_2 -PCCs to gain insights into the relationship of cell cycle progression delays and aberration burden. In metaphase samples about 35 to 65 % of aberrations belong to the category of excess fragments (see tables A.1 to A.5). As shown in fig. 3.5, 3.6, 3.8 and 3.9 the shape of the dose-response curves for the induction of aberrant cells or aberrations was similar for first cycle G_2 -cells and metaphases. However, at any dose- and time-point higher yields were detected in G_2 -PCCs than in metaphase cells. For example, when lymphocytes were exposed to X-rays, about twice as many excess fragments were found in G_2 -cells than metaphases collected at the same time. In addition, this difference did not change

among different sampling times. A similar trend was observed for lymphocytes irradiated with 29 keV/ μm C-ions and 155 keV/ μm Fe-ions.

In contrast, following exposure to particles with $\text{LET} \geq 335$ keV/ μm the number of excess fragments in G_2 -cells at 48 h was >12 times higher than in metaphases, while the difference decreased to 2.5-fold at 84 h. The difference was more pronounced in cells for the 3160 keV/ μm ions, i.e. >22 and >4 times higher yields were detected in G_2 -PCCs than in mitotic cells fixed at 60 and 84 h, respectively. Altogether, these results suggest that after exposure to particles with $\text{LET} \geq 335$ keV/ μm heavily damaged cells suffer a prolonged G_2 -arrest.

3.2.4 Inter-experimental variations in the cytogenetic response to X-ray exposure

To gain information on the inter-experimental variations in the radiation response, in parallel to particle exposure lymphocytes were exposed to 2 Gy X-rays and the frequencies of aberrant cells and aberrations were measured at several time-points post-irradiation in both first cycle metaphases and G_2 -PCC cells and are included in tables A.2 to A.10.

As described above (section 3.2.1 and 3.2.3) analysis of the data sets revealed that after exposure to 2 Gy X-rays the amount of chromosomal damage did not change with sampling time. When the aberration yields were averaged, a frequency of 1.07 ± 0.13 aberrations per first cycle metaphase were found (mean \pm SD from 13 measurements). Accordingly, 1.14 ± 0.17 excess fragments per first cycle G_2 -PCC were measured (mean \pm SD from 12 measurements). The standard deviations were <15 % and are in the range observed in biological experiments indicating that for the present data sets inter-experimental differences in the cytogenetic responses are negligible.

3.2.5 RBE values for the induction of aberrations in metaphases and G_2 -PCC cells

In order to compare the effects of different radiation qualities for the induction of chromosome aberrations in first cycle metaphases or G_2 -PCCs, the relative biological effectiveness (RBE) was estimated. For the RBE calculation, the aberration yields measured at a given sampling time (see fig. 3.5, 3.6, 3.8 and 3.9, right panels) were fit to a linear-quadratic equation (eq. 2.29). Then, the RBE value based on the dose to induce one chromosome aberration in a mitotic cell or one excess fragment in a G_2 -cell was derived as shown in eq. 1.5.

Fig. 3.10 (left panel) shows RBE values obtained from metaphase analysis. The RBE increased with LET reaching a peak at 155 keV/ μm , thereafter the RBE decreased. The lowest RBE value was derived for 3160 keV/ μm Cr-ions. Further-

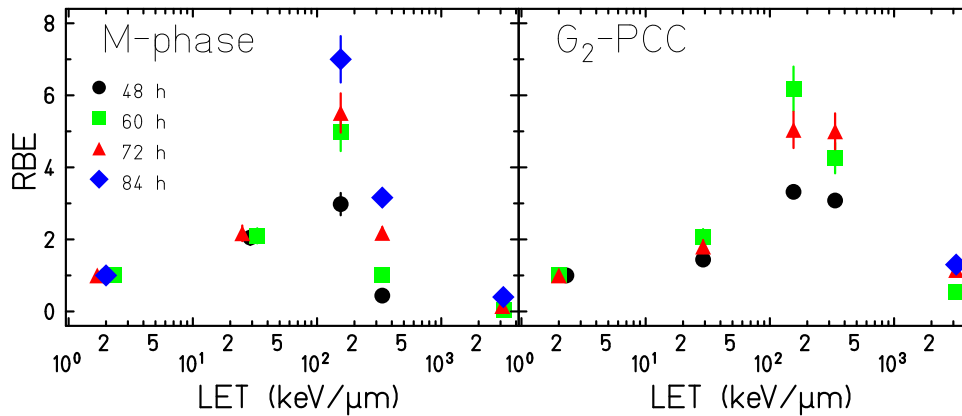


Figure 3.10: Relative biological effectiveness (RBE) as a function of LET. RBE was calculated based on the dose that induces one chromosome aberration per first cycle metaphase (left panel) or one excess fragment per first cycle G_2 PCC (right panel). Errors were derived from eq. 2.30 and were in average 10 %. If absent, error values are smaller than symbols.

more, for lymphocytes irradiated with high LET particles, i.e. $LET \geq 155 \text{ KeV}/\mu\text{m}$, a time-dependent increase in RBE values was observed. For example, the RBE was 3.0 for first cycle metaphase cells collected at 48 h after exposure to $155 \text{ KeV}/\mu\text{m}$ Fe-ions, but after 84 h RBE increased to 7.0. This effect was more significant after irradiation with $335 \text{ KeV}/\mu\text{m}$ Fe-ions: the RBE was 0.44 for cells harvested at 48 h, but $RBE=3.2$ for samples collected at 84 h. Similarly, after irradiation with $3160 \text{ keV}/\mu\text{m}$ Cr-ions, the RBE was less than 0.1 at 60 h post-irradiation reaching 0.4 at 84 h. For low LET C-ions the RBE did not change with sampling time, e.g. 48, 60 and 72 h after irradiation, the values were ~ 2.1 .

Accordingly, fig. 3.10 (right panel) shows the RBE values for the induction of excess fragments in G_2 -PCCs as a function of LET. As in the metaphase study G_2 -PCCs were harvested at several time-points. The trend was similar to that obtained by metaphase analysis (fig. 3.10, left panel), i.e. the RBE increased with LET reaching to maximum at $155 \text{ keV}/\mu\text{m}$, then the RBEs decreased at higher LET. Also, a time-dependent rise in RBEs was detected. However, this effect was less pronounced than that found in metaphase samples. For example, following $335 \text{ keV}/\mu\text{m}$ Fe-ion exposure, RBE values derived from G_2 -PCCs were at 72 h 1.6 times higher than at 48 h, while the RBEs based on metaphase samples increased fivefold within the same time interval.

3.3 Integration analysis

The chromosome aberration yields in first cycle metaphases were time-dependent after high LET irradiation as displayed in fig 3.5 and 3.6. Consequently, the yields measured at a single sampling time reflect only the damage induced within a sub-population. In order to determine the damage induced in the initial cell population, the integration analysis as described in section 2.5.1 was applied.

3.3.1 Fraction of lymphocytes completing first mitosis

Based on the measured mitotic indices and the fraction of metaphases in first, second or later cell generation, the corrected mitotic indices for first cycle cells were calculated by eq. 2.3. As exemplarily shown for lymphocytes irradiated with ~ 2 Gy 335 keV/ μm Fe-ions or X-rays (fig 3.11, left panel) ionizing radiation decreases the number of cells that are able to reach the first mitosis and causes a shift of peak mitotic index to a later time. Generally, a comparable dose of Fe-ions is more effective than X-rays.

Based on the corrected mitotic indices the growth curve of the cell population was reconstructed. As shown in fig. 3.11 (right panel), the fraction of control cells that reached first mitosis amounted to 0.26, while after exposure to 2 Gy

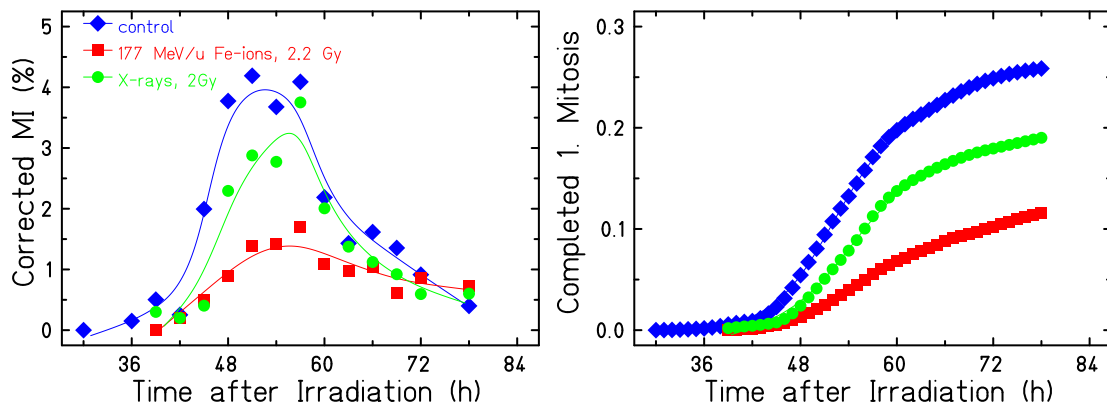


Figure 3.11: Analysis of lymphocyte populations exposed to either 177 MeV/u Fe-ions (LET=335 keV/ μm) or X-rays. Both irradiations were performed in parallel. Left panel: Corrected mitotic indices for cells in first mitosis calculated by eq. 2.3. Right panel: Reconstructed growth curves showing the fractions of the initial cell population that completed first mitosis at a given time after irradiation. Lines are drawn to guide the eye.

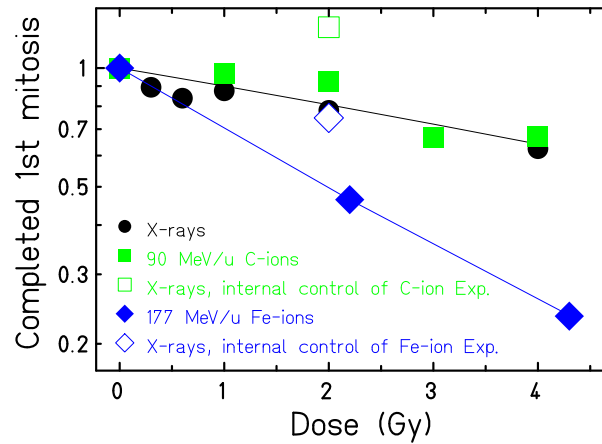


Figure 3.12: Fraction of the initial cell population that completed first mitosis 78 h after exposure to X-rays, 90 MeV/u C-ions (29 keV/ μm) or 177 MeV/u Fe-ions (335 keV/ μm). Data were normalized to the control level.

X-rays and 2.2 Gy Fe-ions (335 keV/ μm) the frequency changed to 0.19 and 0.12, respectively. When the fractions of control cells completing first mitosis measured in all experiments were compared, inter-experimental differences in the cell generation time were found, i.e. 19 to 28 % of the control population capable to enter mitosis.

To compare the proliferation of lymphocytes after exposure to different radiation qualities, each data set was normalized to its control value. As shown in fig. 3.12 for each radiation type the fraction of cells reaching first mitosis declined with dose. Isodoses of X-rays and 29 keV/ μm C-ions showed a similar effectiveness, while 335 keV/ μm Fe-ions were about twice more effective. Furthermore, the data obtained after the exposure of lymphocytes to 2 Gy X-rays (internal control) are plotted in fig. 3.12. The fractions of cells completing first mitosis after 2 Gy X-rays ranged from 0.75 to 1.27 for lymphocytes indicating fluctuations between experiments.

3.3.2 Total amount of chromosome damage in the initial cell population

Based on the number of aberrant first cycle cells or aberrations and the corrected mitotic index, the total amount of damage induced within the initial cell population was determined by integrating the area under the yield time curve as described in section 2.5.1 (also see eq. 2.4 and 2.5). To account for experimental limitations, i.e. aberration data were not available for all time points, a linear interpolation was performed.

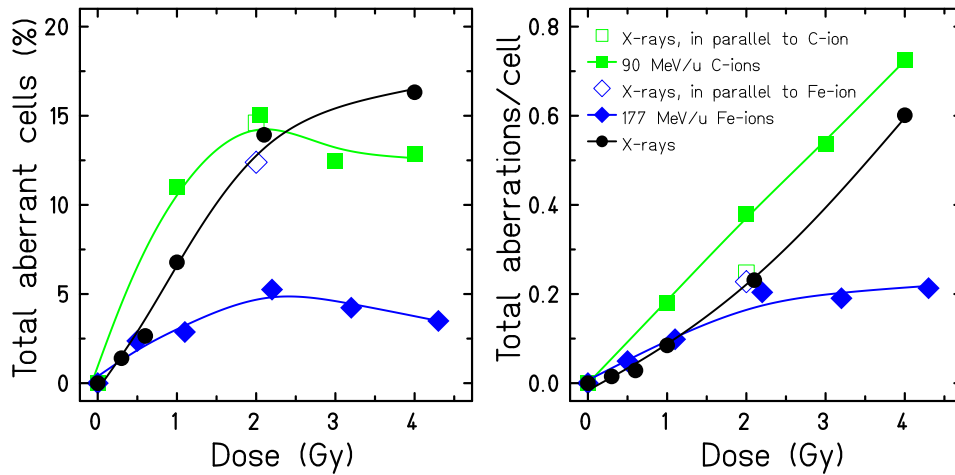


Figure 3.13: Total number of aberrant cells (left panel) and aberrations (right panel) induced within the initial cell population after exposure to X-rays, 90 MeV/u C-ions (29 keV/ μm) and 177 MeV/u Fe-ions (335 keV/ μm). Both irradiations with 2 Gy X-rays and particles were performed in parallel. Lines are drawn to guide the eye.

When the total number of aberrant cells was compared at 1 Gy level, 29 keV/ μm C-ions were 1.5 times more effective in inducing aberrant cells than X-rays, while Fe-ions were 2.5 times less effective (fig. 3.13, left panel). At higher doses (≥ 2 Gy), the total amount of aberrant cells saturated for all radiation types. The saturation can be attributed to the high number of cells that never reached first mitosis (fig. 3.12 and 3.3).

Fig. 3.13 (right panel) displays the total number of aberrations within the dose range investigated. C-ions were found to be more effective than X-rays. The effectiveness of 335 keV/ μm Fe-ions and X-rays was similar for doses up to 2 Gy. However, for higher Fe-ion doses the total yields saturated, although at each sampling time a marked dose-dependent increase in the number of aberrations per cell was detected (see fig. 3.5h). As mentioned above, the saturation is caused by the decrease in the absolute number of cells reaching first mitosis with increasing Fe-ion dose.

Furthermore, when the integrated data obtained for 2 Gy X-rays (three experiments) were compared, a similar number of total aberrations (0.24-0.25/cell) was derived indicating that the fluctuations in total aberration yields were smaller than the fluctuations in proliferation behavior (fig. 3.13, right panel).

3.4 Distribution of chromosome aberrations

Chromosome aberrations were analyzed in cells exposed to X-rays, 29 keV/ μm C-ions, low to high energies of Fe- and iron like particles with 3 to 6 different fluences (for more details, see tables 2.1 and 2.2). Cells were fixed at 3 to 4 different sampling times at 48 to 84 h after exposure. Then, aberrations were measured in 100 to 300 first cycle metaphases or in the first G_2 -phase PCCs per sample. In metaphase samples all aberrations detectable by giemsa staining were recorded (fig. 2.3). In contrast, in G_2 -PCC samples scoring was restricted to the number of excess fragments, because of chromosome morphology as described in section 2.2.4. The number of chromosome aberrations was determined per cell and the frequency distributions of the number of aberrations were obtained for each dose- and time-point.

3.4.1 Distribution of aberrations among first cycle metaphases after exposure to low LET radiation

Distributions of aberrations were analyzed in first cycle mitotic cells after exposure to low LET radiation, i.e. X-rays and 29 keV/ μm C-ions. Exemplarily, in fig. 3.14 the distributions of aberrations in cells collected 48 and 72 h after irradiation with 2 Gy X-rays or C-ions are shown. As shown in the upper left figure, 48 h after exposure to 2 Gy X-rays the average number of aberrations per cell was 1.1. The dominant group was the fraction of cells with one aberration. At 48 h after exposure to 2 Gy C-ions the average number of aberrations was higher, i.e. 2.30 aberrations per cell were detected. Cells with one to three aberrations dominated and the distribution of aberrations was broader.

To analyze further the frequency distributions, the relative variance $\sigma^2/\langle x \rangle$ was determined. For cultures irradiated with low LET radiations the relative dispersion $\sigma^2/\langle x \rangle$ was close to one (see table A.11) indicating that the data can be well described by Poisson statistics (eq. 2.20). After X-ray exposure (three sampling times, five doses), the relative variance ranged from 0.83 to 1.6 resulting in an average value of 1.03 ± 0.18 . Accordingly, for lymphocytes exposed to C-ions (3 sampling times and 6 doses), $\sigma^2/\langle x \rangle$ values ranged from 0.92 to 1.5 with an average value of 1.22 ± 0.15 .

These observations allowed to fit the frequency distributions with the Poisson distribution (see eq. 2.8). A free-parameter Poisson fit resulted that the characteristic parameter a that corresponds to the expected number of aberrations per cell was close to those estimated from the experimental data. Fit parameters and results of the goodness-of-fit test for data measured 48 and 72 h after X-ray and C-ion exposure are listed in table A.11 and are explained in detail in section 3.4.4.

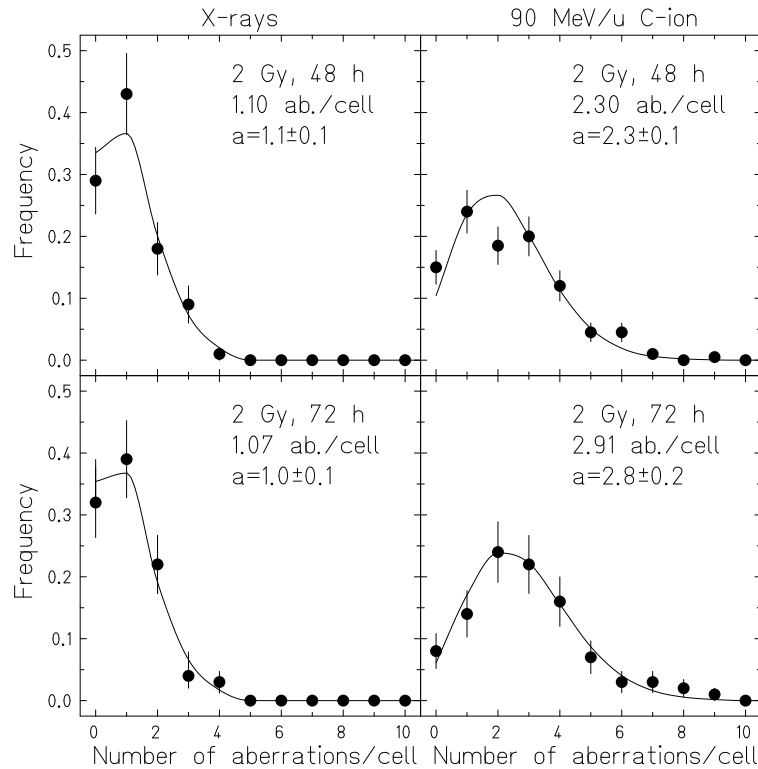


Figure 3.14: Distributions of chromosome aberrations induced by 2 Gy X-rays or 90 MeV/u C-ions (29 keV/ μ m). The relative frequency of first cycle metaphases carrying a distinct number of aberrations is plotted. Vertical bars along frequency values represent statistical errors determined by eq. 2.28. Dose, fixation time and average number of aberrations per cell are displayed in each panel. The solid line represents the best fit to the experimental data by a Poisson distribution with parameter a corresponding to the expected number of aberrations per cell. For each data set a representative average number of aberrations per cells is reported as estimated from frequency histograms.

3.4.2 Distribution of aberrations among first cycle metaphases after exposure to high LET particles

After high LET exposure the distribution of aberrations in first cycle mitotic cells followed a different pattern than after low LET exposure. When lymphocytes were irradiated with high LET ions (155 to 3160 keV/ μm), relatively high frequencies of undamaged cells were observed at early sampling times corresponding the fraction of cells which was not hit by any particle. With increasing fluence and sampling time, the frequency of non-aberrant cells decreased markedly (see fig. 3.15).

Furthermore, for a similar average number of aberrations per cell the distributions in high LET exposed samples were broader than those obtained for cultures exposed to low LET radiation. For instance, a mean number of 1.95 and 2.30 aberrations/cell were measured 84 h after exposure to 1.1 Gy Fe-ions (335 keV/ μm) and 48 h after exposure to 2 Gy C-ions (29 keV/ μm), respectively. Following Fe-ion exposure the distribution ranged from 0 to 12 aberrations/cell, while after C-ion exposure 0 to 9 aberrations per cell were scored. For all frequency histograms obtained for lymphocytes irradiated with high LET particles (>155 keV/ μm) the derived relative dispersions were > 1 indicative for non-Poissonian (eq. 2.20), and hence non-random distributions of lesions (see table A.12). The averaged relative variance was 2.53 ± 0.44 for cells exposed to 155 keV/ μm Fe-ions (12 distributions). Similarly, the averages were 3.21 ± 1.11 for cells irradiated with 335 keV/ μm Fe-ions (20 distributions) and 5.10 ± 2.70 for metaphases after exposure to 3160 keV/ μm Cr-ion (nine distributions).

Because of the apparent overdispersion, most of distributions obtained after high LET exposure could not be fit by Poisson statistics. In fig. 3.15 dotted lines represent the best fits to the experimental data by Poisson distribution with a representative value of the a parameter set to the experimentally assessed average number of aberrations per cell revealing the poor fits to the experimental data. Additionally, the data were fit by a Neyman distribution (eq. 2.11) which takes into account both the stochastics of particle traversals and the stochastics of the number of aberrations induced by a single particle hit. As shown in fig. 3.15, the fit by Neyman statistics (solid lines) agreed better with experimental data as reflected by the χ^2 values of the goodness-of-fit test. From the Neyman fit the parameters λ and μ (cf. eq. 2.11) were derived and compared with their estimators calculated directly from the frequency histograms (see eq. 2.22). These fit parameters and results of the goodness-of-fit test are listed in table A.12 and are explained in detail in section 3.4.4.

3.4.3 Distribution of aberrations among first cycle G_2 -PCCs

Analysis of the distributions of aberrations among first cycle G_2 -PCC cells revealed similar trends as observed in first metaphases: when cells were irradiated with low

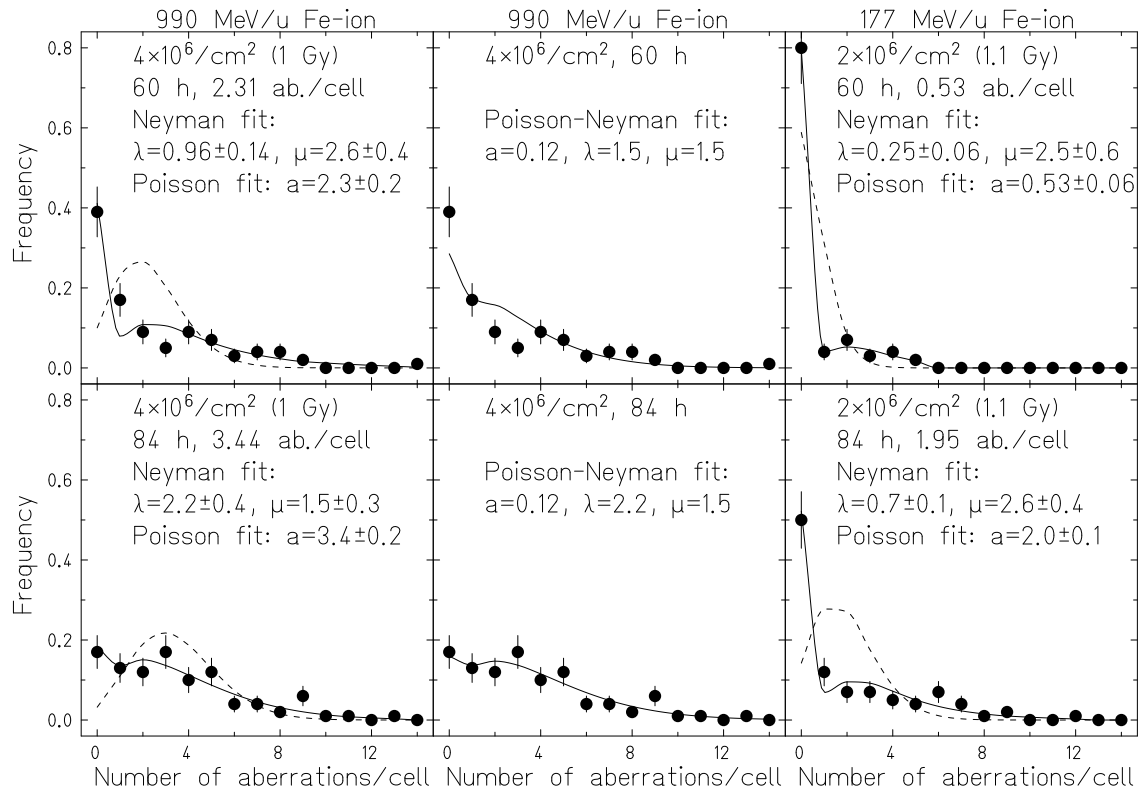


Figure 3.15: Distributions of chromosome aberrations induced by 177 and 990 MeV/u Fe-ions (LET: 155 and 335 keV/ μm). The frequency of first metaphase cells carrying a distinct number of aberrations is plotted. Vertical bars along frequency values represent statistical errors determined by eq. 2.28. Dose, fixation time and average number of aberrations per cell derived from the experimental data are displayed in each panel. Left and right panels: The solid line represents the best fit to the experimental data by Neyman distribution. The fit parameter λ corresponds to the average number of particle hits per nucleus and μ is the average number of aberrations per particle traversal through a cell nucleus. The dotted line represents the best fit to the experimental data by Poisson distribution. Middle panels: The solid line represents the convoluted Poisson-Neyman fit to the experimental data. Fit parameters are shown in the figure.

LET X-rays and C-ions (29 keV/ μm), the relative variances were close to one: The averaged $\sigma^2/\langle x \rangle$ values were 1.18 ± 0.26 (15 distributions) for cells exposed to X-rays and 1.34 ± 0.27 for cells exposed to low LET C-ions (12 distributions).

In contrast, after exposure to high LET ions, all $\sigma^2/\langle x \rangle$ values were larger than 1.5: The averaged $\sigma^2/\langle x \rangle$ values were 2.08 ± 0.38 (nine distributions), 2.83 ± 0.95 (16 distributions) and 7.3 ± 3.22 (nine distributions) for cells exposed to 155, 335 and 3160 keV/ μm Fe- or Fe-like particles, respectively. Similarly to metaphase analysis, the distributions obtained after X-ray and C-ion exposure agreed well with Poisson statistics, while the data obtained after high LET exposure can be well described by Neyman statistics. The summary of the extracted analysis are displayed in table A.13 and A.14 and are explained in detail in section 3.4.4.

3.4.4 Verification of the theoretical fit to the experimental data

To estimate how the Poisson and the Neyman distributions agree with experimental data, the goodness-of-fit χ^2 values per a degree of freedom (χ^2/ndf) were evaluated. The aberration frequency distributions among first metaphases obtained after irradiation with X-rays were fit with Poisson and yielded χ^2/ndf values between 0.01 and 2.2 (mean \pm SD 0.54 ± 0.58 from 15 fits), smaller than averaged χ^2/ndf value 0.75 ± 0.48 (from 0.14 to 1.78 from 18 fits) derived from low LET C-ion experiments. On the other hand, following high LET exposure to lymphocytes, obtained frequency distributions fit to the Poisson statistics yielded large χ^2/ndf values; i.e. 8.65 ± 14.3 (mean \pm SD from 41 distributions). However, the same analysis fit to Neyman statistics resulted lower χ^2/ndf values: i.e. for cells irradiated with 155 keV/ μm Fe-ion, 335 keV/ μm Fe-ions and 3160 keV/ μm Cr-ions, mean values of 1.0 ± 0.39 , 0.85 ± 0.49 and 1.5 ± 0.81 were derived. There was a slight LET-dependent increase in mean χ^2/ndf values. By applying the goodness-of-fit test to the PCC-data the same trend was found, i.e. the mean χ^2/ndf value was 0.96 ± 0.77 for cells exposed to X-rays, while the mean value was 1.2 ± 0.51 for cells irradiated with Cr-ions.

Similar trends were observed when the experimentally measured average number of aberrations per cell were compared with the fit parameters a (Poisson distributions) or $\lambda \times \mu$ (Neyman distributions). Both a and $\lambda \times \mu$ correspond to the expected number of aberrations per cell (see eq. 2.17, 2.22). The comparison revealed a good agreement between experimentally and theoretically determined values for lymphocytes irradiated with X-rays or 29 keV/ μm C-ions. In total 60 distributions obtained for both metaphase and G_2 -PCC analyzed by Poisson statistics: for 49 frequency distributions, the difference between the experimental value and the fit value a was smaller than 10 %. For 11 distributions, the difference ranged from 10 to 18 %. However, the difference became larger after high LET exposure: 75 distributions were fit with Neyman statistics after the exposure of lymphocytes to 155 keV/ μm and 335 keV/ μm Fe-ions and 3160 keV/ μm Cr-ions. For 32 dis-

tributions (40 % of histograms) the difference between the experimental and the products of parameters $\lambda \times \mu$ (eq. 2.22) was smaller than 10 %. For 43 distributions the difference ranged from 10 to 40 %. The poor fits were obtained for Cr-data. The differences between experimental data and Neyman-fits exceeded in most cases 30 %, possibly because the mean number of aberrations was small at early and even late sampling times and high fraction of cells underwent apoptosis.

3.4.5 Parameter λ derived from aberration analysis at early and late sampling time

The parameter λ in Neyman statistics corresponds to the mean number of particle traversal through a cell in the initial population and its value increased at a given time with the particle fluence as reflected in tables A.12 and A.14 and fig. 3.16 and 3.17. For example, when first cycle metaphases were analyzed 48 h after irradiation with 4×10^6 Fe-ions/ cm^2 (335 keV/ μm), which results in a mean number of one hit per cell nucleus, $\lambda=0.6$ was derived, while about twice larger value (i.e. $\lambda=1.0$) was obtained in frequency distribution in samples exposed to 8×10^6 / cm^2 Fe-particles. Moreover, the analysis of data for high and middle energy Fe-ions showed that the λ value increased when aberrations were scored at late sampling times. For example, λ values were 1.4 and 2.7 in metaphases collected at 72 h post-irradiation with 4×10^6 and 8×10^6 Fe-ions/ cm^2 (335 keV/ μm), respectively (fig. 3.16) indicating that the cell cycle transition depends on the number of particle traversals per cell nucleus and consequently on the amount of aberrations carried by a cell.

In contrast to the experiments with high and middle energy Fe-ions, where the value of the parameter λ showed both a time- and a fluence-dependence, after higher LET (3160 keV/ μm) Cr-ion exposure no effect of fluence, but a small effect of time was found. For instance, regardless of particle fluence the λ values ranged from 0.15 to 0.4 for frequency distribution of aberrations measured at 48 h and from 0.86 to 0.96 for distributions obtained at 84 h post-irradiation as shown in fig. 3.16. Although the particle fluence of 12×10^6 / cm^2 corresponds to three particle hits per nucleus, the λ values did not exceed one in cells analyzed at any sampling time providing evidence that cells traversed by more than one stopping particle do not reach mitosis.

A similar trend was observed by analyzing the distributions of aberrations in G_2 -PCCs after exposure to low and high energy Fe- and Fe-like ions as shown in fig. 3.17. The value of the parameter λ increased exhibiting both a time- and a dose-dependence. The λ values were more scattered than the values in metaphase analysis, however most of values were within the confidence limits at one standard deviation. Furthermore, when the λ values were compared between metaphase and G_2 -PCC analysis in cells exposed to the same radiation type, larger λ values were derived for G_2 -PCC cells. For example, for G_2 -PCCs and metaphase cells collected

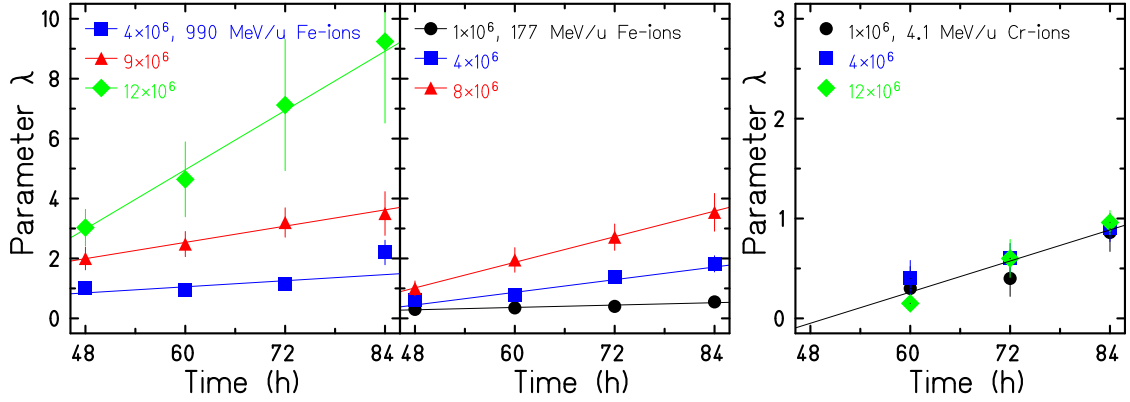


Figure 3.16: Determination of the parameter λ according to the fit by Neyman statistics for frequency distributions of aberrations in first-cycle metaphases analyzed at different sampling times. Error bars were estimated by the **gd** program from experimental errors according to the error analysis algorithms given in Brandt (1992). Note the difference in y axis scaling.

72 h after exposure to $9 \times 10^6 / \text{cm}^2$ of 155 keV/ μm Fe-ions, the parameter λ was 6.1 and 3.2, respectively, further supporting that cells receiving more particle hits are delayed in G_2 -phase.

To gain further insights, the λ values were plotted as a function of sampling time and a linear equation was fit to the data as shown in fig. 3.16 and 3.17. The slopes $\Delta\lambda/\Delta t$ were derived and are displayed in fig. 3.18. In metaphase samples (fig. 3.18, left) there was a fluence-dependent increase in $\Delta\lambda/\Delta t$ after exposure to high and middle energy particles, but the value remained constant after irradiation with stopping particles. For example, for cells irradiated with 990 MeV/u Fe-ions, the ratio $\Delta\lambda/\Delta t$ was 0.017 ± 0.009 after exposure to $4 \times 10^6 / \text{cm}^2$ and the value increased to 0.16 ± 0.057 when a fluences of $12 \times 10^6 / \text{cm}^2$ was applied. When cells were exposed to 4.1 MeV/u Cr-ions, the values were 0.024 ± 0.012 ($1 \times 10^6 / \text{cm}^2$) and 0.034 ± 0.005 ($12 \times 10^6 / \text{cm}^2$) revealing no difference when error values were taken into account. In G_2 -PCC analysis a different trend was observed (fig. 3.18, right). The increase in λ with sampling time was similar for all heavy ions, i.e. $\Delta\lambda/\Delta t$ was around 0.1, independent of energies, fluences or LET. Altogether, these data indicate that the extent of the mitotic delay depends on LET and particle fluence (fig. 3.18, left). In contrast, the G_2 -delay is similar for various LETs and particle fluences (fig. 3.18, right).

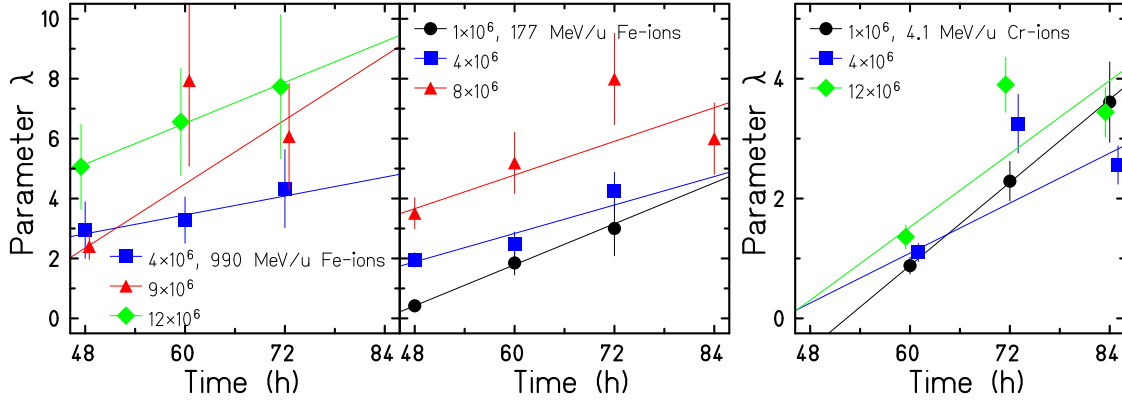


Figure 3.17: Determination of the parameter λ according to the fit by Neyman statistics for frequency distributions of aberrations in G_2 -PCCs analyzed at different sampling times. Error bars were estimated as explained in the caption in fig. 3.16. Note the difference in y axis scaling.

3.4.6 LET dependence of the value of parameter μ

Analysis of fit to Neyman distributions shows that the values of the parameter μ , which corresponds to the mean number of aberrations per particle traversal through a cell nucleus, were scattered exhibiting no significant fluence or time dependence (see tables A.12 and A.14). Therefore, for each particle type the obtained values were averaged over dose and different sampling time as shown in fig. 3.19.

For lymphocytes exposed to $155 \text{ keV}/\mu\text{m}$ and $335 \text{ keV}/\mu\text{m}$ Fe-ions, the averaged μ values obtained from the analysis of frequency distributions of aberrations in first cycle metaphases were 1.8 ± 0.6 and 1.6 ± 0.7 , respectively (see fig. 3.19). Accordingly, G_2 -PCC analysis resulted in μ values of 1.0 ± 0.3 and 1.3 ± 0.4 . The average μ values derived from G_2 -PCC data were lower than those obtained by metaphase data because aberration analysis in G_2 -PCCs is restricted to a subgroup of aberrations (i.e. excess fragments) as described in section 2.2.4.

Finally, analysis of the averaged μ value derived from G_2 -PCC analysis after $3160 \text{ keV}/\mu\text{m}$ Cr-ion exposure was about twice larger than that derived by 155 and $335 \text{ keV}/\mu\text{m}$ Fe-ions, i.e. 2.7 ± 1.1 instead of 1.0 ± 0.3 or 1.3 ± 0.4 . However, the averaged μ value after exposure to low energy Cr-ions yielded for metaphase samples a value of 2.2 ± 2.3 which is not significantly different from the value obtained for medium LET Fe-ions. The data indicate that after high LET exposure heavily damaged cells were able to reach G_2 -phase but never progressed to mitosis.

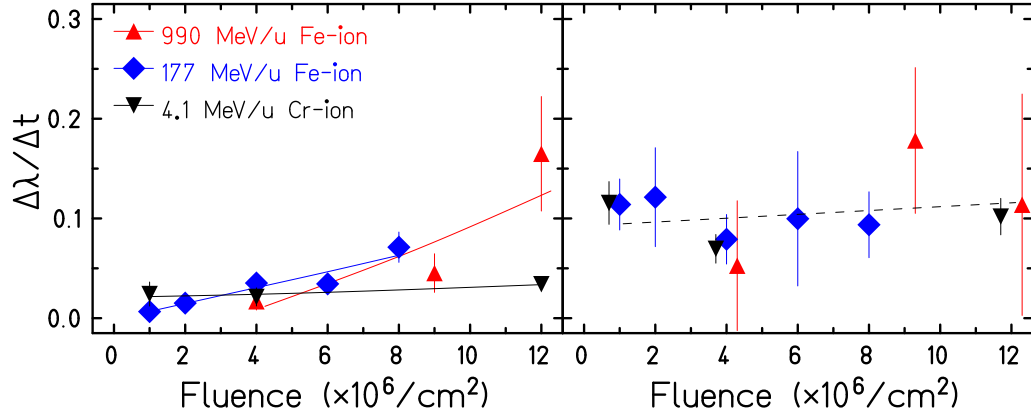


Figure 3.18: $\Delta\lambda/\Delta t$ as a function of particle fluences derived by metaphase analysis (left panel) and G_2 -PCC analysis (right panel). The $\Delta\lambda/\Delta t$ values represent slopes of the linear fit $\lambda(t)$, cf. fig. 3.16 and 3.17. Error bars were estimated as explained in the caption in fig. 3.16.

3.4.7 Fit of the convoluted Poisson-Neyman statistics to the experimental data

Neyman statistics takes into account both the Poisson-stochastics of particle traversals and the Poisson-stochastics of the number of aberrations induced by a single particle hit. However, in case of high energy particle exposure these processes are not independent, e.g. for 990 MeV/u energetic ions, overlap effects from different particle tracks cannot be neglected (see fig. 1.6b). As a first approximation, the distribution of aberrations in lymphocytes after exposure to high energy Fe-ions (155 keV/ μm) was compared to the convoluted Poisson-Neyman statistics (see eq. 2.12) which takes into account that the aberrations are induced by both the dose distributed in the center part of the particle traversal (Neyman component) and the dose distributed like X-rays from the outer part of the particle traversal (Poisson component).

In order to estimate the effect caused by the dose from outer part of a particle traversal, the dose homogeneously distributed, i.e. the background dose, was assumed that the dose is similar to X-rays. Based on the level of the estimated background dose the probability for the induction of additional aberrations were calculated. For example, background dose is 0.5 to 1 Gy for exposure to $9 \times 10^6/cm^2$ 990 MeV/u Fe-ions (see fig. 1.6b). The number of aberrations per lymphocyte induced by ~ 0.5 Gy X-rays was about 0.25 obtained by the dose response curves of the aberrations measured in first metaphases (fig. 3.5, e). Therefore, the parameter in Poisson component is $a = 0.25$ for samples exposed to $9 \times 10^6/cm^2$ (2.3 Gy).

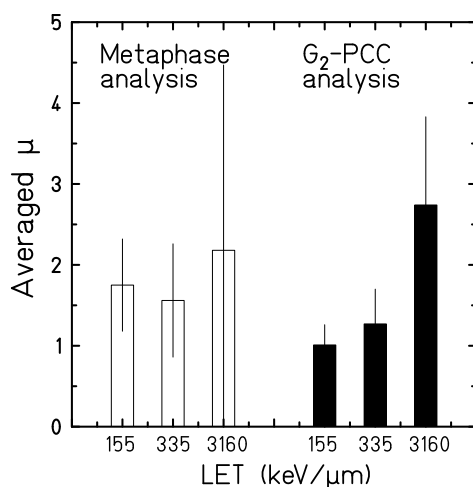


Figure 3.19: LET dependence of the parameter μ derived by metaphase analysis (white columns) and G_2 -PCC analysis (black columns). The μ corresponds to the mean number of aberrations per particle traversal through a cell nucleus. The μ values were averaged by different doses and fixation times. Vertical bars represent standard deviation.

When the parameter was set as $\lambda=2$ in the distribution of cells at 48 h after exposure to 2.3 Gy Fe-ions based on the physical number of particle traversal, the second Neyman parameter was calculated as $\mu=1.5$ by eq. 2.25. Similarly, for each distribution parameter λ was evaluated separately by fixing $\mu=1.5$ and a value estimated from the background dose (i.e. $a=0.12$, 0.25 and 0.33 for cells irradiated with 1, 2,3 and 3 Gy Fe-ions).

The analysis shows that the convoluted Poisson-Neyman fit agreed well with experimental data. For example, the convoluted Poisson-Neyman fit to the experimental data in cells 60 and 84 h after exposure to 1 Gy 990 MeV/u Fe-ions is shown in fig. 3.15. When χ^2 values are compared between different statistical fits, averaged χ^2 value in 12 distributions was 0.20 ± 0.15 for Neyman fits to experimental data as analyzed in section 3.4.2 and 0.23 ± 0.12 for convoluted Poisson-Neyman fits, providing evidence that the both statistical fits similarly agreed well with the experimental data. However, convoluted Poisson-Neyman statistics was better to fit with the experimental data than the Neyman statistics because the former statistics describes better than the latter the cytogenetic effects induced by high energy Fe-ions. For Neyman fits to the experimental data the increase in λ values was dose- and time-dependent, while μ values scattered from 1.1 to 2.7 in 12 distributions revealing no clear trend. On the other hand, experimental data were fit to a convoluted Poisson-Neyman statistics with fixed parameters a and μ and fluence dependent increase in λ . These results clearly shows that chromosome aberrations in lymphocytes after exposure to high energy Fe-ions are induced by the contribu-

tions of two factors: the direct hit of a particle to cell nucleus and the homogeneous dose from the outer part of a particle traversal.

3.5 Radiation-induced apoptosis

To examine to what extent programmed cell death occurs after irradiation, samples were stained with fluorescent dyes and apoptotic cells were identified by characteristic morphological changes of the cell nucleus and the cell membrane (section 2.4.1). The apoptotic response was analyzed at several time-points after irradiation with X-rays, 29 keV/ μm C-ions, 155 keV/ μm and 335 keV/ μm Fe-ion and 3160 keV/ μm Cr-ions (e.g. fig. 3.20). Up to now apoptosis studies focused on resting lymphocytes and several reports related to high LET effects are published (Meijer et al., 1998; Boreham et al., 2000; Wilkins et al., 2002), while studies on high-LET induced apoptosis in PHA-stimulated cells are not available. Since the analysis of cytogenetic damage in G_2 -PCCs and metaphase cells requires proliferating lymphocytes, apoptosis was also analyzed in cycling lymphocytes (section 2.4.1) and the response was compared to that of resting cells. Additionally, after X-ray and C-ion exposure the TUNEL-assay was performed to verify the data obtained by the morphological analysis (for details see section 2.4.2).

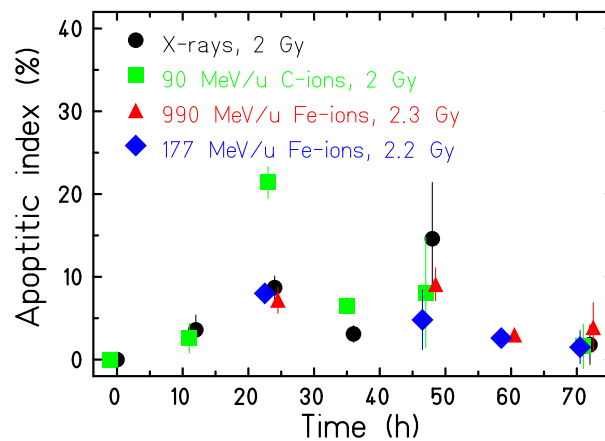


Figure 3.20: Time-response of the apoptotic index in proliferating lymphocytes after irradiation with similar doses of X-rays, 90 MeV/u C-ions (29 keV/ μm), 990 MeV/u Fe-ions (155 keV/ μm) or 177 MeV/u Fe-ions (335 keV/ μm). At each time point the apoptotic index was normalized to the control level. Error bars are standard deviation of 3 measurements on the same slide.

3.5.1 Analysis of the effects of sampling time, dose, LET and inter-experimental variations in proliferating lymphocytes

Analysis of the time-course of apoptosis in stimulated lymphocytes showed that the frequencies of apoptotic cells were $<0.4\%$ in control and irradiated samples directly after initiation of the cultures. In control cultures harvested at later times (12-72 h), the frequency of lymphocytes undergoing apoptosis was $7.0 \pm 3.6\%$ (mean \pm SD from eight experiments, data not shown). Following irradiation the apoptotic index was higher than in the control and tended to reach a maximum between 24 and 48 h post-irradiation. Exemplarily, the time-course of apoptosis induced by ~ 2 Gy X-rays, 29 keV/ μm C-ions, 155 keV/ μm and 335 keV/ μm Fe-ions is shown in fig. 3.20. Analysis of apoptosis by the TUNEL-assay, that detects late apoptotic cells like the applied morphological technique, confirmed this trend (data not shown).

To simplify the comparison of the different data sets, the time-averaged apoptotic indices were determined (2-5 measurements per dose) and normalized to the control level. As shown in fig. 3.21, in all experiments the number of apoptotic cells increased with dose (fluence). Owing to technical reasons only one dose-response curve was generated for Fe-ions and Cr-ions. However, for X-rays and

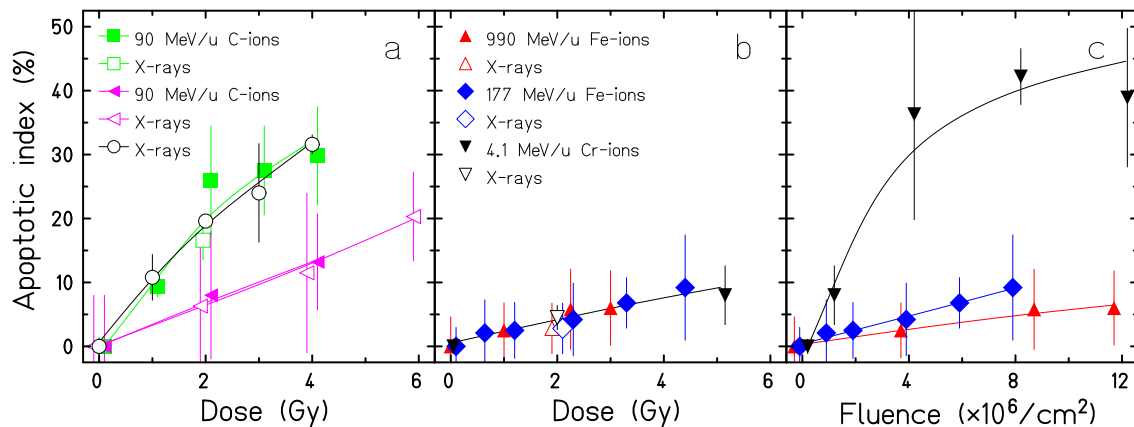


Figure 3.21: Apoptosis in stimulated lymphocyte cultures after exposure to X-rays, 90 MeV/u C-ions with 29 keV/ μm (a), 990 and 177 MeV/u Fe-ions with 155 and 335 keV/ μm , respectively (b, c) and 4.1 MeV/u Cr-ions with 3160 keV/ μm (b, c). For each dose the apoptotic indices were averaged over sampling times and the mean value normalized to the control level was determined. In parallel to particle exposure (closed symbols) aliquots of the cell suspension were irradiated with 2 Gy X-rays (open symbols). Same symbols were used for panel b and c. Error bars are standard deviation of 2-5 measurements between 12 and 72 h post-irradiation.

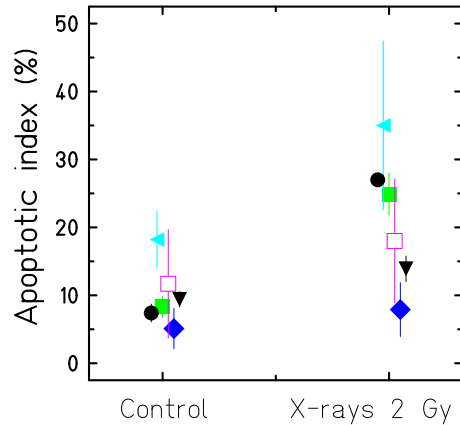


Figure 3.22: Time-averaged apoptotic index detected in proliferating control samples and lymphocytes irradiated with 2 Gy X-rays among six independent experiments. Same symbols were used for control and corresponding X-ray data performed at the same time. Error bars are standard deviations of 2-5 measurements performed between 12 and 72 h post-irradiation.

C-ions two independent experiments could be performed, revealing pronounced inter-experimental variations, although cells of the same donor were used: when the apoptotic indices were compared between the two X-ray experiments, a threefold difference was found (fig. 3.21a). In the same way, the apoptotic indices obtained in two experiments for cultures irradiated with 29 keV/ μm C-ions differed threefold. As mentioned before, in parallel to particle exposure an aliquot of the cell population was exposed to 2 Gy X-rays to account for inter-experimental variations. Accordingly, when the time-averaged apoptotic index induced by 2 Gy C-ions is compared with the corresponding yield induced by 2 Gy X-rays (fig. 3.21a), the effectiveness of both radiation qualities was found to be similar, i.e. RBE=1. Furthermore, as shown in fig. 3.21b, 155 keV/ μm , 335 keV/ μm Fe-ions and 3160 keV/ μm Cr-ions generated a similar apoptotic response and the apoptotic indices were lower than those measured in the cultures exposed to isodoses of C-ions. However, when the proportions induced by 2 Gy heavy ions were compared with the corresponding X-ray data to account for inter-experimental variations, the effectiveness of X-rays, middle and high energy heavy ions for the induction of apoptosis was found to be similar. Consequently, within the LET range investigated, the RBE of particles for the induction of apoptosis is ~ 1 .

Moreover, while after exposure to 5 Gy Cr-ions a low apoptotic index (8 %) was detected, a significant increase in the yield of apoptotic cells was found in cells exposed to 20 to 60 Gy corresponding to particle fluences of 4 to 12×10^6 ions/ cm^2 . As can be inferred from fig. 3.21c in this dose range the frequencies of Cr-ion

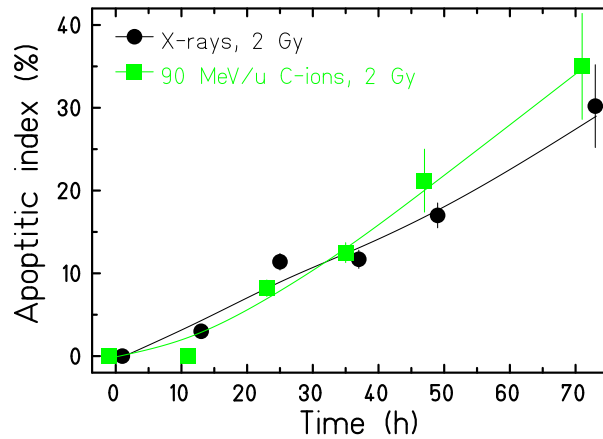


Figure 3.23: Time-response of the apoptotic index in non-proliferating lymphocytes after irradiation with 2 Gy X-rays or 90 MeV/u C-ions (29 keV/ μm). Both experiments were done in parallel. Data were normalized to the control level. Error bars are standard deviation of three measurements on the same slide.

induced apoptotic cells saturated. The analysis of the fluence-response curves showed that similar fluences of 335 keV/ μm Fe-ions were slightly more effective than 155 keV/ μm Fe-ions, whereas 3160 keV/ μm Cr-ions were most effective in inducing apoptosis.

Further insights into experiment-to-experiment variability were gained by the comparison of the apoptotic response of stimulated lymphocytes after exposure to 0 and 2 Gy X-rays obtained in six independent experiments. As described above, time-averaged apoptotic indices were determined and compared (fig. 3.22). In control cultures, the time-averaged apoptotic indices ranged from 5 to 18 %, while after exposure to 2 Gy X-rays indices from 8 to 35 % were measured. As can be inferred from fig 3.22, in three experiments the apoptotic index measured after 2 Gy X-irradiation was 1.5 to 1.6 times higher than in the controls, while in the other experiments the yield was two times higher in irradiated than control sample. Altogether these X-ray data confirm, that there is a pronounced variations in the apoptotic response, even if cells from the same donor are investigated.

3.5.2 Time-course of apoptosis in non-proliferating lymphocytes

Since human lymphocytes reside within the body in a resting state, the G_0 -phase, apoptosis was also measured in non-proliferating cultures. Due to limited beam time, only the effects of X-rays and 29 keV/ μm C-ions were studied. Both experiments were done in parallel. Immediately after irradiation, few apoptotic cells were found (<0.4 %) in unirradiated and irradiated cultures (fig. 3.23). At later

time points (12-72 h) the spontaneous frequencies of apoptotic cells were 3 to 4.5 %. However, after exposure the percentage of apoptotic cells increased with time yielding similar values for both radiation qualities. This time-dependent increase is in contrast to the response of stimulated lymphocytes (fig. 3.20) where the apoptotic index rose slightly up to 24-48 h after exposure, and decreased at later times. This difference in the time-course of apoptosis can be explained by the fact, that in stimulated cultures the number of apoptotic cells is diluted due to cell division, while in non-cycling cultures apoptotic cells accumulate.

Chapter 4

Discussion

4.1 Biological effects of high LET radiation: importance for cancer therapy and manned space explorations

A better knowledge of the biological action of charged particles is of fundamental interest for the application of particle beams in cancer therapy and the health risks posed to crew members in space. In this context, the measurement of the induction of chromosome aberrations gives an indication to judge the risk of late effects like secondary tumor induction after heavy ion therapy. C-ion therapy has several advantages compared to conventional photon therapy. This includes an increased relative biological effectiveness at the end of the particle range (fig. 1.8) and a favorable depth dose distribution to a normal tissue and tumor (fig. 1.2). Following ion treatment high local control rates for tumors and mild early (acute) side effects are reported (e.g. Tsujii et al., 2004; Schulz-Ertner et al., 2004). However, due to the short follow up time, there is little information on late effects like the induction of secondary tumors or fibrosis. Late effects in normal tissue are of great importance for the applicability of C-ion radiation therapy, especially for the treatment of young patients having a long life expectation (Blakely and Chang, 2004).

The major health risks of space flights result from the exposure to cosmic rays. Astronauts in the Earth orbit or outer space receive at least 300 times higher doses than on Earth (NASA, 1997). In addition, the composition of space radiation is different from radiation on Earth. The radiation in space consists mainly of charged particles from protons to Fe-ions (fig. 1.1 and section 1.1). Curtis and Letaw (1989) have estimated the number of particle hits per cell nucleus during a 3-year mission to Mars. Assuming that the average size of a cell nucleus is $100 \mu m^2$ and an aluminum shielding of $4 g/cm^2$ is used, 400 protons and 36 helium particles will traverse each cell nucleus of a human body during this time. Much lower numbers of particle hits were calculated for heavier ions. Among these Fe-ions are of major concern because the probability that a Fe-particle hits a cell nucleus is higher than for ions with $Z \geq 15$. Moreover, the contribution of Fe-ions to the dose equivalent

from the different components of space radiation is high (NASA, 1998), because the radiation dose is proportional to the square of the atomic number (see eq. 1.1 to 1.3).

Information on the dose and the possible health risks associated with radiation exposure can be obtained by the measurement of chromosome aberrations. Chromosome aberrations are a sensitive biomarker which reflects the effects of misrepair of DNA-damages in the genome (section 1.3.2). They are used since more than four decades to quantify the dose to which humans are exposed (overview in IAEA, 2001) and epidemiologic studies have shown that the chromosome aberration yield in peripheral blood lymphocytes correlates with cancer incidence (Bonassi and Au, 2002; Norppa, 2004). To improve the knowledge on the cytogenetic effects of C- and Fe-ions, in the present work aberrations were measured in peripheral blood lymphocytes, which are used *in vivo* and *in vitro* studies (see section 1.4).

4.2 Cytogenetic analysis for radiation risk assessment

4.2.1 Metaphase analysis at single versus multiple sampling times

As described above (section 1.4 and 4.1), chromosome aberrations in lymphocytes are used to estimate the dose to which an individual was exposed, either occupational or accidentally. According to the routinely applied protocol, aberrations are measured in first cycle metaphases collected 48 h after initiation of the culture (IAEA, 2001, and references therein). Then, the yield of aberrations is compared to a dose-response calibration curve, that has been produced by the exposure of blood cells *in vitro* to the same radiation quality. However, evidence is growing that the standard protocol is not reliable after heavy ion exposure (see section 1.3.3 and 1.4.2).

One important factor that may influence the observed frequency of aberrations in lymphocyte cultures is the time of sampling. Heavy charged particles produce more pronounced cell cycle delays than sparsely ionizing radiation (Collyn-d'Hooghe et al., 1981; Scholz et al., 1994; Ritter et al., 1996) and extended time-course studies performed at GSI with rodent cell lines (Nasonova et al., 1998; Ritter et al., 2000, 2002b) or human fibroblasts (Nasonova et al., 2004) have shown that these delays correlate with the number of aberrations harbored by a cell (Gudowska-Nowak et al., 2005, and references therein). If the same holds true for human lymphocytes, the cytogenetic effects of heavy ions will be considerably underestimated, when metaphases are analyzed at one early sampling time as recommended by IAEA (2001). However, only few investigations addressed this question, but they did not examined the full kinetics of aberrations (Anderson et al., 2000; George et al., 2001; Ritter et al., 2002a; Nasonova and Ritter, 2004). Most cytogenetic

studies performed up to now followed the standard protocol and applied one sampling time (Gerasimenko et al., 1980; Edwards et al., 1994; Edwards, 1997; Wu et al., 1997; Testard et al., 1997; Ohara et al., 1998; George et al., 2003).

To gain more insights into the time-course of heavy ion induced chromosomal damage and its LET-dependence, lymphocytes were exposed to particles with LET values in the range of 29-3160 keV/ μm (table 2.1) and aberrations were measured in first cycle metaphase cells collected at multiple sampling times (48-84 h). For comparison, a X-ray study was performed (tables A.1 to A.5). As shown in fig. 3.5e, after the exposure of human lymphocytes to X-rays a stable aberration yield was measured. After exposure to low LET C-ions a minimal increase in the number of aberrations with sampling time was observed (fig. 3.5f). In contrast, after exposure to particles with LET \geq 155 keV/ μm a pronounced rise in the aberration yield occurred (fig. 3.5g,h and 3.6 right) and the extent of this effect depends on LET demonstrating that metaphases collected at a single sampling time after high LET exposure are not representative of the whole cell population. Together with recent information on the time-course of aberrations in human lymphocytes the following trend is visible: after exposure to γ -rays or X-rays (fig. 3.5e; Anderson et al., 2000; George et al., 2001; Hoffmann et al., 2002; Ritter et al., 2002a) or particles with values \sim 30 keV/ μm (fig. 3.5f; George et al., 2001) no or only a minor effect of sampling time on the aberration yield is found. For LET values in the range of 70-160 keV/ μm the aberration yield increases up to three-fold (fig. 3.5g; Anderson et al., 2000; George et al., 2001; Nasonova and Ritter, 2004), for LET \sim 350 keV/ μm seven-fold (fig. 3.5h; Ritter et al., 2002a) and for LET \sim 3000 keV/ μm 20-fold (fig. 3.6 right).

These differences in the time-course of high and low LET induced chromosome damage reflect the spatial energy deposition of both radiation qualities (see also section 4.5). When samples are exposed to sparsely ionizing radiations which deposit the energy fairly uniformly, a homogeneous distribution of aberrations and delay times are induced within the cell population. In contrast, after exposure to high-LET particles, the energy is non-randomly distributed (see fig. 1.6, section 1.2.2) resulting in a different number of particle hits per cell nucleus. Accordingly, cells with a quite different number of aberrations and consequently quite different delay times are found. This effect has been confirmed by the analysis of the frequency distributions of aberrations (see fig. 3.14 and 3.15). The effect of sampling time on the estimated RBE will be discussed in following section.

4.2.2 RBE estimates based on metaphase data

Based on the dose-response curves of chromosome aberrations in first generation metaphases, RBEs were derived. As shown in fig. 3.10 (left), the obtained RBE values reflect the differences in the time-course of X-rays and particle induced chromosomal damage. Following exposure to 29 keV/ μm C-ions, similar RBEs were

derived for early and late arising first cycle metaphases, i.e. the RBE ~ 2 at any time. On the other hand, after irradiation with heavy ions with $\text{LET} \geq 155 \text{ keV}/\mu\text{m}$, RBEs increased with sampling time, e.g. for $335 \text{ keV}/\mu\text{m}$ Fe-ions from 0.44 at 48 h to 3.2 at 84 h, respectively. A similar time-dependent rise in RBE values after high LET exposure was reported for Chinese hamster cells (e.g. Ritter et al., 1996, 2000, 2002b). However, as mentioned above, systematic studies using human lymphocytes have not been performed up to now. Although Anderson et al. (2000) and George et al. (2001) applied several sampling times after high LET exposure, RBE values were not derived, because only one or two dose points were examined and small numbers of cells were scored.

Altogether, the available time-course data (fig. 3.10, Anderson et al., 2000; George et al., 2001) indicated that the conventional method of metaphase analysis 48 h after the stimulation of lymphocytes allows a reasonable estimation of chromosomal damage induced by low LET radiations, i.e. similar RBE values will be derived for early and late appearing first generation metaphases. However, in the case of high LET exposure the true frequency of aberrations will be considerably underestimated, because heavily damaged and drastically delayed cells are excluded from the analysis. In contrast, when lymphocytes are collected at one late sampling time, after high LET exposure the RBE might be overestimated, because the sample is dominated by heavily damaged cells (Ritter et al., 2000, 2002b; Gudowska-Nowak et al., 2005). Therefore, radiation risk assessment based on aberration analysis at one sampling time is not reliable for high LET particles. Alternative approaches will be discussed in the next section.

4.3 Application of new methods for a more reliable biodosimetry

As described above (section 4.2) due to differences in the time-course of high and low LET induced chromosomal damage, derived RBE values will depend on the sampling time chosen for the analysis. To account for this effect, alternative approaches have been proposed, i.e. the integration analysis and the G_2 -PCC assay. Both methods were applied in the present study and the obtained RBE values are compared with those derived from standard metaphase analysis.

4.3.1 Integration analysis

The basic idea of this method is to collect all first cycle metaphases by using several sampling times covering the whole time-interval of the first post-irradiation mitosis (Scholz et al., 1998). Then, at each sampling time the fraction of aberrant cells and the number of aberration are determined and weighted with the corresponding corrected mitotic index (eq. 2.3 to 2.5). Finally, the data are integrated yielding

the total number of aberrant cells and aberrations (eq. 2.6 and 2.7, for more details see section 2.5.1).

In the present study, the integration analysis has been applied for the first time to data measured in human lymphocytes. For X-rays, 29 keV/ μm C-ions and 335 keV/ μm Fe-ions time-course studies with multiple sampling times (≥ 15) covering the time interval from 30 to 90 h post-irradiation were performed.

Analysis of the aberration yields induced within the whole population revealed that C-ions are more effective than X-rays (fig. 3.13 right) in line with data obtained at single sampling times (fig. 3.10). In contrast, the number of aberrations induced by 335 keV/ μm Fe-ions and X-rays was similar in the dose range 0-2 Gy resulting in RBE \sim 1. With increasing Fe-ion dose no further rise in the total aberration yield was observed. Consequently, for doses >2 Gy the RBE is much smaller than one. The saturation effect after Fe-ion exposure is attributable to the low number of lymphocytes capable of reaching the first mitosis (fig. 3.12). Measurements of the mitotic indices (fig. 3.3) and the fractions of cells arrested in G_2 -phase (fig. 3.4) confirm this conclusion. Altogether these data show that after high LET exposure aberration yields measured at single sampling times are not representative of the whole cell population and will result in misleading interpretations. In contrast, for low LET exposure measurements at single times are adequate.

Although the integration analysis provides more precise information on the biological effectiveness of high LET particles, their use as a routine method for biological dosimetry is not practical. The assay requires ≥ 15 times more cells than the classical method and in case of overexposures this amount is not available. Furthermore, the technique is labour-intensive but in case of radiation accident, information on the dose is needed within a few days.

However, the application of the integration analysis in radiobiological *in vitro* studies allows the detection of cell-type specific differences in the expression of cytogenetic damage. For normal human fibroblasts, a saturation of the total aberration yield was already observed after the exposure to low doses of sparsely ionizing radiation (Nasonova et al., 2004), an effect attributable to a dramatic permanent cell cycle arrest of heavily damaged cells. In contrast, the dose-response curves of the integrated aberration yields generated for Chinese hamster V79 cells increased steeply over a wide range of LETs (2-4000 keV/ μm). Accordingly, 40-80 % of the initial cell population were collected in mitosis (Ritter et al., 2000, 2002b). The data obtained in the present study (fig. 3.13) indicate that human lymphocytes in comparison to human fibroblasts and rodent cell lines are characterized by an intermediate radiosensitivity. These cell type specific differences in the expression of radiation-induced chromosomal damage remain undetected, when aberrations are only scored at a single sampling time.

4.3.2 Chromosome aberration measurement in G_2 -PCCs

To overcome the problems resulting from selective mitotic delay of heavily damaged cells, the application of the PCC-technique has been proposed (Durante et al., 1998; Kanda et al., 1999). According to the protocol, PCC is induced by chemicals such as calyculin A and okadaic acid and cytogenetic damages are analyzed in prematurely condensed first cycle G_2 -phase cells (section 1.4.3). Most studies performed up to now restrict the analysis to cells collected at single time-point, mainly 48 h post-irradiation (Durante et al., 2002; Ritter et al., 2002a; George et al., 2003; Nasonova and Ritter, 2004; Johannes et al., 2004). George et al. (2001) scored aberrations in G_2 /M cells collected at 48 and 72 h and found similar aberration yields in cells fixed at both times. However, because in this study cell generations were not differentiated, cell cycle effects are masked (see section 1.3.4).

To examine in more detail to what extent the G_2 -assay accounts for cell cycle delays, the yields of aberrations found in G_2 -cells were compared to the yields measured at the same sampling time in metaphase cells. At any dose- and time-point higher numbers of aberrations were detected in G_2 -PCCs (see tables A.1 to A.10) confirming that heavily damaged cells are arrested in G_2 . For lymphocytes exposed to ≤ 155 keV/ μm particles, the difference was about two-fold at any sampling-time. On the other hand, for particles with higher LET, the difference became larger. For example, 48 h after exposure to 335 keV/ μm Fe-ions >12-times more aberrations were detected in PCC-samples compared to metaphases. Consequently, when the PCC-data at 48 h are used for RBE estimation, much higher values are obtained than in the standard metaphase assay (compare fig. 3.10 left and right panel).

Analysis of the time-course of aberrations in G_2 -PCCs 48-84 h post-irradiation showed after irradiation with X-rays or 29 keV/ μm C-ions only minimal changes in the aberration yield with time (fig. 3.8e,f), while after exposure to particles with LETs ≥ 155 keV/ μm the frequency increased at later sampling times (fig. 3.8g,h and 3.9 right). However, this effect was less pronounced than that observed in metaphases (fig. 3.5 and 3.6) demonstrating that the G_2 -PCC assay accounts to a large part for the selective delay of heavily damaged cells after high LET exposure. Since the aberration yield observable in G_2 -PCCs increases with time for particles with LET ≥ 155 keV/ μm , the obtained RBE values are also time-dependent (fig. 3.10 right). Consequently, also the PCC-assay will underestimate the true frequency of aberrations produced by high LET heavy ions, when aberration analysis is continued to cells collected at 48 h as suggested by Durante et al. (1998) and Kanda et al. (1999).

4.4 Factors that may confound the yield of radiation-induced chromosome damage

4.4.1 Radiation-induced cell cycle effects

To investigate how particle-induced cell cycle delays influence the expression of chromosome aberrations in metaphase cells, the cell cycle progression was monitored by several methods. These include the determination of the BrdU-labeling index and the mitotic index (section 3.1.1 and 3.1.2), a detailed PCC cell-cycle analysis (section 3.1.3, tables A.6 to A.10) and an quantitative estimate of the number of cells capable to progress to the first mitosis post-irradiation (section 3.3.1).

The cumulative BrdU-labeling index was measured to estimate the fraction of lymphocytes that left the G_0 -phase after irradiation and moved to S-phase or later cell cycle stages (see section 2.3.2). Analysis of the labeling curves (e.g. fig. 3.1 left) revealed that in control cultures BrdU-positive cells appeared at ~ 30 h after stimulation. After exposure a delayed entry into mitosis was observed. To facilitate a comparison of the different data sets, the labeling indices measured at 72 h were normalized to the control level and plotted: as shown in fig. 3.2 (left panel), in all experiments the number of BrdU-labeled cells decreased with dose. When isodoses were compared, the effectiveness of X-rays and particles with $LET \leq 335$ keV/ μm was found to be similar, while particles with $LET = 3160$ keV/ μm were less effective resulting in RBEs of ~ 1 and 0.4, respectively. A fluence-based analysis showed that the traversal of a high LET particle through a cell nucleus delays the cell cycle progression more than a hit by a particle with lower LET (fig. 3.2, right panel). Altogether the labeling data indicate that the delayed movement of cells into S-phase is one of the reasons contributing to mitotic delay. However, S-phase delay is not a major confounding factor for measuring high LET induced chromosome aberrations (fig. 3.2, left panel), because over a broad range of LET values (2-335 keV/ μm) isodoses induced a comparable delay.

Further, information on radiation-induced cell cycle progression delays was obtained by the measurement of the mitotic index and the determination of the proportion of metaphases in the first, second or a later cell generation. In irradiated cultures a delayed entry of lymphocytes into mitosis and a lower mitotic activity was observed than in control populations (tables A.1 to A.5; fig. 3.3, left panel). Owing to the pronounced fluctuation in the mitotic indices the fine structure of the kinetics is masked. When the data for first cycle metaphases were analyzed, the delayed entry of cells into mitosis was reflected in a shift of the peak mitotic index to later times (fig. 3.3, right panel). Furthermore, these data clearly show that with increasing dose and LET less cells were able to enter the first post-irradiation mitosis. A dose- and LET-dependent effect was also reported by George et al. (2001). However, George et al. were unable to detect the pronounced radiation-induced

suppression of the mitotic activity clearly seen in fig. 3.3, because they determined only the proportion of cells in first or later mitosis, but not the mitotic index.

An quantitative estimate of the proportion of lymphocytes able to reach the first mitosis can be obtained by the integration analysis (see section 2.5.1; fig. 3.11). As shown in fig. 3.12, in all experiments the total fractions of cells reaching first mitosis decreased with dose. As expected, the effect was similar for cultures irradiated with X-rays and 29 keV/ μm C-ions, while 335 keV/ μm Fe-ions were more effective resulting in RBE-values of ~ 1 and 3, respectively. Furthermore, the integration analysis revealed that only 19 to 28 % of control cells progressed to the first mitosis (section 3.3.1; fig. 3.11, right panel). These low yields can be attributed to the fact that the cell populations used for the experiments contained besides T-lymphocytes other blood cell types (IAEA, 2001). Indeed, immunostaining showed that ~ 70 % of the population were T-lymphocytes, 10 % B-lymphocytes, 10 % monocytes and 10 % granulocytes (S. Conrad, unpublished data). Moreover, not all subsets of T-lymphocytes can be stimulated by PHA (e.g. Azzolina et al., 1990).

Finally, in samples prepared for chromosome aberration analysis in G_2 -cells, the cell cycle stages and the cell generation of prematurely condensed cells were determined. PCC-studies performed up to now (Durante et al., 1998; Kanda et al., 1999; Gotoh et al., 2005) reported only the PCC-index, but a detailed analysis of the cell-cycle distribution is lacking. Analysis of the data sets summarized in tables A.6 to A.10 shows that human lymphocytes suffered a prolonged arrest in the first G_2 -phase after exposure, i.e. at 60 and 72 h larger fractions of first cycle G_2 -PCCs were observed in irradiated samples compared to control cultures. This effect depends on dose and LET as exemplarily shown in fig. 3.4 (left): at 72 h in the control culture ~ 20 % of all PCCs were first generation G_2 -cells. However, after exposure to ~ 2 Gy X-rays and 335 keV/ μm Fe-ions the proportion increased to 40 and 70 %, respectively. Since at ≥ 72 h only low numbers of first cycle metaphases are found (see tables A.1 to A.5, fig. 3.4), it is reasonable to assume that most of the cells accumulated in G_2 will never proceed to mitosis and thus, escape detection in a metaphase assay (section 1.4.1). Apparently, G_2 -arrest is an important factor that should be considered for biological dosimetry.

4.4.2 Spectrum of aberrations

A further problem which affects the accuracy of biodosimetry is the LET-dependent changes in the spectrum of aberrations. In most studies only the number of dicentric has been recorded (e.g. Edwards, 1997; Ohara et al., 1998; IAEA, 2001; Di Giorgio et al., 2004) and it has been assumed that the distribution between different aberration types stays independent from radiation quality. In the present investigations, all aberration-types detectable with Giemsa staining were scored in first generation metaphases (section 2.2.3). Chromatid-type aberrations were included, since the induction of chromatid-type aberration in cells irradiated in

4.4 Factors that may confound the yield of radiation-induced chromosome damage

G_0/G_1 -phase is a specific feature of high LET exposure (Ritter et al., 1996, and references therein).

The analysis of the data shows that for a given radiation quality the aberration spectrum did not change with dose or sampling time (see table A.1 to A.5). Therefore, for each aberration-type the time- and dose-averaged frequencies were determined and compared. As shown in fig. 3.7 (left), after X-ray exposure 42 to 52 % of all aberrations were dicentric. This proportion did not change up to LET values ~ 150 keV/ μ m. At higher LET values the frequency decreased reaching 20 % for particles with LET ~ 3000 keV/ μ m. Accordingly, the frequency of breaks comprising both chromosome and chromatid-type breaks increased for LET values >150 keV/ μ m (see fig. 3.7, right). Similar LET-dependent changes were observed in the few studies recording all aberration types detectable by solid staining: this includes studies on human lymphocytes (Gerasimenko et al., 1980; Bauchinger and Schmid, 1998), human fibroblasts (Nasonova et al., 2004) and various rodent cell lines (Durante et al., 1992; Ritter et al., 1996; Nasonova et al., 1998; Ritter et al., 2000, 2002b).

This change in the aberration spectrum has a pronounced effect on the estimated RBE. As shown in fig. 4.1, RBE estimates based on the number of dicentrics are lower than those derived from the sum of aberrations detectable with Giemsa-staining. This effect is minimal for LET ~ 30 keV/ μ m, but pronounced for LET values ≥ 155 keV/ μ m demonstrating that the restriction of the aberration analysis to dicentrics will result in a significant underestimation of the damage produced by high LET particles.

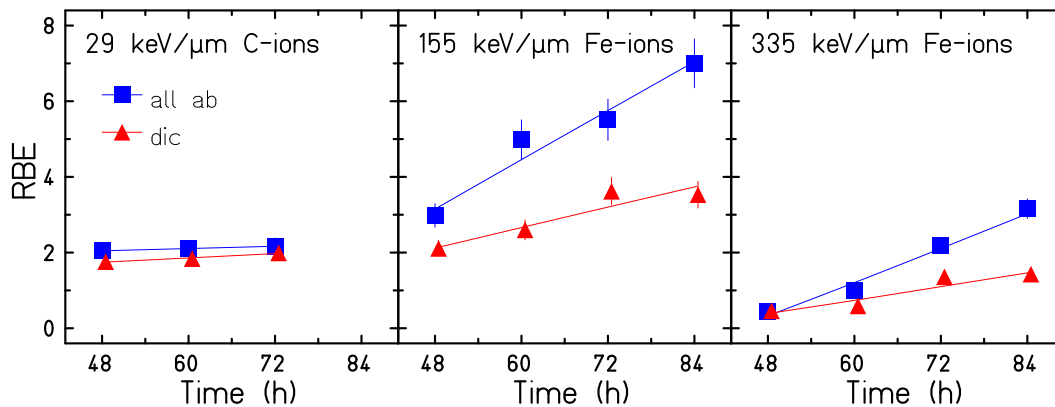


Figure 4.1: Comparison of RBE values of particles for the induction of one chromosome aberration per cell. RBEs were calculated based on the whole number of aberrations visible after Giemsa-staining (all ab, blue square) or on the yield of dicentrics (dic, red triangle) following exposure to 90 MeV/u C-ions (29 keV/ μ m, left panel), 990 MeV/u Fe-ions (155 keV/ μ m, middle panel) and 177 MeV/u Fe-ions (335 keV/ μ m, right panel).

The observed alterations in the aberration spectrum can be explained by changes in the quality of DNA damages as LET increases. As mentioned above (section 1.3.2) modelling studies predict that the yield of clustered lesions increases with LET (Nikjoo et al., 1999) and this has experimentally shown in DNA and chromatin break rejoining studies (Rydberg et al., 1994; Heilmann et al., 1996; Goodwin et al., 1994; Nasonova et al., 2001). More detailed insights into the aberration-types produced by high LET particles are gained by advanced chromosome staining techniques like FISH. Recent FISH studies showed that after high LET exposure the percentage of complex aberrations among the total exchanges is significantly higher than after sparsely ionizing radiation (Griffin et al., 1995; Anderson et al., 2000; Durante et al., 2002). This aberration class originates from three or more breaks in two or more chromosomes and is most likely formed by the interaction of lesions produced close together within a particle track. Data from Griffin et al. (1995) and Anderson et al. (2002) suggest that the induction of a single complex exchange is a consequence of a direct particle traversal through a cell nucleus. In contrast, only after exposure to high doses of X- or γ -rays complex aberrations are formed indicating that they require the interaction of lesions induced by several tracks (e.g. Griffin et al., 1995; Anderson et al., 2000; Durante et al., 2002). In particular, high energy Fe-ions relevant for space research induce a high proportion of complex exchanges. Durante et al. (2002) reported that following exposure to 3 Gy 1 GeV/u Fe-ions (LET: 145 keV/ μ m) 70 % of the cells carried one or more complex aberrations, while the same dose of γ -rays induced only in 20 % of the cells complex aberrations. Since this aberration group is not detectable by solid staining, the aberration frequencies scored in the present study are expected to underestimate the cytogenetic effects of heavy ions. Further time-course studies are in progress to address this problem by combining the techniques of M-FISH (fig. 1.11b) and differential staining of chromatids (fig. 2.2 and section 2.2.2).

4.4.3 Radiation-induced apoptosis

Apoptosis or programmed cell death is a well regulated process that occurs during the normal development of organs and tissues, but is also induced by DNA-damaging agents such as chemicals or ionizing radiation. In the latter cases apoptosis is thought to remove genetically damaged cells from the cell population (see section 1.3.3). Therefore, it can be expected that apoptosis affects the aberration yield observable at metaphase and thus can cause a considerable underestimation of the radiation exposure.

Although DNA-damage induced apoptosis is the typical radiation response of human lymphocytes, little is known on the LET-dependence of this pathway. Most studies on the LET dependence of apoptotic cell death have been performed with rodent cell lines. These studies showed that the RBE increased with LET reaching a maximum of about three at 110-230 keV/ μ m (Sasaki et al., 1997; Aoki et al.,

4.4 Factors that may confound the yield of radiation-induced chromosome damage

2000). However, these results cannot be directly applied to human lymphocytes, because the apoptotic response differs among cell lines as reviewed by Dewey et al. (1995). Also, a recent X-ray study indicates that apoptosis is more pronounced in resting compared to proliferating lymphocyte cultures (Carloni et al., 2001).

Investigations of radiation-induced apoptosis in human lymphocytes were usually performed with resting cells. Meijer et al. (1998) measured apoptosis in resting lymphocytes after exposure to γ -rays and nitrogen ions (LET=140 keV/ μ m) and reported RBE values in the range of 1.3-3.0. For particles with lower LET values such as fast neutrons (LET=20 keV/ μ m) and protons (LET \approx 0.5 keV/ μ m), RBEs \sim 1 were found (Vral et al., 1998; Radojic and Crompton, 2001). However, for proliferating lymphocytes data on the effect of LET on radiation induced apoptosis are not available.

To clarify, to what extent the proliferative status of lymphocytes affects their apoptotic response, radiation-induced apoptosis was compared between cycling and non-cycling lymphocytes after exposure to 2 Gy X-rays or 29 keV/ μ m C-ions. As shown in fig. 3.23, in non-stimulated cultures the number of apoptotic cells increased significantly with time after exposure in line with data reported by several authors (Meijer et al., 1998; Boreham et al., 2000; Wilkins et al., 2002). In contrast, when lymphocytes were stimulated with PHA to enter the cell cycle, the proportion of apoptotic cells increased slightly with time and tended to reach a maximum at 24-48 h. At later times the yields declined to the control level (see fig. 3.20). This decline reflects probably the dilution of the number of apoptotic cells due to division of undamaged cells. Carloni et al. (2001) studied apoptosis in both PHA stimulated and non-stimulated cells following exposure to 1.5 and 3 Gy X-rays and observed the same trend, i.e. a marked increase in the apoptotic index with time in non-proliferating cultures and lower frequencies in proliferating cultures.

To facilitate a comparison of the different data sets generated for proliferating cells (tables A.1 to A.10), the time-averaged apoptotic indices were determined. The data showed that for all exposure conditions the frequency of apoptotic cells increased with dose. However, a pronounced experiment-to-experiment variability was observed, although cells of the same donor were used for all experiments (fig. 3.21a). To account for this effect, the apoptotic indices induced by 2 Gy particles were related to the X-ray yields measured in parallel demonstrating that the effectiveness of X-rays and particles is similar, i.e. RBEs of \sim 1 were derived for all particle exposures. As expected, comparison of the effect induced by the same fluence, corresponding to the same number of particle hits per cell nucleus, showed an increase in the apoptotic index with LET (fig. 3.21c).

Altogether, the data confirm that the apoptotic response of non-stimulated and stimulated lymphocytes differs significantly consistent with the view that stimulation rescues blood lymphocytes from radiation-induced apoptotic cell death (Carloni et al., 2001). The observation that similar doses of charged particles and X-rays show the same effectiveness in experiments using stimulated lymphocytes suggests

that apoptosis is not a confounding factor for cytogenetic studies investigating chromosomal damage in metaphase cells.

4.4.4 Inter-experimental variations

To reduce inter-experimental variations, all studies were performed under the same conditions and for all experiments blood cells from the same donor were used. Therefore, the occurrence of variations in the radiation-response can be interpreted as inter-donor variability. To account for this effect, in all particle experiments an aliquot of the cell population was irradiated with 2 Gy X-rays. This X-ray sample serves as an internal control and allows to distinguish between effects caused by radiation quality and those originating from inter-donor variability.

Only a few studies addressed the problem of variations in the radiosensitivity and its importance for radiation risk assessment. Inter-individual differences have for example been attributed to DNA-repair fidelity, while intra-individual differences have been related to the hormone status (Ricoul et al., 1997). Comparison of the aberration yields measured in first cycle G_2 -PCCs and metaphases of the same donor after exposure to 2 Gy X-rays in four independent experiments (tables A.1 to A.10) showed only small variations ($<15\%$ SD). Similarly, Vral et al. (2004) analyzed cytogenetic damage in lymphocytes of 14 donors by means of the micronucleus assay. Repeated experiments revealed differences in intra-individual variations in the range of 3 to 39 % (SD). In contrast, several authors reported larger variations than those detected in the present study and by Vral et al. (2004). Größer (2002) investigated the aberration yield in lymphocytes of the same donor after exposure to X-rays and C-ions at two occasions and found a two-fold difference. Similarly, Kakati et al. (1986) found an up to four-fold difference, when lymphocytes of the same donor were collected at four occasions. Since in the present study the aberration yields induced by 2 Gy X-rays are similar, it is reasonable to assume, that the generated data sets are not confounded by intra-individual variations in the radiosensitivity and thus, can be directly used for estimating RBE values.

Furthermore, when the frequencies of apoptotic cells were analyzed in both control cultures and samples irradiated with 2 Gy X-rays (six experiments, fig. 3.22), differences up to a factor of four were found (50 % SD). Data on intra-individual variations in radiation-induced apoptosis in lymphocytes stimulated with PHA that can be used for comparison are not available. As mentioned above (section 4.4.3) apoptosis has been generally examined in resting lymphocytes and data are contradictory (Boreham et al., 1996, 2000; Wilkins et al., 2002). However, the observation in this study that variations in X-ray induced chromosomal damage are smaller than variations in the induction of apoptosis suggests that programmed cell death does not affect the observable aberration yields, when proliferating human lymphocytes are investigated.

4.5 Insights into radiation quality gained by the distribution of aberrations among cells

4.5.1 Overdispersion of the frequency distribution in lymphocytes irradiated with high-LET particles

When radiation-induced chromosome aberrations were analyzed in metaphase or G_2 -PCC cells, the number of the different aberrations per cell was recorded providing information on the distribution of chromosome aberrations among the cells (e.g. fig. 3.14 and 3.15). The analysis of the relative variance ($\sigma^2/\langle x \rangle$), that is an useful indicator of the dispersion of a distribution, revealed that the distributions were different for low and high LET radiation. After low-LET exposure, e.g. X-rays and 29 keV/ μm C-ions, the time- and dose-averaged $\sigma^2/\langle x \rangle$ for a given radiation type was 1.0~1.3 showing that the chromosome aberrations observed in metaphases or G_2 -cells are Poisson-distributed (see fig. 3.14). On the other hand, when lymphocytes were irradiated with 155 and 335 keV/ μm Fe-ions and 3160 keV/ μm Cr-ions, the averaged relative variance increased with LET from 2.1 to 7.3 (see section 3.4.1 to 3.4.3 and tables A.11 to A.14). A similar, LET-dependent trend has been reported by Goodwin et al. (1994) for aberrations in Chinese hamster ovary cells after exposure to particles with LET value in the range of 0.6 to 2700 keV/ μm by means of PCC-fusion technique. Edwards et al. (1979, 1980) analyzed dicentrics in human lymphocytes at the first mitosis demonstrating that the $\sigma^2/\langle x \rangle$ was about one for γ -rays and X-rays but >1 for after exposure to neutrons and α -particles.

This differences in the distributions of aberrations induced by low and high LET radiations can be explained by the spatial energy deposition of radiations. For low LET radiation, the doses are uniformly distributed within the cell producing random numbers of events (e.g. chromosome aberrations) as representatively shown in fig. 4.2. Therefore, these distributions can be well described with Poisson statistics as shown in fig. 3.14. In contrast, particles deposit their energies inhomogeneously along the trajectory inducing aberrations which are non-randomly distributed within a cell (see fig. 4.2). For low particle energies, the dose is concentrated in areas much smaller than the cell nucleus and the tracks are randomly distributed over the cell nuclei. Under this irradiation conditions the experimental data were better described by Neyman type A statistics than Poisson statistics (see fig. 3.15) in line with previous studies investigating the distribution of high LET induced aberrations in various mammalian cell systems (Virsik and Harder, 1981; Goodwin and Blakely, 1992; Durante et al., 1994; Ritter et al., 1996; Nasonova et al., 2001; Gudowska-Nowak et al., 2005).

But the assumption of Poisson-distributed tracks where the effects (i.e. the chromosome aberrations) are again Poisson-distributed is not correct. The dose distribution inside the track is not homogeneous causing a Poisson event distribution. It

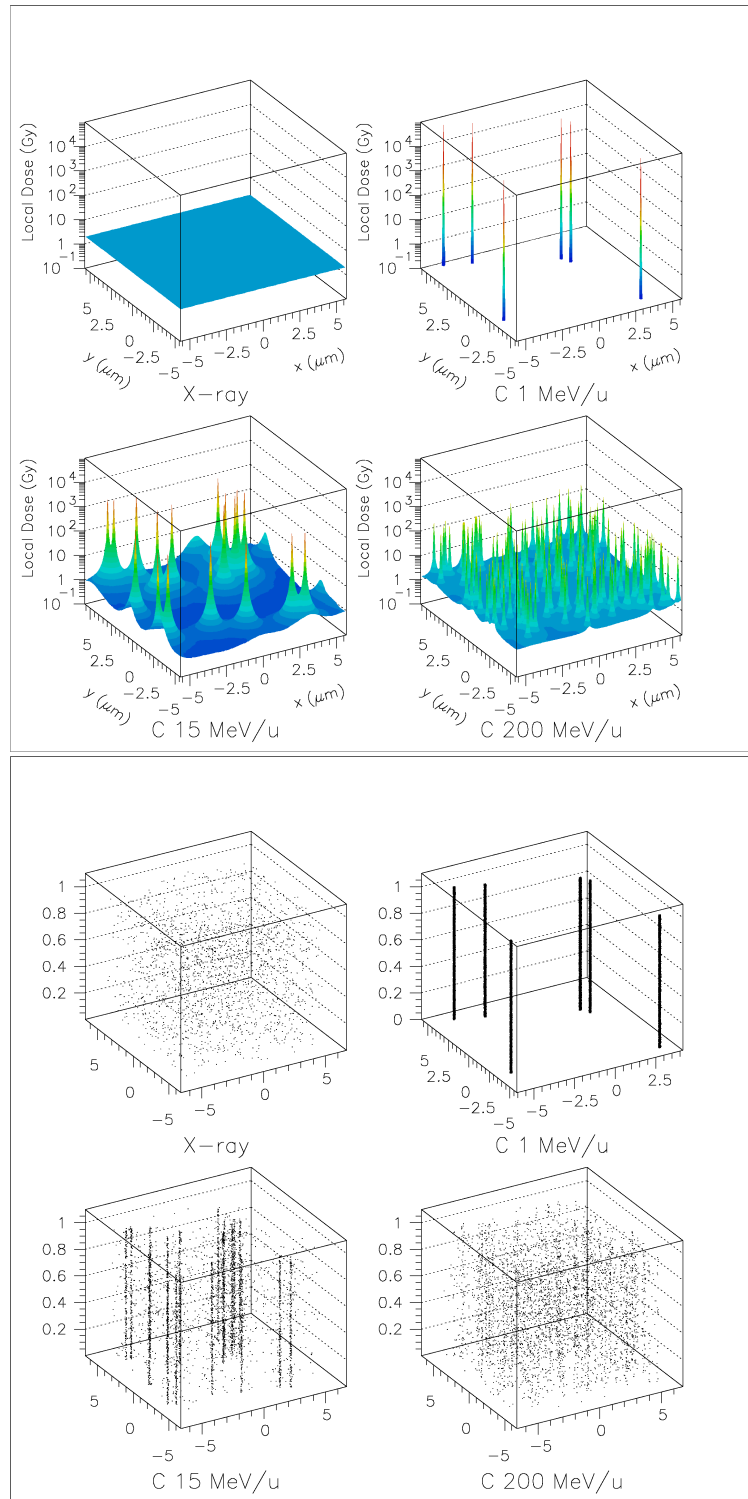


Figure 4.2: Microscopic dose distributions (upper panel) and corresponding event distributions (lower panel) of X-rays or C-ions with different energies in μm scale. For all radiation types, averaged dose is 2 Gy yielding 200 events/Gy/cell (Courtesy M. Scholz).

is rather inhomogeneous (see fig. 4.2) with extreme dose-spikes in the center of the track reaching values of hundreds of kilo Gray for very heavy particles. However, the biological action of these dose-spikes is reduced by early diffusion processes that take place before the biological damage is produced (Brons et al., 2003) and up to now these processes are not quantitatively understood.

In order to simulate the situation at least for the intermediate energies the Neyman type A distribution has been combined with a Poisson distribution: the basic approximation is to simulate the tracks with their high dose area with a Neyman A distribution and to add to this part a background of a more or less homogeneous distributed dose, which is caused by the low dose parts of the tracks at large distances from the center. This is obvious from the fig. 4.2. For 15 MeV/u C-ions nearly half of the dose is dispersed homogeneously over the nuclear volume, while the other half is concentrated in solid tracks. At even higher energies these concentrated parts of the track centers decrease and the homogeneous fraction become more intense (see section 4.5.2).

4.5.2 Analysis of data by Neyman and Poisson-Neyman statistics fit to experimental distributions

Several types of theoretical distributions have already been fit to overdispersed aberration yields. Goodwin and Blakely (1992) compared the initial chromosome breakage induced by high LET particles to a Neyman type A statistics (Poisson-Poisson form) or an other Neyman distribution (Poisson-binomial form) and no significant difference between both approaches. Brame and Groer (2002) claimed that the negative-binomial model is a better descriptor of the dicentric yields measured in human lymphocytes after neutron exposure than the Poisson statistics and in an early study Virsik and Harder (1981) showed that the Neyman type A distribution fits the dicentric aberration frequencies induced in lymphocytes by α -particles better than the negative-binomial statistics.

To address this question, each distribution of aberrations obtained for lymphocytes irradiated with high-LET particles were fit by the Neyman distribution and the parameters λ and μ were determined (table A.12 and A.14, fig. 3.15). As can be inferred from formula 2.11, the Neyman statistics is expressed as a time-independent distributions. However, due to the selective delay of heavily damaged cells (fig. 3.5 and 3.6) the parameter λ changed with time. The analysis revealed that the parameter λ was time- and dose-dependent for cells exposed to 155 and 335 keV/ μm Fe-ions as displayed in fig. 3.16. For example, after irradiation with $12 \times 10^6/\text{cm}^2$ of 155 keV/ μm Fe-ions, the parameter λ increased from 3.0 at 48 h to 9.2 at 84 h. When samples were irradiated with 3160 keV/ μm Cr-ions, derived λ values were time-dependent, but similar for different doses providing evidence that

multiple >3000 keV/ μm particle traversals in a cell nucleus induce cell cycle stop or cell death before reaching metaphase.

In contrast, the parameter μ , which corresponds to the number of aberrations induced by a particle hit in a cell nucleus fluctuated showing no dose- or time-dependence (e.g. table A.12 and A.14). Therefore, the cell cycle delay of heavily damaged cells influenced more the parameter λ than the parameter μ . The increase in λ value with sampling time has already been observed in previous experiments of our group (Ritter et al., 1996; Nasonova et al., 2001; Gudowska-Nowak et al., 2005) performed with V79 Chinese hamster cells. The time-dependence of the λ value reveals that with increasing the number of particles hits per cell nucleus, more chromosome aberrations are produced in the cell and according to the extent of damage, cell cycle is delayed.

Additionally, the distribution of aberrations induced by 990 MeV/u Fe-ions were compared with a convoluted Poisson-Neyman statistics (eq 2.12) in order to take into account the energy deposition of the high energy ions within the cell nucleus (see fig. 4.2). The fit describes well the distribution of aberrations induced by two different quality of the energy deposition: the center part of a particle traversal and the quasi-uniform dose deposition consisted of the outer part of neighboring particle traversals. Moreover, the analysis shows that heavily damaged cells were delayed to enter mitosis and that the delay correlates with the number of direct particle hits.

Chapter 5

Summary

The analysis of radiation-induced cytogenetic damages in human lymphocytes is an established method to estimate both the health risks resulting from radiation exposure and the dose to which an individual has been exposed (IAEA, 2001). The standard assay relies on the scoring of aberrations in first cycle metaphases collected 48 h after initiation of the culture. However, recent data suggest, that this assay results in an underestimation of the effects of high LET exposure due to a pronounced cell cycle delay of heavily damaged cells. Since the delayed entry of severely damaged cells has been attributed to a G_2 -arrest, the analysis of aberrations in G_2 -cells collected 48 h after irradiation by means of chemically induced premature chromosome condensation (PCC), has been proposed as an alternative method.

In this context, human lymphocytes were exposed to X-rays, C-ions (LET: 29 keV/ μm) and Fe and Fe-like particles (155, 335 and 3160 keV/ μm) and the time-course of particle induced chromosomal damage was investigated in detail in metaphase and interphase cells. To account for inter-individual variations in radiosensitivity, for all experiments lymphocytes of the same donor were used. Analysis of aberrations in cells at the first mitosis after exposure to X-rays revealed a relatively stable aberration yield over time. Similarly, after exposure to C-ions the effect of sampling time was minimal, i.e. relative biological effectiveness (RBE) was similar for early and late arising first cycle metaphases. However, after exposure to particles with $\text{LET} \geq 155 \text{ keV}/\mu\text{m}$ the number of aberrations increased drastically with time and this effect was more pronounced with a further increase in LET. Thus, when aberrations are analyzed according to the standard protocol, the true frequency of high LET produced damages will be considerably underestimated, because heavily damaged cells are not included in the analysis.

Similarly, the investigation of the time-course of aberrations in G_2 -phase cells revealed a time-dependent increase after high LET exposure. However, the effect was smaller than that detected by metaphase analysis demonstrating that the G_2 -PCC assay accounts to a large part for the selective delay of heavily damaged cells. Furthermore, when the aberration yields measured at the same time in metaphase

and G_2 -cells were compared, higher frequencies were found in G_2 -cells confirming that aberrant cells are arrested in G_2 .

To account for the different time-course of high and low LET induced damage, the total amount of aberrations induced within the entire population was determined by means of a mathematical approach (Scholz et al., 1998). The method relies on the scoring of aberrations at multiple sampling times together with the corresponding mitotic index. Analysis of the data showed that the total number of aberrations was higher in cultures irradiated with 29 keV/ μm C-ions than in those exposed to X-rays in accordance with data measured at single sampling times. However, the number of aberrations induced by 335 keV/ μm Fe-ions and X-rays was similar in the dose range 0-2 Gy. Consequently, for these Fe-ions RBE=1 is obtained and this value is significantly higher than the value estimated by the standard assay. At higher doses the yields saturate due to a pronounced decrease in the mitotic activity and RBE<1 is estimated.

Furthermore, special emphasis was placed on radiation-induced apoptosis, because this cellular response may influence the aberration yield seen in metaphase cells. The frequency of apoptotic cells was found to increase with dose. Since similar doses of X-rays and charged particles showed the same effectiveness, it can be concluded that apoptosis is not a confounding factor for cytogenetic studies.

Detailed analysis of the frequency distributions of aberrations among metaphase and PCC cells showed that after X-rays or low LET C-ion exposure, aberrations were randomly distributed among cells. This is expected, because both radiation types deposit the dose homogeneously in the cell nucleus. Thus, the obtained frequency distributions agreed well with Poisson statistics. On the other hand, the inhomogeneous dose distribution of high LET particles induced a broad variation in the distribution of aberrations among cells, i.e. distributions were overdispersed. These overdispersed distributions were well described by Neyman or convoluted Poisson-Neyman statistics and revealed that the delay of late arising heavily damaged cells is related to the number of particle hits per cell nucleus.

Appendix A

Tables

Dose (Gy)	Time (h)	BrdU		Cells at 1st cycle (%)	Scored 1st mitoses	Aberrant cells (%)	Aberration types per 100 metaphases							Aberrations per cell	Excess fragments per cell
		LI (%)	MI (%)				ctb	csb	dmin	dic	r	cte	t		
0	48	47	3.7	97.0	300	1	1	0	0	0	0	0	0	0.01	0
	60	71	3.9	30.8	100	0	0	0	0	0	0	0	0	0	0
	72	83	6.5	6.9	100	5	4	1	0	0	0	0	0	0.05	0.01
0.3	48	43	2.1	99.3	300	5	0	3	0	2	0	0	0	0.05	0.03
	60	65	4.5	37.7	100	6	1	3	0	1	1	0	0	0.06	0.04
	72	81	6.2	17.8	100	16	5	9	2	4	0	0	0	0.2	0.11
0.6	48	44	3.3	99.5	300	13	1	8	0	3	2	0	1	0.15	0.09
	60	67	3.3	33.4	100	11	0	4	3	5	0	0	0	0.12	0.07
	72	80	6.0	14.3	100	20	3	6	0	11	1	0	0	0.21	0.07
1.0	48	41	3.3	99.3	100	30	1	15	3	17	1	0	0	0.37	0.20
	60	65	3.4	38.7	100	33	1	15	4	22	0	0	0	0.42	0.19
	72	79	6.2	11.3	100	36	10	13	4	14	0	0	1	0.42	0.16
2.0	48	34	1.6	100	100	71	6	26	11	59	6	1	1	1.10	0.39
	60	62	3.0	50.5	100	63	6	28	16	61	2	0	2	1.15	0.45
	72	73	4.2	14.8	100	68	4	32	8	57	5	1	0	1.07	0.46
4.0	48	35	0.9	100	100	99	9	87	37	168	12	0	10	3.23	1.38
	60	-	2.4	67.9	100	94	9	97	40	187	15	0	6	3.54	1.47
	72	67	3.0	29.4	100	97	13	119	39	171	9	3	12	3.66	1.71

Table A.1: Effects of X-ray irradiation on the frequency of chromosome aberrations in first cycle metaphases, the corresponding mitotic index (MI) and BrdU-labeling index (LI) 48, 60 and 72 h after exposure of human lymphocytes. At further time-points (section 2.2) only the MI, the cell generation of metaphases and the LI were determined. For reasons of space these data are not included in the table. The abbreviated terms for chromosome aberrations are used as shown in fig. 2.3: ctb, chromatid break; csb, chromosome break; dmin, acentric ring; dic, dicentric chromosome; r, centric ring; cte, chromatid exchange; t, translocation.

Dose (Gy)	Time (h)	BrdU		Cells at 1st cycle (%)	Scored 1st mitoses	Aberrant cells (%)	Aberration types per 100 metaphases							Aberrations per cell	Excess fragments per cell
		LI (%)	MI (%)				ctb	csb	dmin	dic	r	cte	t		
0	48	45	2.5	97.8	100	1	1	0	0	0	0	0	0	0.01	0
	60	67	3.0	44.0	100	2	2	0	0	0	0	0	0	0.02	0
	72	77	3.3	14.7	100	3	4	0	0	0	0	0	0	0.04	0
0.3	48	-	1.2	100	100	18	0	6	3	9	0	0	1	0.19	0.09
	60	-	3.1	67.1	100	18	2	8	4	7	3	0	0	0.24	0.15
	72	-	1.7	37.5	100	22	5	5	6	8	2	0	0	0.26	0.13
0.6	48	-	2.8	97.8	100	39	2	17	6	30	0	0	2	0.57	0.23
	60	-	4.6	38.0	100	47	4	38	3	26	0	0	1	0.72	0.41
	72	-	2.6	15.0	100	43	1	20	14	23	1	0	1	0.60	0.35
1	48	43	2.5	99.6	100	62	10	25	10	41	3	1	6	0.96	0.40
	60	66	2.5	45.0	100	60	4	22	13	64	4	0	1	1.08	0.39
	72	74	2.9	14.2	100	69	10	40	6	64	4	0	1	1.25	0.50

Continued on next page

Table A.2: Effects of 90 MeV/u C-ion irradiation (LET=29 keV/ μ m) on the frequency of chromosome aberrations in first cycle metaphases, the corresponding mitotic index (MI) and BrdU-labeling index (LI) 48, 60 and 72 h after exposure of human lymphocytes. At further time-points (section 2.2) only the MI, the cell generation of metaphases and the LI were determined. For reasons of space these data are not included in the table. For further details and abbreviations, see table caption A.1.

Dose (Gy)	Time (h)	BrdU		Cells at 1st cycle (%)	Scored 1st mitoses	Aberrant cells (%)	Aberration types per 100 metaphases							Aberrations per cell	Excess fragments per cell
		LI (%)	MI (%)				ctb	csb	dmin	dic	r	cte	t		
2	48	35	2.4	99.8	200	85	7	61	26	129	6	1	2	2.32	0.92
	60	58	2.0	57.5	100	92	16	59	32	142	23	0	0	2.72	1.14
	72	69	1.8	25.2	100	92	6	85	26	149	21	4	0	2.91	1.33
3	48	35	0.9	99.8	200	96	9	108	39	188	18	3	0	3.65	1.66
	60	57	1.6	73.1	100	100	5	156	51	225	5	1	2	4.45	2.13
	72	66	1.9	36.9	200	99	12	138	68	227	17	4	4	4.70	2.25
4	48	35	0.6	99.9	200	97	7	150	40	246	16	3	3	4.65	2.05
	60	56	1.5	79.9	200	100	12	146	60	315	25	3	2	5.63	2.32
	72	64	1.8	44.6	200	100	9	195	89	298	22	2	4	6.19	3.05
2 X-rays	48	36	1.9	100	100	59	6	28	7	61	1	0	2	1.05	0.37
	60	63	2.7	47.5	100	57	8	32	8	43	3	1	1	0.96	0.43
	72	76	4.1	17.2	100	65	6	37	12	53	1	1	0	1.10	0.51

Table A.2: (continued) Effects of 90 MeV/u C-ion irradiation (LET=29 keV/ μm) on the frequency of chromosome aberrations in first cycle metaphases, the corresponding mitotic index (MI) and BrdU-labeling index (LI) 48, 60 and 72 h after exposure of human lymphocytes. At further time-points (section 2.2) only the MI, the cell generation of metaphases and the LI were determined. For reasons of space these data are not included in the table. For further details and abbreviations, see table caption A.1.

Dose (Gy)	Time (h)	BrdU		Cells at 1st cycle (%)	Scored 1st mitoses	Aberrant cells (%)	Aberration types per 100 metaphases								Aberrations per cell	Excess fragments per cell
		LI (%)	MI (%)				ctb	csb	dmin	dic	r	cte	t			
0	48	58	5.0	96.5	100	4	3	2	0	0	0	0	0	0.05	0.02	
	60	71	5.1	36.0	100	10	7	0	0	0	0	3	0	0.1	0	
	72	74	5.1	10.6	50	6	4	0	0	0	0	0	4	0.08	0	
1	48	44	3.3	100	100	54	8	47	14	71	7	3	0	1.5	0.70	
	60	58	4.6	55.6	100	61	14	78	24	86	19	10	0	2.31	1.22	
	72	71	2.0	21.6	100	67	23	98	19	124	9	11	0	2.84	1.27	
	84	75	4.3	8.5	100	83	32	139	35	122	5	11	0	3.44	1.87	
2.3	48	37	2.3	100	100	81	20	105	36	146	13	5	0	3.25	1.59	
	60	59	2.8	65.0	100	89	20	166	43	227	19	8	0	4.83	2.34	
	72	64	2.0	40.0	100	96	36	266	64	271	24	21	0	6.82	3.58	
	84	59	2.8	17.8	100	94	34	279	68	267	25	18	0	6.91	3.80	
3	48	36	0.7	100	100	91	16	158	46	180	20	13	0	4.33	2.31	
	60	45	1.6	78.5	100	95	16	238	41	223	20	15	0	5.53	3.06	
	72	58	2.5	46.5	100	97	38	345	80	332	32	26	0	8.53	4.74	
	84	61	2.8	31.6	100	99	61	391	78	331	27	32	0	9.20	5.20	
2 X-rays	48	39	2.2	100	100	60	7	38	14	47	3	2	2	1.13	0.55	
	60	55	3.9	44.0	100	76	8	50	8	60	1	0	1	1.28	0.59	
	72	62	2.8	16.0	100	70	9	51	13	60	2	1	2	1.38	0.66	
	84	76	4.0	6.0	100	74	5	51	9	59	1	0	0	1.25	0.60	

Table A.3: Effects of 990 MeV/u Fe-ion irradiation (LET=155 keV/ μ m) on the frequency of chromosome aberrations in first cycle metaphases, the corresponding mitotic index (MI) and BrdU-labeling index (LI) 48, 60, 72 and 84 h after exposure of human lymphocytes. Because the irradiations with 990 MeV/u and 177 MeV/u Fe-ions were performed at the same day only one set of X-rays data was generated to both Fe-ion data. For further details and abbreviations, see table caption A.1.

Dose (Gy)	Time (h)	BrdU		Cells at 1st cycle (%)	Scored 1st mitoses	Aberrant cells (%)	Aberration types per 100 metaphases							Aberrations per cell	Excess fragments per cell
		LI (%)	MI (%)				ctb	csb	dmin	dic	r	cte	t		
0	48	41	3.6	98.3	100	2	2	1	0	0	0	0	0	0.03	0.01
	60	65	4.1	42.5	100	6	3	4	0	0	0	0	0	0.07	0.04
	72	77	4.8	12.6	100	5	4	1	0	0	0	0	0	0.05	0.01
	84	80	4.5	4.9	100	9	5	6	0	0	1	0	1	0.13	0.07
0.54	48	-	2.7	99.3	100	12	2	8	0	7	0	1	0	0.18	0.07
	60	-	4.2	39.7	100	16	2	18	2	8	0	0	0	0.30	0.20
	72	-	4.2	14.6	100	17	4	15	1	14	0	2	0	0.36	0.16
	84	-	2.6	3.5	100	37	20	50	7	19	0	2	0	0.98	0.58
1.1	48	-	1.8	98.5	100	15	4	7	4	6	0	0	0	0.21	0.11
	60	-	3.0	39.9	100	20	3	25	4	17	0	3	1	0.53	0.29
	72	-	3.6	15.8	100	40	9	82	14	52	1	5	0	1.63	0.97
	84	-	4.7	4.4	100	50	27	114	4	44	4	2	0	1.95	1.23

Continued on next page

Table A.4: Effects of 177 MeV/u Fe-ion irradiation (LET=335 keV/ μm) on the frequency of chromosome aberrations in first cycle metaphases, the corresponding mitotic index (MI) and BrdU-labeling index (LI) 48, 60, 72 and 84 h after exposure of human lymphocytes. At further time-points (section 2.2) only the MI, the cell generation of metaphases and the LI were determined. For reasons of space these data are not included in the table. For further details and abbreviations, see table caption A.1.

Dose (Gy)	Time (h)	BrdU		Cells at 1st cycle (%)	Scored 1st mitoses	Aberrant cells (%)	Aberration types per 100 metaphases							Aberrations per cell	Excess fragments per cell
		LI (%)	MI (%)				ctb	csb	dmin	dic	r	cte	t		
2.2	48	29	0.9	99.7	100	27	4	21	5	16	0	0	1	0.47	0.27
	60	48	2.1	47.9	100	47	16	60	8	55	2	4	0	1.45	0.73
	72	62	3.4	20.7	100	72	28	148	16	105	1	10	4	3.12	1.65
	84	66	3.7	9.9	100	81	38	213	27	100	3	13	0	3.94	2.44
3.2	48	-	0.7	99.5	100	33	6	27	2	12	2	0	0	0.49	0.31
	60	-	0.9	59.5	100	54	11	74	6	62	2	2	0	1.57	0.83
	72	-	1.9	26.8	100	78	48	202	31	127	8	18	1	4.35	2.42
	84	-	2.7	19.3	100	86	70	257	25	175	3	18	1	5.49	2.86
4.3	48	21	0.4	100	100	48	8	39	6	47	3	1	1	1.05	0.48
	60	32	0.9	63.4	100	77	8	137	30	95	3	4	0	2.77	1.71
	72	54	1.9	36.2	111	91	51	240	56	188	18	26	2	5.81	3.21
	84	52	1.6	20.1	100	96	90	423	73	188	8	42	3	8.27	5.11

Table A.4: (continued) Effects of 177 MeV/u Fe-ion irradiation (LET=335 keV/ μ m) on the frequency of chromosome aberrations in first cycle metaphases, the corresponding mitotic index (MI) and BrdU-labeling index (LI) 48, 60, 72 and 84 h after exposure of human lymphocytes. At further time-points (section 2.2) only the MI, the cell generation of metaphases and the LI were determined. For reasons of space these data are not included in the table. For further details and abbreviations, see table caption A.1.

Dose (Gy)	Time (h)	BrdU		Cells at 1st cycle (%)	Scored 1st mitoses	Aberrant cells (%)	Aberration types per 100 metaphases							Aberrations per cell	Excess fragments per cell
		LI (%)	MI (%)				ctb	csb	dmin	dic	r	cte	t		
0	60	64	4.2	64.6	100	5	4	1	0	0	0	0	0	0.05	0.01
	72	73	6.0	21.6	100	7	5	3	0	0	0	0	0	0.08	0.03
5.1	60	58	1.9	55.0	100	13	7	3	1	3	0	1	0	0.15	0.05
	72	63	3.6	18.0	100	19	12	14	2	7	1	2	2	0.40	0.17
	84	76	2.2	12.3	100	48	30	61	10	29	2	10	0	1.42	0.77
20.3	60	42	1.6	72.4	100	20	11	18	3	16	0	0	0	0.48	0.21
	72	49	3.1	31.0	100	40	32	93	11	31	1	4	0	1.72	1.09
	84	67	2.3	7.4	100	61	63	185	16	73	7	17	0	3.61	2.16
60.8	60	16	0.8	78.2	100	10	3	10	2	11	1	0	0	0.27	0.15
	72	29	1.8	22.6	150	32	17	61	4	19	3	0	0	1.04	0.67
	84	47	2.0	8.8	120	63	147	338	30	73	10	26	0	6.24	3.88
2 X-rays	60	58	2.1	84.8	100	63	11	29	10	37	7	3	0	0.97	0.46
	72	63	3.7	23.8	100	61	18	19	7	47	0	0	0	0.91	0.26
	84	70	1.9	12.3	100	67	18	43	8	41	2	2	0	1.14	0.56

Table A.5: Effects of 4.1 MeV/u Cr-ion irradiation (LET=3160 keV/ μm) on the frequency of chromosome aberrations in first cycle metaphases, the corresponding mitotic index (MI) and BrdU-labeling index (LI) 60, 72 and 84 h after exposure of human lymphocytes. For further details and abbreviations, see table caption A.1.

Dose (Gy)	Time (h)	Scored PCC cells	Aberrant cells (%)	Excess fragments per cell	PI (%)	Prematurely condensed cells (%)									
						S	1st G_2	M	2nd			3rd			
							G_1	G_2	M	G_1	G_2	M	G_1	G_2	M
0	48	100	16	0.16	26.6	58.3	9.4	11.7	10.7	6.5	2.9	0.5	0	0	
	60	100	13	0.16	30.9	53.2	9.9	2.6	5.7	16.0	0.7	8.4	3.1	0.5	
	72	100	13	0.18	19.3	42.2	6.1	1.3	2.4	9.8	0.9	7.5	25.6	4.3	
0.3	48	100	36	0.52	17.3	50.9	35.7	3.2	8.2	2.0	0	0	0	0	
	60	100	30	0.38	20.2	42.2	21.9	1.2	11.7	11.2	0.9	8.8	2.0	0	
	72	100	32	0.45	25.0	47.6	8.2	0.6	4.9	9.7	1.1	12.9	14.1	0.9	
0.6	48	100	36	0.47	16.4	44.4	44.3	3.2	7.6	0.3	0	0.1	0	0	
	60	100	36	0.50	38.5	39.4	17.1	2.3	15.1	14.9	0.5	8.6	1.8	0.2	
	72	100	40	0.58	43.8	39.3	8.4	1.1	5.5	11.7	0.8	12.9	18.1	2.2	
1.0	48	100	50	0.69	17.7	41.7	40.0	7.0	9.9	0.8	0.6	0	0	0	
	60	100	63	0.91	23.0	42.4	17.4	2.1	12.9	12.7	1.2	8.7	1.5	1.0	
	72	100	43	0.71	28.3	44.0	7.2	1.3	4.4	11.5	0.6	11.4	17.3	2.3	
2.0	48	100	76	1.37	15.2	39.7	47.6	3.2	8.7	0.4	0.4	0	0	0	
	60	200	67	1.21	32.2	42.9	23.6	1.8	10.5	14.4	1.0	5.5	0.2	0.1	
	72	200	83	1.63	33.0	38.1	14.0	1.0	5.1	17.6	1.1	9.4	12.1	1.6	
4.0	48	100	95	2.74	12.2	47.5	47.0	1.5	4.0	0	0	0	0	0	
	60	200	95	2.69	27.8	31.9	45.5	2.0	5.9	11.8	0.4	2.1	0.3	0	
	72	200	98	3.20	31.3	29.2	22.4	0.8	4.7	26.2	0.9	6.6	8.0	1.1	

Table A.6: Effects of X-ray irradiation on the frequency of excess fragments in first cycle G_2 -PCCs, the corresponding PCC index (PI) and the cell cycle distribution of PCCs 48, 60 and 72 h after exposure of human lymphocytes.

Dose (Gy)	Time (h)	Scored PCC cells	Aberrant cells (%)	Excess fragments per cell	PI (%)	Prematurely condensed cells (%)								
						S	1st G_2		2nd G_1		3rd G_2			M
0	48	250	16	0.20	32.8	54.8	22.9	5.0	16.3	0.9	0	0	0	0
	60	100	19	0.23	25.7	61.9	11.2	3.1	6.7	7.4	3.1	6.3	0.4	0
	72	100	30	0.37	28.0	59.3	3.7	0.1	4.5	8.3	0.7	16.2	6.7	0.4
1.0	48	200	64	1.14	19.0	55.5	24.2	2.1	17.5	0.5	0	0.2	0	0
	60	200	73	1.51	22.7	49.8	20.6	0.9	7.4	12.3	0.8	8.1	0.1	0
	72	200	72	1.51	17.2	48.6	9.0	0	4.7	11.5	1.0	13.4	11.0	0.9
2.0	48	200	82	1.83	28.6	56.9	27.8	2.5	12.7	0	0	0	0	0
	60	100	86	2.60	18.7	51.4	26.4	2.1	3.7	12.5	1.5	2.1	0.4	0
	72	200	90	2.71	17.2	50.8	12.6	0.9	3.9	14.3	0.9	10.7	5.1	0.6
3.0	48	200	95	3.20	22.2	58.4	34.7	1.3	5.6	0	0	0	0	0
	60	100	97	3.86	35.1	48.3	37.5	2.0	3.4	7.0	0.7	1.1	0	0
	72	100	97	4.18	21.7	48.9	26.1	2.8	4.7	9.5	1.0	4.9	1.9	0.1
4.0	48	100	98	4.17	10.7	57.5	37.4	1.3	3.8	0	0	0	0	0
	60	100	98	4.70	22.0	38.9	47.8	2.1	2.0	7.7	0.4	1.0	0.1	0
	72	200	100	4.68	13.9	44.0	34.3	1.6	2.9	11.7	0.6	3.9	1.0	0
X-rays	2.0	48	100	72	1.28	20.8	55.4	29.7	2.1	12.4	0.3	0.2	0	0
	60	100	67	1.15	33.0	46.1	21.1	2.4	8.6	11.3	2.0	7.8	0.7	0.1
	72	100	71	1.28	36.3	53.9	11.0	1.2	6.2	8.0	0.4	14.1	4.5	0.6

Table A.7: Effects of 90 MeV/u C-ion irradiation (LET=29 keV/ μ m) on the frequency of excess fragments in first cycle G_2 -PCCs, the corresponding PCC index (PI) and the cell cycle distribution of PCCs 48, 60 and 72 h after exposure of human lymphocytes.

Dose (Gy)	Time (h)	Scored PCC cells	Aberrant cells (%)	Excess fragments per cell	PI (%)	Prematurely condensed cells (%)								
						S	1st G_2	M	2nd G_1 G_2		3rd G_1 G_2 M			
0	48	100	13	0.16	49.5	45.5	24.6	3.9	24.2	1.2	0.1	0.4	0	0
	60	50	20	0.24	51.0	49.9	7.9	1.2	9.8	11.9	0.9	16.4	1.1	0.8
	72				55.0	32.1	4.1	0.3	4.0	11.9	0.6	27.7	15.2	4.2
1.0	48	100	81	2.44	31.4	39.3	36.5	3.2	20.2	0.7	0	0	0	0
	60	100	90	3.92	51.6	44.1	25.1	1.6	13.9	10.1	0.3	4.2	0.3	0.4
	72	100	92	3.66	45.4	35.3	13.6	1.1	3.9	17.1	0.4	20.6	6.7	1.6
2.3	48	100	87	3.39	34.0	47.5	46.3	1.1	5.1	0	0	0	0	0
	60	100	96	5.84	37.4	40.2	38.1	4.4	11.3	6.0	0	0	0	0
	72	100	98	5.82	36.6	29.0	34.5	1.4	5.5	15.3	0.6	8.2	4.1	1.3
3.0	48	100	96	5.60	29.0	40.5	53.7	1.7	3.7	0.2	0	0	0	0
	60	100	98	7.60	27.0	28.0	58.6	2.9	6.5	3.8	0	0.2	0	0
	72	100	99	6.43	37.0	26.6	40.3	3.1	8.1	14.7	0.5	3.7	2.9	0.3
2.0 X-rays	48	200	69	1.26	36.7	35.0	44.4	3.4	17.0	0.1	0	0	0	0
	60	200	71	1.52	38.4	38.9	19.6	0.9	17.8	11.2	1.6	9.6	0.4	0
	72	200	70	1.26	45.3	40.4	9.2	0.7	12.9	9.9	0.4	21.1	4.9	0.5

Table A.8: Effects of 990 MeV/u Fe-ion irradiation (LET=155 keV/ μ m) on the frequency of excess fragments in first cycle G_2 -PCCs, the corresponding PCC index (PI) and the cell cycle distribution of PCCs 48, 60, 72 and 84 h after exposure of human lymphocytes. Because the irradiations with 990 MeV/u and 177 MeV/u Fe-ions were performed at the same day only one set of X-rays data was generated to both Fe-ion data.

Dose (Gy)	Time (h)	Scored PCC cells	Aberrant cells (%)	Excess fragments per cell	PI (%)	Prematurely condensed cells (%)								
						S	1st G_2	M	2nd G_1	G_2	M	3rd G_1	G_2	M
0	48	200	11	0.12	42.7	48.0	25.4	3.2	22.5	0.7	0	0.1	0	0
	60	200	14	0.15	43.1	51.2	15.7	1.8	10.2	10.9	1.8	7.8	0.1	0.5
	72	200	20	0.28	36.9	50.5	3.9	0.7	6.8	6.4	0.1	22.1	8.4	1.0
0.54	48	100	37	0.93	36.8	45.6	32.8	2.2	18.6	0.7	0	0	0	0
	60	100	73	2.10	42.0	47.7	19.2	1.7	13.1	10.2	0.8	7.3	0	0
	72	100	83	2.43	51.3	41.4	9.6	1.2	7.0	9.2	0.7	23.4	6.8	0.6
1.1	48	100	65	2.10	32.2	49.7	32.4	1.9	15.7	0.3	0	0	0	0
	60	100	82	2.58	26.1	54.6	25.6	1.7	3.5	8.4	1.3	3.6	0.9	0.4
	72	100	92	3.55	46.8	49.7	9.8	0.7	10.7	6.1	0.3	16.2	5.7	0.9
2.2	48	200	80	3.36	26.3	43.8	43.8	1.9	9.9	0.6	0	0	0	0
	60	100	90	4.75	37.9	36.4	44.1	1.8	8.1	4.9	1.2	2.8	0.5	0.1
	72	200	97	5.66	46.5	38.2	28.9	0.8	7.1	7.8	0.4	11.1	5.1	0.6
3.2	48	200	93	4.52	33.0	51.2	41.0	0.8	6.8	0.2	0	0	0	0
	60	200	97	5.88	37.6	29.3	57.8	1.3	3.1	5.4	0.3	2.3	0.3	0.1
	72	200	98	6.25	36.4	38.9	41.0	1.1	3.4	5.3	0.5	5.7	3.6	0.7
4.3	48	200	94	5.53	28.8	60.3	37.4	0.3	2.0	0	0	0	0	0
	60	100	99	8.09	37.0	26.2	64.5	0.9	4.1	2.3	0.5	1.5	0	0
	72	200	100	7.85	34.0	39.3	48.1	1.1	3.1	2.5	0.9	3.5	1.3	0.2
	84	200	100	10.9	49.2	32.1	42.9	0.7	7.5	6.3	1.3	6.2	2.6	0.3

Table A.9: Effects of 177 MeV/u Fe-ion irradiation (LET=335 keV/ μ m) on the frequency of excess fragments in first cycle G_2 -PCCs, the corresponding PCC index (PI) and the cell cycle distribution of PCCs 48, 60, 72 and 84 h after exposure of human lymphocytes.

Dose (Gy)	Time (h)	Scored PCC cells	Aberrant cells (%)	Excess fragments per cell	PI (%)	Prematurely condensed cells (%)								
						S	1st G_2		2nd G_1		3rd G_2			M
0	60	100	24	0.33	26.0	45.8	15.5	3.7	14.4	12.7	0.7	5.5	0	1.8
	72	100	31	0.49	73.0	54.8	4.4	0.7	3.8	9.0	0.7	16.6	7.7	2.3
	84				59.0	40.4	1.7	0.5	0.8	8.1	0.3	31.7	13.5	3.0
5.1	60	100	58	2.96	25.0	48.0	21.9	2.8	9.7	11.7	0.6	4.8	0.1	0.4
	72	100	89	6.10	57.0	46.6	12.1	1.2	5.4	8.8	1.0	15.4	7.4	2.1
	84	100	96	6.83	46.0	43.7	6.4	1.2	2.7	6.4	0.5	23.8	12.5	3.0
20.3	60	100	71	4.64	13.0	47.4	23.0	2.7	16.1	6.3	0.2	3.2	0.2	1.0
	72	100	96	10.2	41.5	37.1	28.0	1.4	3.7	10.3	0.6	11.1	5.5	2.2
	84	100	93	11.2	31.0	41.4	17.0	0.5	2.2	5.4	0.3	19.0	11.9	2.3
60.8	60	100	73	5.50	11.0	53.4	19.1	1.9	20.1	4.4	0.7	0.5	0	0
	72	100	99	15.7	25.0	52.2	27.9	1.0	2.9	5.6	1.4	7.0	1.9	0.2
	84	100	98	16.0	19.0	39.7	31.0	1.1	1.4	4.3	0.3	14.1	6.0	2.0
2.0 X-rays	60	100	72	1.50	28.4	42.5	27.0	2.4	18.9	7.0	0.6	1.6	0	0
	72	100	81	1.64	54.0	44.1	10.0	2.3	5.3	21.0	2.2	11.5	2.5	1.0
	84	100	83	1.73	48.0	41.6	4.2	0.9	3.2	12.0	0.6	24.5	11.0	2.0

Table A.10: Effects of 4.1 MeV/u Cr-ion irradiation (LET=3160 keV/ μ m) on the frequency of excess fragments in first cycle G_2 -PCCs, the corresponding PCC index (PI) and the cell cycle distribution of PCCs 60, 72 and 84 h after exposure of human lymphocytes.

Particle fluence (ions/cm ²)	Dose (Gy)	Time (h)	Averaged no. of ab./cell ($\langle x \rangle$)	Dispersion (σ^2)	Relative dispersion ($\sigma^2/\langle x \rangle$)	Poisson fit (a)	χ^2	p
X-rays								
	1.0	48	0.37	0.37	1.0	0.38 ± 0.07	0.34	0.21
	1.0	72	0.42	0.38	0.91	0.41 ± 0.06	0.31	0.13
	2.0	48	1.10	0.91	0.83	1.1 ± 0.10	0.80	0.47
	2.0	72	1.07	0.97	0.91	1.0 ± 0.10	0.78	0.46
	4.0	48	3.23	3.0	0.92	3.4 ± 0.16	2.2	0.97
	4.0	72	3.66	3.6	0.98	3.6 ± 0.19	1.2	0.68
90 MeV/u C-ions								
22×10^6	1.0	48	0.96	0.98	1.0	0.95 ± 0.10	0.39	0.18
22×10^6	1.0	72	1.25	1.6	1.3	1.2 ± 0.11	0.52	0.21
43×10^6	2.0	48	2.30	3.1	1.3	2.3 ± 0.12	1.8	0.92
43×10^6	2.0	72	2.91	3.6	1.2	2.8 ± 0.17	0.47	0.11
86×10^6	4.0	48	4.64	5.5	1.2	4.7 ± 0.17	0.71	0.27
86×10^6	4.0	72	6.18	7.3	1.2	6.2 ± 0.18	0.49	0.06

Table A.11: Analysis of the frequency distributions of aberrations in first-cycle mitotic cells produced by X-rays and 90 MeV/u C-ions. Experimental data have been compared to the Poisson distribution. For reasons of space only selected time- and dose-points are included in the table. Averaged no. of ab./cell stands for the averaged number of aberrations per cell. The parameter a is the average number of aberrations per cell. Results of the goodness-of-fit test, χ^2 values are given per a degree of freedom. p is the probability of finding a higher value of χ^2 .

Particle fluence (ions/cm ²)	Dose (Gy)	Time (h)	Averaged no. of ab./cell ($\langle x \rangle$)	Dispersion (σ^2)	Relative dispersion ($\sigma^2/\langle x \rangle$)	Neyman fit (λ)	Neyman fit (μ)	χ^2	p	Expected no. of ab./cell ($\lambda\mu$)
990 MeV/u Fe-ions										
4×10^6	1.0	48	1.50	3.3	2.2	1.0 ± 0.18	1.7 ± 0.34	0.49	0.18	1.69
4×10^6	1.0	72	2.84	8.8	3.1	1.2 ± 0.16	2.7 ± 0.38	1.0	0.55	3.11
12×10^6	3.0	48	4.33	10.1	2.3	3.0 ± 0.61	1.4 ± 0.30	0.74	0.28	4.25
12×10^6	3.0	72	8.53	18.8	2.2	7.1 ± 2.19	1.3 ± 0.41	0.88	0.40	9.19
177 MeV/u Fe-ions										
4×10^6	2.2	48	0.47	1.0	2.1	0.60 ± 0.26	0.60 ± 0.27	0.63	0.32	0.36
4×10^6	2.2	72	3.12	10.3	3.3	1.4 ± 0.21	2.1 ± 0.33	0.77	0.32	2.93
8×10^6	4.3	48	1.05	2.5	2.4	1.0 ± 0.25	1.1 ± 0.31	1.1	0.64	1.06
8×10^6	4.3	72	5.80	23.9	4.1	2.7 ± 0.44	1.7 ± 0.28	1.3	0.82	4.51
4.1 MeV/u Cr-ions										
4×10^6	20.3	60	0.48	2.1	4.3	0.40 ± 0.18	0.64 ± 0.31	0.72	0.39	0.26
4×10^6	20.3	84	3.61	19.6	5.4	0.90 ± 0.13	5.2 ± 0.52	1.3	0.77	4.62
12×10^6	60.8	60	0.27	0.90	3.3	0.15 ± 0.04	3.1 ± 0.79	0.30	0.09	0.46
12×10^6	60.8	84	6.23	63.2	10.1	0.96 ± 0.12	6.7 ± 0.58	1.2	0.78	6.41

Table A.12: Analysis of the frequency distributions of aberrations in first-cycle mitotic cells produced by 990 MeV/u Fe-ions, 177 MeV/u Fe-ions and 4.1 MeV/u Cr-ions. Experimental data have been compared to the Neyman distribution. For reasons of space only selected time- and dose-points are included in the table. Further data set is plotted in fig. 3.16. The parameter λ is the average number of particle traversals per cell nucleus, while μ is the average number of aberrations per particle hit. For more details see the caption in table A.11.

Particle fluence (ions/cm ²)	Dose (Gy)	Time (h)	Averaged no. of ab./cell ($\langle x \rangle$)	Dispersion (σ^2)	Relative dispersion ($\sigma^2/\langle x \rangle$)	Poisson fit (a)	χ^2	p
X-rays								
	1.0	48	0.69	0.67	0.97	0.63 ± 0.07	0.74	0.44
	1.0	72	0.71	1.4	1.9	0.55 ± 0.07	0.78	0.42
	2.0	48	1.37	1.9	1.4	1.3 ± 0.11	0.84	0.48
	2.0	72	1.63	1.6	0.96	1.6 ± 0.09	1.1	0.62
	4.0	48	2.74	2.9	1.1	3.0 ± 0.17	3.4	1.0
	4.0	72	3.20	2.8	0.86	3.2 ± 0.12	0.90	0.48
90 MeV/u C-ions								
22×10^6	1.0	48	1.14	1.5	1.3	1.1 ± 0.08	0.85	0.47
22×10^6	1.0	72	1.51	2.1	1.4	1.4 ± 0.08	1.2	0.72
43×10^6	2.0	48	1.83	2.0	1.1	1.8 ± 0.10	0.56	0.21
43×10^6	2.0	72	2.71	3.6	1.3	2.7 ± 0.12	0.87	0.44
86×10^6	4.0	48	4.17	4.7	1.1	4.2 ± 0.23	0.90	0.47
86×10^6	4.0	72	4.68	5.7	1.2	4.5 ± 0.14	1.0	0.57

Table A.13: Analysis of the frequency distributions of aberrations in first-cycle G_2 -PCC cells produced by X-rays and 90 MeV/u C-ions. Experimental data have been compared to the Poisson distribution. For reasons of space only selected time- and dose-points are included in the table. For more details see the caption in table A.11.

Particle fluence (ions/cm ²)	Dose (Gy)	Time (h)	Averaged no. of ab./cell ($\langle x \rangle$)	Dispersion (σ^2)	Relative dispersion ($\sigma^2/\langle x \rangle$)	Neyman fit (λ)	Neyman fit (μ)	χ^2	p	Expected no. of ab./cell ($\lambda\mu$)
990 MeV/u Fe-ions										
4×10^6	1.0	48	2.44	5.3	2.2	3.0 ± 0.94	0.71 ± 0.24	1.9	0.95	2.10
4×10^6	1.0	72	3.66	6.4	1.8	4.3 ± 1.3	0.84 ± 0.26	0.42	0.06	3.63
12×10^6	3.0	48	5.60	11.1	2.0	5.1 ± 1.4	1.2 ± 0.35	0.43	0.04	5.86
12×10^6	3.0	72	6.43	11.9	1.8	7.7 ± 2.4	0.82 ± 0.27	0.71	0.22	6.36
177 MeV/u Fe-ions										
4×10^6	2.2	48	3.36	9.5	2.8	2.0 ± 0.24	1.7 ± 0.21	0.77	0.32	3.23
4×10^6	2.2	72	5.66	14.5	2.6	4.2 ± 0.64	1.3 ± 0.21	1.0	0.56	5.51
8×10^6	4.3	48	5.53	20.1	3.6	3.5 ± 0.52	1.5 ± 0.22	0.51	0.04	5.15
8×10^6	4.3	72	7.85	20.2	2.6	8.0 ± 1.5	0.91 ± 0.18	1.3	0.85	7.27
4.1 MeV/u Cr-ions										
4×10^6	20.3	60	4.64	32.2	6.9	1.1 ± 0.15	2.1 ± 0.31	1.9	0.99	2.29
4×10^6	20.3	84	11.2	67.1	6.0	2.6 ± 0.32	4.6 ± 0.62	0.89	0.36	11.7
12×10^6	60.8	60	5.50	80.3	14.6	1.4 ± 0.20	2.5 ± 0.38	1.1	0.64	3.46
12×10^6	60.8	84	16.0	110.3	6.9	3.4 ± 0.41	4.5 ± 0.62	0.70	0.09	15.4

Table A.14: Analysis of the frequency distributions of aberrations in first-cycle G_2 -PCC cells produced by 990 MeV/u Fe-ions, 177 MeV/u Fe-ions and 4.1 MeV/u Cr-ions. Experimental data have been compared to the Neyman distribution. For reasons of space only selected time- and dose-points are included in the table. Further data set is plotted in fig. 3.17. For more details see the captions in table A.11 and A.12.

Appendix B

Abbreviated terms

BrdU	5-bromo-2'-deoxyuridine
csb	chromosome fragment
ctb	chromatid break
cte	chromatid exchange
dic	dicentric with fragment
dmin	acentric ring
DNA	2'-deoxyribonucleic acid
DSBs	DNA double strand breaks
eq.	equation
FCS	fetal calf serum
fig.	figure
FISH	fluorescence in situ hybridization
FITC	fluorescein-5-isothiocyanate
FPG	Fluorescence plus Giemsa
GSI	Gesellschaft fr Schwerionenforschung mbH
ISCN	international system for human cytogenetic nomenclature
LET	linear energy transfer
M-Phase	mitosis of cell cycle
MI	mitotic index

Appendix B Abbreviated terms

MPF	mitosis promoting factor
PBS	phosphate buffered saline
PCC	premature chromosome condensation
PHA	phytohemagglutinin
PI	PCC index
r	centric ring with fragment
RBE	relative biological effectiveness
RNA	ribonucleic acid
rpm	revolutions per minute
RT	room temperature
S-Phase	synthesis phase of cell cycle
SD	standard deviation
SIS	heavy ion synchrotron (Schwer-Ionen-Synchrotron)
SSC	saline sodium citrate
t	translocation
UNILAC	universal linear accelerator
UV	Ultraviolet

Appendix C

List of materials, products and laboratory equipments

C.1 Materials

C.1.1 Chemicals

Acetic acid, GR for analysis (Merck, Darmstadt)
Acridine orange (Molecular probes, Leiden, Netherlands)
BrdU: 5-Bromo-2'-deoxyuridine (Roche, Mannheim)
Calyculin A, 100 μg (Wako, Osaka, Japan)
Citric acid (Merck, Darmstadt)
Colcemid, 10 $\mu\text{g}/\text{ml}$ (Roche, Mannheim)
Deoxycytidine (Serva, Heidelberg)
Disodium hydrogen phosphate: $\text{Na}_2\text{HPO}_4 \cdot 12\text{H}_2\text{O}$ (Merck, Darmstadt)
Ethanol, absolute GR for analysis (Merck, Darmstadt)
Eukitt (O. Kindler, Freiburg)
Fetal calf serum (Lot no. p950425, PAN, Aidenbach)
Giemsa (Merck, Darmstadt)
Hoechst No.33258 (Sigma, St.Louis, USA)
Hoechst No.33342 (Sigma, St.Louis, USA)
Isoton: Casyton (Schaerfe, Reutlingen)
L-glutamine 200 mM (Biochrom, Berlin)
Methanol, GR for analysis (Merck, Darmstadt)
Paraformaldehyde (Merck, Darmstadt)
PBS without Ca^{2+} and Mg^{2+} (Biochrom, Berlin)
Penicillin and streptomycin, 10000 U/10000 $\mu\text{g}/\text{ml}$ (Biochrom, Berlin)
Phytohemagglutinin, M-form: PHA (Gibco, Paisley, UK)
Potassium dihydrogen phosphate: KH_2PO_4 (Merck, Darmstadt)
RPMI 1640 medium (Gibco, Paisley, UK)
Sodium chloride (Merck, Darmstadt)
Sodium citrate·2 H_2O (Merck, Darmstadt)

Sodium heparin: Liquemin N25000, 5000 U/ml (Roche, Mannheim)

C.1.2 Test kits

TUNEL-test

ApoDIRECT *in situ* DNA fragmentation assay kit (BioCat, Heidelberg) contains following reagents

1. Wash buffer
2. Staining solution by mixing reaction buffer, TdT enzymes and FITC-dUTP
3. Rinse buffer
4. PI/RNase staining buffer

C.1.3 Solutions and buffers

Buffer during UV exposure (for FPG-staining)

19.45 ml	0.2 M Disodium hydrogen phosphate (Na_2HPO_4)
0.55 ml	0.1 M Citric acid

Complete medium

400 ml	RPMI 1640 medium
100 ml	Fetal calf serum
5 ml	L-glutamine
5 ml	Penicillin and streptomycin
1 ml	Sodium heparin

Fixative solution (for chromosome preparation)

75 %	Methanol
25 %	Acetic acid

Giemsa staining solution, pH 6.8

3 %	Giemsa
1 fraction	0.067 M Disodium hydrogen phosphate (Na_2HPO_4)
1 fraction	0.067 M Potassium dihydrogen phosphate (KH_2PO_4)

20×SSC

175.3 g	Sodium chloride (3 M)
88.4 g	Sodium citrate·2H ₂ O (0.3 M)
Add up to 1000 ml	distilled deionized water

C.2 Disposable products

Cell culture flask: 25 and 75 cm^2 (Becton Dickinson, Franklin Lakes, USA)
Centrifuge tube: 15 and 50 ml (TPP, Trasadingen, Switzerland)
Centrifuge tube for cell culture: 10 ml (Nunc, Roskilde, Denmark)
Cover glass: 60 mm \times 24 mm (IDL, Nidderau)
Disposable hypodermic needle: long needle (Braun, Melsungen)
Petri dish: 35 mm diameter (Nunc, Roskilde, Denmark)
Pipettes: 2, 5, 10, 25 ml (TPP, Trasadingen, Switzerland)
Pokalon foil: Polycarbonate foil (LOFO High Tech Film, Weil am Rhein)
Pasteur pipette (Greiner, Frickenhausen)
Slide glass: 76 mm \times 26 mm (IDL, Nidderau)
Tipps: 10, 200, 1000 μm (Brand, Wertheim)
Vacutainer CPT, Cell preparation tube (Becton Dickinson, Franklin Lakes, USA)
Vacutainer systems, Blood collection set: needle for taking blood (Becton Dickinson, Franklin Lakes, USA)

C.3 Laboratory equipments

Autoclave: Varioklav-Dampfsterilisator (H+P Labortechnik, Oberschleissheim)
Centrifuge: Megafuge 1.0 (Kendro-Heraeus instruments, Hanau)
Cell counter: Casy 1 model TT (Schaerfe system, Reutlingen)
Clean bench: Hera Safe HSP12 (Kendro-Heraeus instruments, Hanau)
Fluorescence microscope: BX61 (Olympus, Tokyo, Japan)
Incubator: BBD6220 (Kendro-Heraeus instruments, Hanau)
Pipettes: Eppendorf research (Eppendorf, Hamburg)
Pipette aid: Pipetus-akku (Hirschmann Laborgeraete, Eberstadt)
Ultrapure water supply-system: Milli-Q Plus (Millipore, Eschborn)
UV lamp: VL-15L (Novodirect, Karlsruhe)
UV lamp: VL-115L (Bioblock scientific, Illkirch, France)
Water bath: M12 (Lauda, Lauda-Koenigshofen)
X-ray machine: IV320-12 (Seifert, Ludwigshafen)

Bibliography

- Alberts, B., Bray, D., Lewis, J., Raff, M., Roberts, K., Watson, J., 1994. *Molecular biology of the cell*. Garland Publishing, New York.
- Amaldi, U., Kraft, G., July/Aug. 2005. Recent applications of Synchrotrons in cancer therapy with Carbon Ions. *Europhysics news* July/Aug., 114–118.
- Anderson, R., Marsden, S., Wright, E., Kadhim, M., Goodhead, D., Griffin, C., Jan 2000. Complex chromosome aberrations in peripheral blood lymphocytes as a potential biomarker of exposure to high-LET alpha-particles. *Int J Radiat Biol* 76 (1), 31–42.
- Anderson, R. M., Stevens, D. L., Goodhead, D. T., Sep 2002. M-fish analysis shows that complex chromosome aberrations induced by alpha -particle tracks are cumulative products of localized rearrangements. *Proc Natl Acad Sci U S A* 99 (19), 12167–12172.
- Aoki, M., Furusawa, Y., Yamada, T., Jun 2000. LET dependency of heavy-ion induced apoptosis in V79 cells. *J Radiat Res (Tokyo)* 41 (2), 163–175.
- ATIMA, 2006. The ATIMA program online documentation.
URL <http://www-linux.gsi.de/weick/atima/>
- Azzolina, L. S., Stevanoni, G., Tommasi, M., Tridente, G., Jul-Sep 1990. Phenotypic analysis of human peripheral blood lymphocytes by automatic sampling flow cytometry after stimulation with mitogens or allogeneic cells. *Ric Clin Lab* 20 (3), 209–216.
- Barkas, H., 1963. *Nuclear research emulsions*. Vol. 1. Academic Press, New York and London.
- Bauchinger, M., Oct 1995. Quantification of low-level radiation exposure by conventional chromosome aberration analysis. *Mutat Res* 339 (3), 177–189.
- Bauchinger, M., Schmid, E., Jul 1998. LET dependence of yield ratios of radiation-induced intra- and interchromosomal aberrations in human lymphocytes. *Int J Radiat Biol* 74 (1), 17–25.

- Bender, M. A., Gooch, P. C., Dec 1966. Somatic chromosome aberrations induced by human whole-body irradiation: the "recuplex" criticality accident. *Radiat Res* 29 (4), 568–582.
- Bethe, H., 1930. Zur Theorie des Durchgangs schneller Korpuskularstrahlen durch Materie. *Ann Phys* 5, 325–400.
- Beyer, W. H., 1968. Handbook of tables for probability and statistics. Cleveland: Chemical Rubber Co., 1968, 2nd ed., edited by Beyer, William H.
- Blakely, E. A., Chang, P. Y., Dec 2004. Late effects from hadron therapy. *Radiother Oncol* 73 Suppl 2, 134–140.
- Bloch, F., 1933. Zur Bremsung rasch bewegter Teilchen beim Durchgang durch Materie. *Ann Phys* 16, 287–321.
- Bonassi, S., Au, W. W., Mar 2002. Biomarkers in molecular epidemiology studies for health risk prediction. *Mutat Res* 511 (1), 73–86.
- Boreham, D., Dolling, J., Maves, S., Siwarungsun, N., Mitchel, R., May 2000. Dose-rate effects for apoptosis and micronucleus formation in gamma-irradiated human lymphocytes. *Radiat Res* 153 (5 Pt 1), 579–586.
- Boreham, D., Gale, K., Maves, S., Walker, J., Morrison, D., Nov 1996. Radiation-induced apoptosis in human lymphocytes: potential as a biological dosimeter. *Health Phys* 71 (5), 685–691.
- Brame, R., Groer, P., 2002. Bayesian analysis of overdispersed chromosome aberration data with the negative binomial model. *Radiat Prot Dosimetry* 102 (2), 115–119.
- Brandt, S., 1992. Datenanalyse. BI Wissenschaftsverlag.
- Brons, S., Taucher-Scholz, G., Scholz, M., Kraft, G., Apr 2003. A track structure model for simulation of strand breaks in plasmid dna after heavy ion irradiation. *Radiat Environ Biophys* 42 (1), 63–72.
- Carloni, M., Meschini, R., Ovidi, L., Palitti, F., Mar 2001. PHA-induced cell proliferation rescues human peripheral blood lymphocytes from X-ray-induced apoptosis. *Mutagenesis* 16 (2), 115–120.
- Coco-Martin, J. M., Begg, A. C., Mar 1997. Detection of radiation-induced chromosome aberrations using fluorescence in situ hybridization in drug-induced premature chromosome condensations of tumour cell lines with different radiosensitivities. *Int J Radiat Biol* 71 (3), 265–273.

- Collyn-d'Hooghe, M., Hemon, D., Gilet, R., Curtis, S., Valleron, A., Malaise, E., 1981. Comparative effects of ^{60}Co gamma-rays and neon and helium ions on cycle duration and division probability of EMT 6 cells. A time-lapse cinematography study. *Int J Radiat Biol Relat Stud Phys Chem Med* 39 (3), 297–306.
- Cornforth, M. N., Goodwin, E. H., Jul 1991. The dose-dependent fragmentation of chromatin in human fibroblasts by 3.5-mev alpha particles from ^{238}Pu : experimental and theoretical considerations pertaining to single-track effects. *Radiat Res* 127 (1), 64–74.
- Cucinotta, F. A., Schimmerling, W., Wilson, J. W., Peterson, L. E., Badhwar, G. D., Saganti, P. B., Dicello, J. F., Nov 2001. Space radiation cancer risks and uncertainties for mars missions. *Radiat Res* 156 (5 Pt 2), 682–688.
- Cullings, H., Fujita, S., 2003. The way to DS02: Resolving the neutron discrepancy. *RERF Update* 14, 17–23.
URL <http://www.rerf.or.jp/top/datae.htm>
- Curtis, S. B., Letaw, J. R., 1989. Galactic cosmic rays and cell-hit frequencies outside the magnetosphere. *Adv Space Res* 9 (10), 293–298.
- Dewey, W. C., Ling, C. C., Meyn, R. E., Nov 1995. Radiation-induced apoptosis: relevance to radiotherapy. *Int J Radiat Oncol Biol Phys* 33 (4), 781–796.
- Di Giorgio, M., Edwards, A. A., Moquet, J. E., Finnon, P., Hone, P. A., Lloyd, D. C., Kreiner, A. J., Schuff, J. A., Tajal, M. R., Vallerga, M. B., López, F. O., Burlón, A., Debray, M. E., Valda, A., 2004. Chromosome aberrations induced in human lymphocytes by heavy charged particles in track segment mode. *Radiat Prot Dosimetry* 108 (1), 47–53.
- Durante, M., Furusawa, Y., Gotoh, E., Oct 1998. A simple method for simultaneous interphase-metaphase chromosome analysis in biodosimetry. *Int J Radiat Biol* 74 (4), 457–462.
- Durante, M., George, K., Wu, H., Cucinotta, F., Nov 2002. Karyotypes of human lymphocytes exposed to high-energy iron ions. *Radiat Res* 158 (5), 581–590.
- Durante, M., George, K., Yang, T. C., Nov 1997. Biodosimetry of ionizing radiation by selective painting of prematurely condensed chromosomes in human lymphocytes. *Radiat Res* 148 (5 Suppl), 45–50.
- Durante, M., Gialanella, G., Grossi, G., Nappo, M., Pugliese, M., Bettega, D., Calzolari, P., Chiorda, G., Ottolenghi, A., Tallone-Lombardi, L., Apr 1994. Radiation-induced chromosomal aberrations in mouse 10T1/2 cells: dependence on the cell-cycle stage at the time of irradiation. *Int J Radiat Biol* 65 (4), 437–447.

- Durante, M., Grossi, G., Napolitano, M., Pugliese, M., Gialanella, G., Nov 1992. Chromosome damage induced by high-LET alpha-particles in plateau-phase C3H 10T1/2 cells. *Int J Radiat Biol* 62 (5), 571–580.
- Edwards, A., Finnon, P., Moquet, J., Lloyd, D., Darroudi, F., Natarajan, A., 1994. The effectiveness of high energy neon ions in producing chromosomal aberrations in human lymphocytes. *Radiat Prot Dosim* 52, 299–303.
- Edwards, A., Lloyd, D., Purrott, R., Apr 1979. Radiation induced chromosome aberrations and the Poisson distribution. *Radiat Environ Biophys* 16 (2), 89–100.
- Edwards, A., Purrott, R., Prosser, J., Lloyd, D., Jul 1980. The induction of chromosome aberrations in human lymphocytes by alpha-radiation. *Int J Radiat Biol Relat Stud Phys Chem Med* 38 (1), 83–91.
- Edwards, A. A., Nov 1997. The use of chromosomal aberrations in human lymphocytes for biological dosimetry. *Radiat Res* 148 (5 Suppl), 39–44.
- Evans, H., 1974. Effects of ionizing radiation on mammalian chromosomes. John Wiley and Sons, New York.
- Fournier, C., Scholz, M., Weyrather, W. K., Rodemann, H. P., Kraft, G., Jun 2001. Changes of fibrosis-related parameters after high- and low-let irradiation of fibroblasts. *Int J Radiat Biol* 77 (6), 713–722.
- Fournier, C., Taucher-Scholz, G., Dec 2004. Radiation induced cell cycle arrest: an overview of specific effects following high-let exposure. *Radiother Oncol* 73 Suppl 2, 119–122.
- GD, 2006. The gd program online documentation.
URL <http://www-aix.gsi.de/bio/DOCS/gd.html>
- George, K., Durante, M., Willingham, V., Wu, H., Yang, T., Cucinotta, F., Oct 2003. Biological effectiveness of accelerated particles for the induction of chromosome damage measured in metaphase and interphase human lymphocytes. *Radiat Res* 160 (4), 425–435.
- George, K., Wu, H., Willingham, V., Furusawa, Y., Kawata, T., Cucinotta, F., Feb 2001. High- and low-LET induced chromosome damage in human lymphocytes: a time-course of aberrations in metaphase and interphase. *Int J Radiat Biol* 77 (2), 175–183.
- Gerasimenko, V., Govorun, R., Ryzhov, N., Mar-Apr 1980. [Effect of accelerated boron, carbon, and neon ions on human lymphocyte chromosomes in vitro] in Russian. *Radiobiologiya* 20 (2), 206–211.

- Goodhead, D. T., Jan 1994. Initial events in the cellular effects of ionizing radiations: clustered damage in dna. *Int J Radiat Biol* 65 (1), 7–17.
- Goodwin, E., Blakely, E., 1992. Heavy ion-induced chromosomal damage and repair. *Adv Space Res* 12 (2-3), 81–89.
- Goodwin, E., Blakely, E., Tobias, C., Jun 1994. Chromosomal damage and repair in G1-phase Chinese hamster ovary cells exposed to charged-particle beams. *Radiat Res* 138 (3), 343–351.
- Gotoh, E., Asakawa, Y., Kosaka, H., 1995. Inhibition of protein serine/threonine phosphatases directly induces premature chromosome condensation in mammalian somatic cells. *Biomed Res* 16, 63–68.
- Gotoh, E., Tanno, Y., Takakura, K., Jan 2005. Simple biodosimetry method for use in cases of high-dose radiation exposure that scores the chromosome number of giemsa-stained drug-induced prematurely condensed chromosomes (pcc). *Int J Radiat Biol* 81 (1), 33–40.
- Griffin, C. S., Marsden, S. J., Stevens, D. L., Simpson, P., Savage, J. R., Apr 1995. Frequencies of complex chromosome exchange aberrations induced by 238pu alpha-particles and detected by fluorescence in situ hybridization using single chromosome-specific probes. *Int J Radiat Biol* 67 (4), 431–439.
- Größer, T., 2002. Untersuchung zur biologischen dosimetrie von schwerioneninduzierten chromosomenschäden in peripheren blutlymphozyten. Ph.D. thesis, TU Darmstadt.
- Gudowska-Nowak, E., Kleczkowski, A., Nasonova, E., Scholz, M., Ritter, S., Jan 2005. Correlation between mitotic delay and aberration burdens, and their role for the analysis of chromosomal damage. *Int J Radiat Biol* 81 (1), 23–32.
- Haberer, T., Becher, W., Schardt, D., Kraft, G., 1993. Magnetic scanning system for heavy ion therapy. *Nucl. Instr. Meth.* A330, 296–365.
- Hayata, I., Kanda, R., Minamihisamatsu, M., Furukawa, M., Sasaki, M. S., Sep 2001. Cytogenetical dose estimation for 3 severely exposed patients in the jco criticality accident in tokai-mura. *J Radiat Res (Tokyo)* 42 Suppl, 149–155.
- Heilmann, J., Taucher-Scholz, G., Haberer, T., Scholz, M., Kraft, G., Feb 1996. Measurement of intracellular dna double-strand break induction and rejoining along the track of carbon and neon particle beams in water. *Int J Radiat Oncol Biol Phys* 34 (3), 599–608.

- Heinrich, W., Wiegel, B., Kraft, G., 1991. Tables of dE/dx range and restricted energy loss of heavy ions in the energy range from 1 to 3000 MeV/u. Vol. 91-30. GSI-Report.
- Hoffmann, G., Sayer, A., Littlefield, L., Sep 2002. Higher frequency of chromosome aberrations in late-arising first-division metaphases than in early-arising metaphases after exposure of human lymphocytes to X-rays in G0. *Int J Radiat Biol* 78 (9), 765–772.
- Holgerson, A., Jernberg, A., Persson, L., Edgren, M., Lewensohn, R., Nilsson, A., Brahme, A., Meijer, A., Aug 2003. Low and high LET radiation-induced apoptosis in M059J and M059K cells. *Int J Radiat Biol* 79 (8), 611–621.
- IAEA, 2001. Cytogenetic analysis for radiation dose assessment. a manual. Tech. Rep. 405, International Atomic Energy Agency.
- ICRU, 1970. Linear Energy Transfer. Tech. Rep. 16, International Commission on Radiation Units and Measurements.
- ICRU, 1986. The quality factor in radiation protection. Tech. Rep. 40, International Commission on Radiation Units and Measurements.
- ISCN, 1978. An international system for human cytogenetic nomenclature (1978). Report of the Standing Committee on Human Cytogenetic Nomenclature. *Cytogenet Cell Genet* 21 (6), 309–409.
- Jakob, B., Scholz, M., Taucher-Scholz, G., Oct 2000. Immediate localized cdkn1a (p21) radiation response after damage produced by heavy-ion tracks. *Radiat Res* 154 (4), 398–405.
- Jenner, T. J., Fulford, J., O'Neill, P., Nov 2001. Contribution of base lesions to radiation-induced clustered dna damage: implication for models of radiation response. *Radiat Res* 156 (5 Pt 2), 590–593.
- Johannes, C., Horstmann, M., Durante, M., Chudoba, I., Obe, G., May 2004. Chromosome intrachanges and interchanges detected by multicolor banding in lymphocytes: searching for clastogen signatures in the human genome. *Radiat Res* 161 (5), 540–548.
- Kakati, S., Kowalczyk, J., Gibas, Z., Sandberg, A., Jun 1986. Use of radiation induced chromosomal damage in human lymphocytes as a biological dosimeter is questionable. *Cancer Genet Cytogenet* 22 (2), 137–141.
- Kanda, R., Hayata, I., Lloyd, D., Apr 1999. Easy biodosimetry for high-dose radiation exposures using drug-induced, prematurely condensed chromosomes. *Int J Radiat Biol* 75 (4), 441–446.

- Kaufman, G., Miller, M., Savage, J., Papworth, D., Mar 1974. Chromosome aberration yields from multiple fixation regimens. *J Theor Biol* 44 (1), 91–103.
- Kerr, J. F., Wyllie, A. H., Currie, A. R., Aug 1972. Apoptosis: a basic biological phenomenon with wide-ranging implications in tissue kinetics. *Br J Cancer* 26 (4), 239–257.
- Kiefer, J., Straaten, H., Nov 1986. A model of ion track structure based on classical collision dynamics. *Phys Med Biol* 31 (11), 1201–1209.
- Kraft, G., 1997. Radiobiology of heavy charged particles. *Advances in Hadron therapy*. Elsevier Science, Amsterdam, talk given at the Advanced Seminar on Hadron Therapy, Geneva, Switzerland, 20–24 Nov 1995.
- Kraft, G., 2000. Tumor therapy with heavy charged particles. *Prog Part Nucl Phys* 45 (suppl 2), S473–S544.
- Kraft, G., Daues, H., Fischer, B., Kopf, U., Leibold, H., Quis, D., Stelzer, H., Kiefer, J., Schoepper, R., Schneider, E., Weber, U., Wulf, H., Dertinger, H., 1980. Irradiation chamber and sample changes for biological samples. *Nuclear Instruments and Methods* 168, 175–179.
- Krämer, M., Kraft, G., 1994. Calculations of heavy-ion track structure. *Radiat Environ Biophys* 33 (2), 91–109.
- Lewis, B. J., McCall, M. J., Green, A. R., Bennett, L. G., Pierre, M., Schrewe, U. J., O'Brien, K., Felsberger, E., 2001. Aircrew exposure from cosmic radiation on commercial airline routes. *Radiat Prot Dosimetry* 93 (4), 293–314.
- Lindhard, J., Sorensen, A. H., Apr 1996. Relativistic theory of stopping for heavy ions. *Phys Rev A* 53 (4), 2443–2456.
- Meijer, A., Kronqvist, U., Lewensohn, R., Harms-Ringdahl, M., Feb 1998. RBE for the induction of apoptosis in human peripheral lymphocytes exposed in vitro to high-LET radiation generated by accelerated nitrogen ions. *Int J Radiat Biol* 73 (2), 169–177.
- Munro, T. R., Jun 1970. The relative radiosensitivity of the nucleus and cytoplasm of chinese hamster fibroblasts. *Radiat Res* 42 (3), 451–470.
- NASA, 1997. Modeling human risk: Cell and molecular biology in context. Tech. Rep. LBNL-40278, Lawrence Berkeley National Laboratory.
- NASA, 1998. Strategic program plan for space radiation health research. Tech. rep., NASA.

- Nasonova, E., Füssel, K., Berger, S., Gudowska-Nowak, E., Ritter, S., Sep 2004. Cell cycle arrest and aberration yield in normal human fibroblasts. I. Effects of X-rays and 195 MeV u(-1) C ions. *Int J Radiat Biol* 80 (9), 621–634.
- Nasonova, E., Gudowska-Nowak, E., Ritter, S., Kraft, G., Jan 2001. Analysis of Ar-ion and X-ray-induced chromatin breakage and repair in V79 plateau-phase cells by the premature chromosome condensation technique. *Int J Radiat Biol* 77 (1), 59–70.
- Nasonova, E., Ritter, S., 2004. Cytogenetic effects of densely ionising radiation in human lymphocytes: impact of cell cycle delays. *Cytogenet Genome Res* 104 (1-4), 216–220.
- Nasonova, E., Ritter, S., Fomenkova, T., Kraft, G., 1998. Induction of chromosomal damage in CHO-K1 cells and their repair-deficient mutant XRS5 by X-ray and particle irradiation. *Adv Space Res* 22 (4), 569–578.
- National Research Council, 1999. Health Effects of Exposure to Radon: BEIR VI. National Academy Press, Washington, DC.
- Neyman, J., 1939. On a new class of 'contagious' distributions, applicable in entomology and bacteriology. *Annals of Mathematical Statistics* 10, 35–57.
- Nikjoo, H., O'Neill, P., Terrissol, M., Goodhead, D. T., May 1999. Quantitative modelling of dna damage using monte carlo track structure method. *Radiat Environ Biophys* 38 (1), 31–38.
- Norppa, H., 2004. Cytogenetic biomarkers. *IARC Sci Publ* 157, 179–205.
- Ohara, H., Okazaki, N., Monobe, M., Watanabe, S., Kanayama, M., Minamihisamatsu, M., 1998. Induction of asymmetrical type of chromosomal aberrations in cultured human lymphocytes by ion beams of different energies at varying let from himac and rrc. *Adv Space Res* 22 (12), 1673–1682.
- Pantelias, G. E., Maillie, H. D., Jul 1984. The use of peripheral blood mononuclear cell prematurely condensed chromosomes for biological dosimetry. *Radiat Res* 99 (1), 140–150.
- Perry, P., Wolff, S., Sep 1974. New Giemsa method for the differential staining of sister chromatids. *Nature* 251 (5471), 156–158.
- Pietenpol, J. A., Stewart, Z. A., Dec 2002. Cell cycle checkpoint signaling: cell cycle arrest versus apoptosis. *Toxicology* 181-182, 475–481.

- Pinkel, D., Straume, T., Gray, J. W., May 1986. Cytogenetic analysis using quantitative, high-sensitivity, fluorescence hybridization. *Proc Natl Acad Sci U S A* 83 (9), 2934–2938.
- PTCOG, 2006. Particle therapy facilities in a planning stage or under construction. URL <http://ptcog.web.psi.ch/newptcentres.html>
- Radojcic, M., Crompton, N., Jun 2001. Age dependence of T-lymphocyte apoptosis induced by high-energy proton exposure. *Radiat Environ Biophys* 40 (2), 131–135.
- Ricoul, M., Sabatier, L., Dutrillaux, B., Mar 1997. Increased chromosome radiosensitivity during pregnancy. *Mutat Res* 374 (1), 73–78.
- Ritter, S., Nasonova, E., Furusawa, Y., Ando, K., Dec 2002a. Relationship between aberration yield and mitotic delay in human lymphocytes exposed to 200 MeV/u Fe-ions or X-rays. *J Radiat Res (Tokyo)* 43 Suppl, 175–179.
- Ritter, S., Nasonova, E., Gudowska-Novak, E., Mar 2002b. Effect of LET on the yield and quality of chromosomal damage in metaphase cells: a time-course study. *Int J Radiat Biol* 78 (3), 191–202.
- Ritter, S., Nasonova, E., Gudowska-Nowak, E., Scholz, M., Kraft, G., Feb 2000. High-LET-induced chromosome aberrations in V79 cells analysed in first and second post-irradiation metaphases. *Int J Radiat Biol* 76 (2), 149–161.
- Ritter, S., Nasonova, E., Scholz, M., Kraft-Weyrather, W., Kraft, G., Feb 1996. Comparison of chromosomal damage induced by X-rays and Ar ions with an LET of 1840 keV/micrometer in G1 V79 cells. *Int J Radiat Biol* 69 (2), 155–166.
- Roesch, W. (Ed.), 1987. US-Japan joint reassessment of atomic bomb radiation dosimetry in Hiroshima and Nagasaki, Final report. Vol. 1 and 2. Radiation Effects Research Foundation, Hiroshima.
URL <http://www.rerf.or.jp/shared/ds86/ds86a.html>
- Roy, L., Buard, V., Delbos, M., Durand, V., Paillole, N., Grégoire, E., Voisin, P., 2004. International intercomparison for criticality dosimetry: the case of biological dosimetry. *Radiat Prot Dosimetry* 110 (1-4), 471–476.
- Rydberg, B., Cooper, B., Cooper, P. K., Holley, W. R., Chatterjee, A., May 2005. Dose-dependent misrejoining of radiation-induced dna double-strand breaks in human fibroblasts: experimental and theoretical study for high- and low-let radiation. *Radiat Res* 163 (5), 526–534.

- Rydberg, B., Löbrich, M., Cooper, P. K., Aug 1994. Dna double-strand breaks induced by high-energy neon and iron ions in human fibroblasts. i. pulsed-field gel electrophoresis method. *Radiat Res* 139 (2), 133–141.
- Sancar, A., Lindsey-Boltz, L., Unsal-Kacmaz, K., Linn, S., 2004. Molecular mechanisms of mammalian dna repair and the dna damage checkpoints. *Annu Rev Biochem* 73, 39–85.
- Sasaki, H., Yatagai, F., Kanai, T., Furusawa, Y., Hanaoka, F., Zhu, W., Mehnati, P., Nov 1997. Dependence of induction of interphase death of Chinese hamster ovary cells exposed to accelerated heavy ions on linear energy transfer. *Radiat Res* 148 (5), 449–454.
- Sasaki, M. S., Hayata, I., Kamada, N., Kodama, Y., Kodama, S., Sep 2001. Chromosome aberration analysis in persons exposed to low-level radiation from the jco criticality accident in tokai-mura. *J Radiat Res (Tokyo)* 42 Suppl, 107–116.
- Savage, J., Apr 1976. Classification and relationships of induced chromosomal structural changes. *J Med Genet* 13 (2), 103–122.
- Schall, I., Schardt, D., Geissel, H., Irnich, H., Kankeleit, E., Kraft, G., Magel, A., Mohar, M., Munzenberg, G., Nickel, F., Scheidenberger, C., Schwab, W., 1996. Charge-changing nuclear reactions of relativistic light-ion beams ($5 \leq Z \leq 10$) passing through thick absorbers. *Nucl Instr Methods B* 117, 221–234.
- Scheidenberger, C., Geissel, H., 1998. Penetration of relativistic heavy ions through matter. *Nucl Inst and Meth in Phys Res B* 135, 25–34.
- Schimmerling, W., Cucinotta, F. A., Wilson, J. W., 2003. Radiation risk and human space exploration. *Adv Space Res* 31 (1), 27–34.
- Scholz, M., 2003. Effects of ion radiation on cells and tissues. *Adv Polym Sci* 162, 95–155.
- Scholz, M., Kraft-Weyrather, W., Ritter, S., Kraft, G., Jul 1994. Cell cycle delays induced by heavy ion irradiation of synchronous mammalian cells. *Int J Radiat Biol* 66 (1), 59–75.
- Scholz, M., Ritter, S., Kraft, G., Sep 1998. Analysis of chromosome damage based on the time course of aberrations. *Int J Radiat Biol* 74 (3), 325–331.
- Schulz-Ertner, D., Nikoghosyan, A., Didingner, B., Debus, J., Dec 2004. Carbon ion radiation therapy for chordomas and low grade chondrosarcomas—current status of the clinical trials at gsi. *Radiother Oncol* 73 Suppl 2, 53–56.

- Silver, L., Schardt, D., Kanai, T., 1998. Depth-dose distributions of high-energy carbon, oxygen and neon beams in water. *Jpn J Med Phys* 18 (1), 1–21.
- Simpson, J., 1983. Elemental and isotopic composition of the galactic cosmic rays. *Ann Rev of Nucl Part Sci* 33, 323–381.
- Sisterson, J., 2005. Particles. A newsletter for those interested in proton, light ion and heavy charged particle radiotherapy 36, 11.
URL <http://ptcog.web.psi.ch/archive.html>
- Skarsgard, L. D., Kihlman, B. A., Parker, L., Pujara, C. M., Richardson, S., 1967. Survival, chromosome abnormalities, and recovery in heavy-ion and x-irradiated mammalian cells. *Radiat Res Suppl* 7, 208–221.
- Space Studies Board, 1996. Radiation hazards to crews of interplanetary missions. Biological issues and research strategies. National academy press, Washington, DC.
- Tanaka, S. I., Sep 2001. Summary of the jco criticality accident in tokai-mura and a dose assessment. *J Radiat Res (Tokyo)* 42 Suppl, 1–9.
- Testard, I., Dutrillaux, B., Sabatier, L., Oct 1997. Chromosomal aberrations induced in human lymphocytes by high-LET irradiation. *Int J Radiat Biol* 72 (4), 423–433.
- Tsujii, H., Mizoe, J. E., Kamada, T., Baba, M., Kato, S., Kato, H., Tsuji, H., Yamada, S., Yasuda, S., Ohno, T., Yanagi, T., Hasegawa, A., Sugawara, T., Ezawa, H., Kandatsu, S., Yoshikawa, K., Kishimoto, R., Miyamoto, T., Dec 2004. Overview of clinical experiences on carbon ion radiotherapy at nirs. *Radiother Oncol* 73 Suppl 2, 41–49.
- Virsik, R., Harder, D., Jan 1981. Statistical interpretation of the overdispersed distribution of radiation-induced dicentric chromosome aberrations at high LET. *Radiat Res* 85 (1), 13–23.
- Vral, A., Cornelissen, M., Thierens, H., Louagie, H., Philippé, J., Strijckmans, K., De Ridder, L., Mar 1998. Apoptosis induced by fast neutrons versus ⁶⁰Co gamma-rays in human peripheral blood lymphocytes. *Int J Radiat Biol* 73 (3), 289–295.
- Vral, A., Thierens, H., Baeyens, A., De Ridder, L., Apr 2004. Chromosomal aberrations and in vitro radiosensitivity: intra-individual versus inter-individual variability. *Toxicol Lett* 149 (1-3), 345–352.
- Ward, J. F., Nov 1994. The complexity of dna damage: relevance to biological consequences. *Int J Radiat Biol* 66 (5), 427–432.

- Weyrather, W. K., Ritter, S., Scholz, M., Kraft, G., Nov 1999. Rbe for carbon track-segment irradiation in cell lines of differing repair capacity. *Int J Radiat Biol* 75 (11), 1357–1364.
- Wilkins, R., Wilkinson, D., Maharaj, H., Bellier, P., Cybulski, M., McLean, J., Jan 2002. Differential apoptotic response to ionizing radiation in subpopulations of human white blood cells. *Mutat Res* 513 (1-2), 27–36.
- Wojcik, A., Stephan, G., Sommer, S., Buraczewska, I., Kuszewski, T., Wieczorek, A., Gózd, S., Dec 2003. Chromosomal aberrations and micronuclei in lymphocytes of breast cancer patients after an accident during radiotherapy with 8 mev electrons. *Radiat Res* 160 (6), 677–683.
- Wu, H., Durante, M., George, K., Yang, T. C., Nov 1997. Induction of chromosome aberrations in human cells by charged particles. *Radiat Res* 148 (5 Suppl), 102–107.
- Wyllie, A. H., Apr 1980. Glucocorticoid-induced thymocyte apoptosis is associated with endogenous endonuclease activation. *Nature* 284 (5756), 555–556.
- Ziegler, J., Biersack, J., Littmark, U., 1985. The stopping and range of ions in solids. Pergamon Press, New York.

Acknowledgements

This PhD study has been performed at the biophysics group of Gesellschaft für Schwerionenforschung (GSI, Darmstadt) and supervised by Prof Dr Gerhard Kraft and Dr Sylvia Ritter since April 2002. The work was supported by BMBF (Bonn, Germany) under contract number 02S8203.

First of all, I want to express my gratitude to Prof Dr Gerhard Kraft for giving me the opportunity to work in this group, for his advices and valuable discussions. I am grateful to Prof D.H.H. Hoffmann for his interest in my work and undertaking the co-referee of the PhD work.

It was a great pleasure that I did my research together with wonderful ladies. I especially thankful to Dr Sylvia Ritter, who suggested me to do PhD at GSI and helped me for everything during my stay in Darmstadt, e.g. painting the walls of my flat, performing irradiation experiment with hundreds samples, correcting the manuscript, etc. I appreciate skillful helps from Ms Petra Hessel for taking blood cells and analyzing samples. I want to acknowledge Dr Elena Nasonova (JINR, Russia) for showing me the chromosome world, i.e. teaching me how to fix samples, prepare slides and score complicated aberrations. I greatly acknowledge Prof Dr Ewa Gudowska-Nowak (Jagellonian University, Poland) for introducing me into mathematical approaches such as the integration analysis or the fitting of frequency distributions. I appreciate Dr Annelie Meijer (Karolinska Institute, Sweden) for teaching me the morphological analysis of apoptotis. I want to thank Dr Claudia Fournier for her advices and kind help during my experiments.

I am grateful to Doppel Michaels, Dr M. Scholz and Dr M. Krämer, for their valuable advices and discussions and for providing figures of the simulation of dose distributions. I want to thank Mr Marek Tylutki from Kraków, who was a summer school student at GSI in 2005, for developing a part of the program for frequency distribution analysis. I also appreciate the help from Mr Wolfgang Becher, Mr Günter Lenz and Mr Cornelius Neitzert for their excellent technical support during irradiation. I want to thank Mr Marcus Winter, Dr Hiroshi Iwase and Dr Christoph Bert for their kind help, when computer software problems occurred.

I am grateful to all biophysics members to share a nice time in good atmosphere and I particularly appreciate volunteers from the group to be a blood donor. I also acknowledge to my Japanese friends at GSI and TU Darmstadt for spending a pleasant time. I am thankful to my boyfriend, Masayuki Muramatsu for his heart warming massages via email or telephone. Finally, many thanks to my family in Japan for their support to let me go to Germany for the study.

Curriculum Vitae

Name: Ryonfa Lee
Date of Birth: 19 Jan 1975
Place of birth: Yamagata, Japan
Marital status: Single
Nationality: Democratic People's Republic of Korea

Education and Qualifications

1981 – 1983 Kisai Town Elementary School (Saitama, Japan)
1983 – 1990 Saitama Korean Elementary and Middle School (Saitama, Japan)
1990 – 1993 Kasukabe Kyohei High School (Saitama, Japan)
1993 – 1997 International Christian University (Tokyo, Japan);
Physics (Bachelor of Arts) Thesis title: Irradiation effect of soft-X-rays on DNA-platinum complex
1997 – 1999 International Christian University (Tokyo, Japan);
Physics (Master of Arts in Science) Thesis title: The relation between cell killing and DNA strand break induction after heavy-ion irradiation
Since Apr 2002 Promotion supervised by Prof Dr G. Kraft, TU Darmstadt; the study has been performed at GSI Darmstadt, Biophysics group

Work Experience

1999 – 2001 Technical staff at International Space Radiation Laboratory, National Institute of Radiological Sciences (Chiba, Japan)
2001 – 2002 Technical staff at Frontier Research Center, National Institute of Radiological Sciences (Chiba, Japan)